Alma Mater Studiorum · Universit di Bologna

DOTTORATO DI RICERCA IN
SCIENZE E TECNOLOGIE AGRARIE, AMBIENTALI E ALIMENTARI

Ciclo XXXI

Settore Concorsuale: 07/C1
Settore Scientifico Disciplinare: AGR/10

Study of ventilation strategies in agricultural buildings through CFD modeling and experimental analysis

Supervisore:
Prof.ssa
Patrizia Tassinari

Co-superivisore:
Ing.
Stefano Benni

Prof.ssa
Beatrice Pulvirenti

Presentato da:
Enrica Santolini

Coordinatore Dottorato:
Massimiliano Petracci

Esame finale anno 2019

Abstract

English version

Environmental control in agricultural and agro-industrial buildings is a very important and topical subject which falls within the domain of precision agriculture and smart food processing. In fact, environmental conditions can have an impact on the quality, safety and health of the product, on the uniformity and therefore on the traceability of food chains, as well as the effects on sustainability, environmental and economic aspects of the sector. Considering the global interest and need to focus on energy consumption and also considering the policies at European level in the sector, there is a growing interest in the study of systems able to combine active and passive environmental control techniques, as well as for the development of systems and methodologies for modeling and simulating the environmental conditions of the various possible environments in the agro-industrial sector. These ones need an appropriate process of validation and experimental calibration, but they certainly have the positive aspect of opening the doors to many possibilities to investigate specific aspects and variations of the thermo-fluidynamic phenomena involved in the control of environmental parameters.
Precisely, these opportunities can be given by the computational fluid dynamics application (CFD), in this sector. In fact, over the last 20-30 years there was a noticeable increase in CFD applied to sectors such as greenhouse agriculture and animal farming. This approach presented some application limitations due mainly to the computational power of computers that has significantly increased nowadays. Computational fluid dynamics have been used to study various aspects, i.e. animal comfort in farms, distribution of temperature and humidity in greenhouses. It has been exploited for the structural improvement of greenhouses the proper materials to use for the covers, such as polyethylene, glass or other materials. Furthermore, CFD has been applied for the study of space-time distributions of air velocity with precision techniques, but also for investigating the most effective ventilation strategies. In fact, the optimization of both natural and mechanical ventilation has proved to be an extremely important field of application, given the direct effects of correct air circulation on different aspects of production (evaporation control

of fluids and mold formation, air exchange and cooling for natural ventilation, control of the concentration of both useful and harmful gases, etc.), and in general, considering the close relationship with the thermo-hygrometric control of production environments, on the wider field of the thermo-fluidodynamic investigations, applied to agricultural structures.
This thesis is specifically focused on the ventilation aspects in agricultural buildings. In fact, the main aim is to consider improvement actions, by the application of CFD approach, to optimize and act on airflow conditions in two types of structures: an experimental greenhouse and a cellar. They are two very different structures but in which climate control is extremely important and of interest. Specifically, the natural ventilation of a glass greenhouse has been investigated with a particular focus on the effects of internal shading screens on the internal fluidynamic and on the crop growing conditions. Considering the first results, a deep focus on the characterization of this type of screens has been carried out, with also the aim of identifying applicable methodologies, including the use of CFD, for this purpose. Finally, with regards to ventilation, a smart system has been created, considering to placed it in a cellar, for the improvement of the air flows around the barrels, which would thus prevent the formation of molds and eliminate the air stagnation areas behind the barrels. Therefore, different configurations have been analyzed and compared to identify the optimal design of the system.
The future step would be to conduct an evaluation of the effect of the system inside the cellar and then to make choices about the position and the number of this system needed. About ventilation of the greenhouse, the future step would be to to evaluate not only the choice of the type of cloth but also a better positioning of them within the structure.
In conclusion, CFD approach, in addiction to the specific results obtained, has allowed, in every aspect treated, to reach conclusions on possible decisions or strategies to improve the ventilation respecting a specific purpose: to improve the production and food quality conditions.

Keywords: Computational Fluid Dynamics, Agricultural Buildings, Ventilation, Wind Tunnel, Shading Screens.

Italian Version

Il ruolo del controllo dei parametri ambientali in edifici agricoli e agroindustriali fa parte delle tematiche inerenti all'agricoltura di precisione e dello smart food processing. Di fatto, le condizioni ambientali possono avere effetti sulla qualitá, sicurezza e salubritá del prodotto, sull'uniformitá e quindi sulla tracciabilitá delle filiere alimentari, cosí effetti anche sulla sostenibilitá ambientale ed economica del comparto. Considerando l'interesse e la necessit a livello globale di intevenire sui consumi energetiche e viste anche le politiche a livello europeo nel settore, sta quindi crescendo l'interesse per lo studio di sistemi in grado di combinare tecniche attive e passive di controllo ambientale, cosí come per la messa a punto di sistemi e metodologie per la modellazione e la simulazione delle condizioni ambientali dei diversi ambienti possibili nel settore agro-industriale. Questi ultimi ovviamente hanno bisogno di un processo opportuno di validazione e calibrazione sperimentale, ma hanno sicuramente l'aspetto positivo di aprire le porte a moltissime possibilitá di indagare specifici aspetti e varianti dei fenomeni termofluidodinamici coinvolti nel controllo dei parametri ambientali.
Proprio queste possibilitá possono essere date dall' applicazione fluidodinamica computazionale (CFD), in questo settore. Di fatto, negli ultimi 20-30 anni si é visto un notevole incremento della CFD applicata a settori come l' agricoltura in serra e nell' allevamento. Questo approccio all' inizio peró presentava delle limitazioni applicative dovute principalmente al potere computazionale dei computer che peró é andato sempre piú ad aumentare. La fluidodinamica computazionale é stata impiegata per lo studio di diversi aspetti, come ad esempio il benessere animale negli allevamenti, la distribuzione di temperatura e umiditá in serre. Essa é stata sfruttata per la scelta delle forme e dei materiali di copertura piú adatti per unéfficiente controllo ambientale. Inoltre, é stata applicata per lo studio delle distribuzioni spazio-temporali della velocitá dell' aria con tecniche di precisione, ma anche delle piú efficaci strategie di ventilazione.
Infatti, l' ottimizzazione della ventilazione sia naturale sia meccanica si é dimostrato essere un campo di applicazione di estrema rilevanza, visti gli effetti diretti che puó avere una corretta circolazione dell' aria su diversi aspetti della produzione (controllo dell' evaporazione di liquidi e formazione di muffe, ricambio dell' aria e raffrescamento per ventilazione naturale, controllo della concentrazione di gas sia utili che nocivi, ecc.), nonché piú in generale, vista la stretta relazione con il tema del controllo termoigrometrico degli ambienti di produzione, sul piú ampio dominio delle indagini termofluidodinamiche applicate alle strutture agricole.
Proprio sugli aspetti di ventilazione é incentrato il lavoro di tesi. L'obiettivo principale di questo lavoro é stato valutare e verificare, grazie all'utilizzo della CFD, azioni migliorative per le condizioni di ventilazione in due tipologie di strutture: una serra sperimentale ed una cantina. Sono due strutture di per sé molto diverse

ma dove il controllo climatico é di estrema importanza e di significativo interesse. In specifico, la ventilazione naturale di una serra é stata analizzata in diverse condizioni, con un focus in piú sugli effetti dati dalla presenza di schermi interni per l' ombreggiatura. I risultati ottenuti sono motivanti per dare vita ad un approfondimento sulla caratterizzazione di questa tipologia di teli, con l'intento di identificare delle metodologie applicabili, compreso l' utilizzo della CFD, per tale scopo. Infine, in merito alla tematica della ventilazione, é stato ideato, progettato e testato un sistema smart di ventilazione, pensato per un utilizzo in cantine, con lo scopo di migliorare i flussi di aria intorno a botti e barriques, in modo tale da eliminare le zone di stagnazione dell' aria dietro le barriques e da ridurre la formazione di muffe. In pratica, diverse ipotetetiche configurazioni del sistema sono state analizzate e confrontate per ottenerne il design ottimale.
La prospettiva futura é di passare alla valutazione del sistema ultimato all'interno della cantina, dove sará necessario individuare il suo posizionamento ottimale e quante unitá risulteranno necessarie. Per quanto riguarda invece la ventilazione della serra, un'aspetto da investigare, oltre alla scelta della tipologia di telo, sar l'ottimizazzione del posizionamento dei teli all'interno della struttura.
In conclusione, l'utilizzo della CFD ha consentito, al di lá degli specifici risultati ottenuti, di giungere a conclusioni in merito a possibili decisioni o strategie per migliorare la ventilazione seguendo il ben preciso intento di migliorare le condizioni di produzione e la qualitá del prodotto agroalimentare.

Keywords: Fluidodinamica Computazionale, Edifici Rurali, Ventilazione, Galleria del vento, Teli Ombreggianti.

Contents

Chapter 1

Introduction and goals

The importance of environmental control in agricultural and agro-industrial buildings is part of precision agriculture / smart food processing. This is because environmental conditions can have effects on quality, safety and wholesomeness of the product, on uniformity / constancy of its characteristics, and therefore on the traceability of food chains (Ceglie et al., 2018; Annese and De Venuto, 2015). Obviously it can also affect environmental sustainability, considering energy and resource consumption, and the economic aspect of the sector totally, in line with the new environmental policies. (Campiotti et al., 2013; Blanco et al., 2017)
At the same time has increased the interest in the development of systems and methodologies for the modeling and simulation of the environmental conditions of production and processing environments of agricultural and food products, in order to support the design of optimized and innovative systems, speeding up the phases of development with respect to processes on a purely empirical basis. Obviously, such simulation systems need appropriate validations and experimental calibrations, but they open the doors to many possibilities to investigate specific aspects and variations of the therm-fluid-dynamic phenomena involved in the control of environmental parameters, allowing to outline the better strategies and actions to apply (Fabrizio et al., 2015).
The theme is extremely important in various types of agricultural and zoo-technical buildings, as well as in storage, processing and processing of both plant and animal products. The study of these issues is particularly interesting and challenging in the case of buildings for protected crops, where the interaction between external and internal environment requires a study of the dynamics of environmental parameters such as temperature, velocity and humidity of the air tightly integrated both in thermal and fluid dynamic field, and where the dynamic control of the environmental conditions and their spatial distribution takes great advantage from precision modeling and simulation techniques able to take into account the characteristics of the greenhouses and the progress of the internal and external environmental

conditions (Tanny, 2013).
Similarly, a sector that for a long time has been significantly supporting the theme of quality related to sustainability - even with important repercussions on the image and marketing level - is the wine production sector. In this context, several researchers have focused on the development of methods for monitoring, analyzing and controlling environmental parameters that can guarantee the correct production and conservation of wine, while at the same time improving the environmental and economic sustainability of the structures. While considerable attention has been paid to optimizing the thermal control of the production and conservation environments and to the relative energy saving, an increasing interest is given to the topic of ventilation and micro-ventilation, due to the importance of maintaining homogeneous conditions in therm-hygrometric terms and, consequently, to the application of optimized systems with a low environmental impact (Tate, 2013; Barbaresi et al., 2015).
To all this, it should be considered also that in many cases solutions and monitoring and control systems developed for large companies may not be accessible or optimized for the needs of small and medium-sized farms and agro-industries, which are a very important part of the Italian agricultural and food production fabric and several other European countries and beyond. According to what has been said, the Computational Fluid Dynamic (CFD) approach certainly fits in with those methodologies that support the design and optimization phases not only of residential and industrial, but also of agricultural buildings (Norton, 2013). In fact, are several years that in this sector CFD has been applied with different goals, for example the animal comfort in livestock or the micro-climatic conditions of plant growth in greenhouses (Rong et al., 2016; Teitel et al., 2008).
Taking into account all these prospective, the idea of this study is to apply the Computational Fluid Dynamic to ventilation systems in agricultural field. In particular, it is focused in crop and wine production sectors. The reasons that lead me to deepen these arguments are several, starting from the importance of ventilation in the environmental control, *i.e.* for the optimal growth of the plants or the wine aging process. The ventilation also is related to energy consumption because could allow the reduction of temperature and humidity, avoiding the use of air conditioning systems. At final, also the versatility and the power that this technique has reached is an interesting aspect. This work is about mixed and natural ventilation systems. The mixed ventilation consists on the application of both mechanical and natural ventilation technique. In particular, natural ventilation efficiency is conditioned by a lot of factors, such as solar radiation, wind magnitude and direction, opening dimensions and obstacles presence, like insect and shading screens. The last one is another aspect developed in this work.
The main aim of this thesis is to study different configurations of ventilation in

order to be able to improve the existent condition in two different environments, a greenhouse and a wine cellar, both with a high level of technology use. One is for the vegetable garden and flower nursery production, the other one is for the for the finishing phase in the wine production chain. It is investigated and identified the magnitude of the effect on the natural ventilation of a greenhouse, caused by the presence of shading screens. The modeling of shading screens leads to carry out a deepening on the shading screens characterization with the goal of defining of an applicable methodology for porosity, permeability and inertial coefficient determination for shading screens, now available on the market, which doesn't have an easy and homogeneous texture. In parallel, it has been investigated the design of a perforated polyethylene tube that is going to be placed, as additional ventilation system, in a natural ventilated wine cellar, with the scope of improving the air flow around the barrels. The results searched are a better homogenization of temperature and humidity but mainly an optimal air velocity, in order to control or limit not only the mold formation but also the wine losses due to evapo-transpiration.
The thesis is structured in five chapters: the first chapter is a general explanation of ventilation in buildings, with few more specific words about the state of the art in crop and wine production; in the second one are introduced and clarified the modeling methods used in CFD, the assumptions, limitations and application examples. In this chapter are presented in detail the model formulations which will be applied in the specific case studies. In the third chapter are reported the case studies performed and analyzed: a greenhouse ventilation study to evaluate the effect of the presence of the screens, an experimental characterization and modeling of shading screens types, in order to consider how the choice of a type screen could modify the air flow patterns and the volume of air entering in the structure. Moreover, has been carried out a design case of a ventilation system for a wine cellar, deciding which could be the better set up of the tube to be placed in the room. The last chapter is dedicated to the conclusions, which summarize also the connections within the works conducted.

Chapter 2

State of the art: Buildings ventilation

The control of environmental parameters is an hot topic in buildings management, in particular in agricultural sector for the optimization of any type of production. Proper planning of agricultural and agro-industrial buildings, as well as an appropriate management strategy of the structures and related environmental control systems, is in fact fundamental to guarantee the maintenance of a controlled environment in terms of air temperature, humidity and velocity. The use of techniques of analysis, modeling and precision design applied to agro-industrial building allows an accurate prior assessment of the effects of multiple design variables and their relationships. Therefore, it allows the identification of the most effective and efficient construction solutions for the control of microclimate within structures, optimized according to the specific needs of crops and food products, and in relation to the environmental and climatic conditions of the place. At the same time, a correct selection of the various design variables can guarantee a good level of flexibility for agricultural structures (Maher et al., 2016). This not only allows, in different cases, to extend the areas and production periods, maximizing the operability, economic and environmental sustainability of the facilities, but also, in general, to increase production quality and quantity, to ensure the maintenance of predefined objectives and quality standards, as well as ensuring the requirements of food safety, also encouraging the traceability of supply chains (Sravani et al., 2018). Moreover, it is an optimized building design and management, with a smart use of passive and active systems, it is very important to reduce the operating costs and the environmental impact related to energy and resource consumption (Hemraj and Sukesha, 2014). In this context, the study of time and space distribution of air velocity with precision techniques and the most effective ventilation strategies proves to be an extremely important field of application itself, given the direct effects of a correct circulation of the air, air on different aspects of production (evaporation of fluids

and mold formation, air exchange and cooling for natural ventilation, control of the concentration of both useful and harmful gases, etc.). More in general, it gives the close relationship with the topic of thermo-hygrometric control of production environments, in the broader domain of thermo-fluid dynamics surveys applied to agricultural structures (Robles, 2017). The growing attention paid to this field of study is also due to the growing diffusion of increasingly sophisticated techniques of computer modeling and simulation of air flows, and in particular of fluid dynamics computation (CFD), which has found increasing and new applications both in field of buildings for plant productions (in this regard, the greenhouses are used as a case study), which in the context of agro-industrial transformation buildings (within which this thesis focuses on the cellars) (Bournet et al., 2007; Barbaresi et al., 2014; De Rosis et al., 2014). These computerized techniques, appropriately validated through validations and calibrations conducted through experimental campaigns, allow to evaluate in a very accurate way the effects of the different technical-design and management choices related to these structures. This work aim to investigate the ventilation in agricultural buildings (natural and hybrid), focusing on the optimization of the air flow distributions inside the structure as already presented in the introduction. In this chapter are introduced the concept of ventilation and the types of ventilation system applicable in structures, with a specific focus on greenhouse and wine cellar cases. Moreover, it is presented a literature overview in order to give an idea on how is significantly important the climatic control in agricultural sector and on the role played by ventilation efficiency, anticipating also what role can have CFD in this type of studies. At the end, are presented the theoretical principles underlying the movements of air, that are basic for understanding the computational dynamic fluid, described in the next chapter.

2.1 Methods of ventilation

The definition of ventilation can be the intentional introduction of new air from the outside into a building. Moreover, are considered different variants of ventilation system that can be used to positively control the environmental parameters within a building (Almuhanna, E. A. , 2016). A ventilation system is formed from all the elements that contribute to the air exchange level and the distribution of fresh air within the building. In most applications in agriculture, the ventilation system consists of an air inlet and distribution system, an air outlet system and some control equipment. The purpose of ventilation is to supply fresh air to the spaces, to meet the heating/cooling and to reach air quality requirements for occupants within an indoor environment. It fulfills this purpose by bringing fresh air into the airspace and dilute the heat, moisture, and gaseous and particulate

contaminants that eventually build up indoors. The effectiveness of this process noticeably depends on the ventilation system design and air distribution within the space. Ventilation effectiveness has been increasingly used in studies of ventilation and air quality control. In fact, the ventilation control systems can be crucial for management of production environment for all kind of agricultural buildings, such as greenhouses, livestock and also wine cellar. However, basically two solutions can be adopted to achieve the desired ventilation rate of any building: natural or mechanical (forced) ventilation, or a combination of the two. Despite the increasing complexity of the ventilation systems in buildings, a hierarchy of ventilation systems can be identified as visible in figure 2.1 below (Etheridge D., 2012).

Contingency is the system where the natural ventilation is used but the building has been realized to predict the later installation of mechanical system (Etheridge D., 2012). Instead, the **zoned** type considers different systems in different part of the building and the **complementary** type contemplates natural and mechanical systems, operating in different times. In this work, the focus is on the natural ventilation of a greenhouse and a mixed system used in a wine cellar.

2.2 Natural and mechanical ventilation

Natural ventilation is the flow generated by temperature differences and by the wind. The governing nature of this flow is the exchange between an interior space and the external ambient. Although, the wind may often appear to be the dominant driving mechanism, but in many circumstances temperature variations play a controlling feature on the ventilation since the directional buoyancy force has a large influence on the flow patterns within the space and on the nature of exchange with the outside (Etheridge D., 2012). The forces ruling the natural ventilation are wind and buoyancy. In fact, air exchange is generated by the wind pressure differences along the facedes and by the temperature differences between indoor and outdoor. The ventilation rate is based on strength and direction of these forces and flow path resistance. These physical processes are complicated and connected, and this makes it difficult to predict the ventilation rate. Hence, the control of natural ventilation is a challenge for obtaining optimal indoor environmental conditions. In particular for greenhouses, ventilation is the main way to remove solar radiation heating, to manage the level of humidity, to supply CO_2 for photosynthesis of plants. In wine cellar, the ventilation has a role of controller of temperature and humidity but also it helps to avoid formation of molds. However, a strong air velocity could increase wine losses due to evapo-transpiration. A well designed air distribution contemplates that fresh air is consistently delivered to all interior regions of a structure. This parameter is more qualitative than air exchange, which is definable by a number. For all buildings, dimensions, shape and layout are really

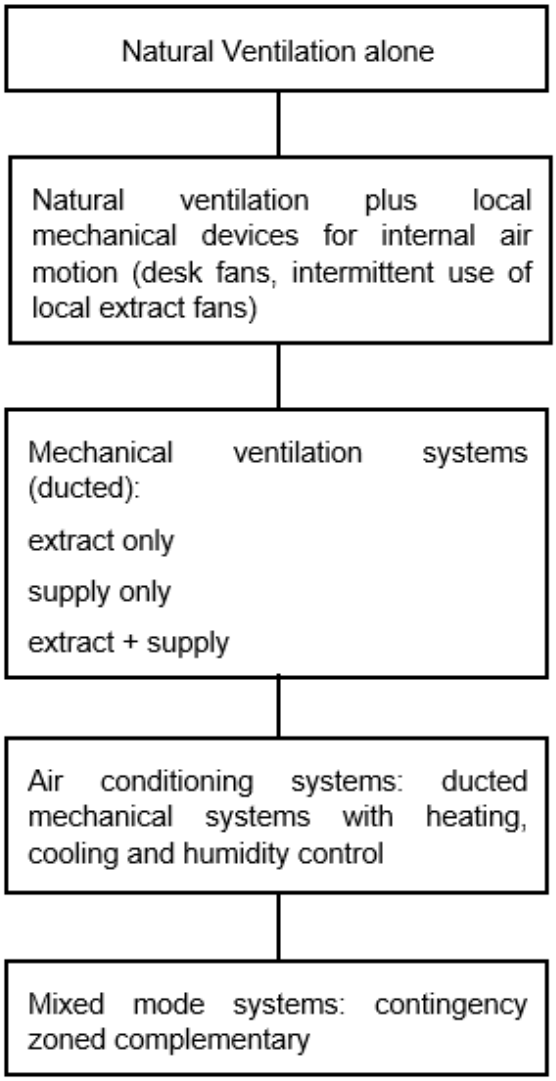

Figure 2.1: Diagram showing the hierarchy of ventilation systems.

important factors of air distribution, such as plant disposition, room volume or barrel dispositions, just about greenhouses and wine cellar. Additionally, interior layout (roof, slope and design, ceiling) affects air flow patterns. Several methods can be suggested in attempt to control ventilation rate in agricultural buildings but most of these have proved inadequate, resulting in poor indoor climatic conditions. Data from literature and field researches have demonstrated that the possible benefits obtainable by highly sophisticated control algorithms, improved ventilation and heating systems, improved building envelope or high-tech equipment would be

only realizable with a more efficient way of ventilation rate control (Berckmans,D. and Vranken, E. and Geers, R. and Goedseels, V.; Vranken et al., 1991).
However, back to the systems, mechanical ventilation takes advantage of the work of machines that move air and can also modify its characteristics. Usually this system consists in one or more fans to create a pressure difference over the building envelope, obtaining an air stream through the structure. At constant voltage, the ventilation rate increases when fan static pressure decreases. The ventilation rate depends not only on the applied voltage but also on the static pressure difference over the ventilation opening, in which the fan is placed. Consequently, to modify the ventilation rate different basic methods can be applied (Randall, J. M. and Boon, C. R.):

1. keeping fan voltage constant and recirculating a proportion of the building air;

2. keeping fan voltage constant and changing the pressure difference over the ventilation opening;

3. modifying the voltage applied to the fan, altering the number of fans in operation.

The mechanical ventilation includes also the use of cooling and heating systems, which are highly energy consuming.

2.2.1 Greenhouse ventilation systems

The greenhouse industry is a growing sector worldwide. First of all, the greenhouse separates the crop from the environment, thus providing some way of a protection from the direct influence of the external conditions. This permits the production of crops that otherwise could not be produced at that specific location. Secondly, the greenhouse enclosure allows the manipulation of the crop environment. In fact, in the greenhouse it is possible for the grower to lead the cultivation in a desirable direction, obtaining higher crop yield, longer production period, better quality, and less use of protective chemicals. However, the disadvantage of intensification production is the high energy demand per unit area for resources, caused by the current greenhouse designs. The energy consumption can be of different natures depending on the location of the production. On one hand, in moderate climate zones heating is necessary for some periods, on the other hand, in (semi) arid zones, the cooling and water supply are major issues. Nevertheless, from a sustainability point of view, after all aspects viewed, the greenhouse is a solar collector and this will ultimately be another factor that contributes to the growth of the greenhouse sector in the future. As matter of fact, greenhouse management and everyday

working can be influenced by operating adjustments on several components such as heating input, window opening, screening, and CO_2 dosage. Hence, it can be expected that the way these controls are conducted affects the final economic result. For sure, the final result depends on an essential and inescapable aspect: the variations of the weather, which is beyond the control of the grower and will always lead to year-by-year variability in income. No action on environment is possible but a good control strategy could conduct to opportunities and contributes for the net profit of the grower. The ventilation optimization and investigation of related aspects, having an important role in the indoor climate, are the focus here. Considering a good ventilation essential for maintaining an optimal growth plants environment, it is clear that it plays a key role for improving the overall efficiency of a greenhouse. In fact, ventilation has been confirmed as crucial for both good temperature and humidity management. Cooling process could be critical in the Italian and Mediterranean countries and usually it is achieved using passive roof ventilation, through which is pulled in cooler air by movement of hot air up and out of the roof vents. Ventilation is also necessary for air circulation and carbon dioxide supply. As a matter of fact, poor air circulation decreases plant activity and can cause problems with humidity and disease management. If carbon dioxide levels are not maintained, plant growth is badly affected. Ventilation depends on number of air exchanges. Large volumes of air need to be moved during hot conditions. Greenhouse's air exchange number achieves at least 30 to 45 units per hour, but ideally should be 60 air changes per hour one air exchange every minute to assure a good greenhouse environment in hot sunny conditions. This result can be assured passively or actively, by vents or by mechanical solutions.

Greenhouse types

The horticultural sector considers the presence of a multiple types of structures for crops production. Regarding the outline profiles, the typologies of structure can be summarized in two main categories:

- **tunnel type** (figure 2.2), a semicircular or elliptical vault, mainly used for the production of vegetables, flowers, mushrooms and protected grapes. Usually, the upper and perimeter covering are made by polyethylene films, stretched on the structure by means of a winding roller system. However, depending on the necessities, the tunnel could be realized with other types of plastic materials. On one hand, this type of greenhouse can be mechanically ventilated by the presence of fans, placed along the structure or at final wall. On the other hand, the structure can be ventilated by vents on the gutter, manually or motorized opened, and eventually on the lateral part.

- **double-pitched type** (figure 2.3), that can have a symmetrical or asymmetrical pitches, whose intended use is the production of vegetables, flowers, succulents and any other type of crops. For the ventilation, it is possible to install manual or motorized openings near the ridge and on the sides. This type of structure is suitable often for the installation on the roof of photovoltaic modules, thanks to the appropriate inclination of the pitches that allows the right incidence of solar rays on the photovoltaic panels.

Figure 2.2: Image example of a tunnel greenhouse, covered by plastic.

Greenhouses can be categorized also by the type of air conditioning system, dependent on the crop grown. In fact, they can be defined as cold greenhouse, if there are not air conditioned, or as temperate, when the temperature is forcibly maintained between $10°C$ and $14°C$, during the night. Moreover, they can be classified as warm when they are warmed up to $16 - 20\ °C$ during night.
Anyway, the greenhouse structures are made by steel in any case, because they have to support not only its own weight together with the secondary structure and roof, but also the accidental loads, caused by wind and snow. The covering materials condition the type of structure, the shape and the dimensions and are substantially possible to be used glass, plastic and plastic films. Rigid plastic materials are also used, such as polycarbonate, reinforced polyester resins and vinyl polychloride (PVC). In particular, polycarbonate has getting a considerable diffusion in greenhouse and tunnel roofs, while the polyester resin essentially concerns tunnel

Figure 2.3: Picture of a double-pitched greenhouse with several spans, of an experimental structure of Unibo, in Imola.

structures. Plastic films are applied in tunnels especially in horticulture and for ornamental plants with lower thermal requirements. The most common materials are polyethylene and PVC, produced in various thicknesses, which the duration generally does not go beyond twelve months. Regarding the ventilation systems, the increasing concern about the high cost of energy required to operate on greenhouses and today this is one of the main cause for the reborn emphasis about natural ventilation systems for greenhouses. Usually in greenhouses with natural ventilation system, sidewall vents and ridge vents along the full length of the building can be opened with different angles and frequencies to allow air to move through the house. As said before, natural ventilation is based on the pressure difference between the indoor of the greenhouse and the external environment (Perone et al., 2017). Moreover, natural ventilation efficiency is function of the design characteristic of the greenhouse (e.g. size, shape and position of the openings). When only natural ventilation is used to control the climate condition the greenhouse is considered an open-system (Fuchs et al., 2006). In order to obtain a satisfying ventilation, both sidewall and ridge vents should be present in the structure. In fact, the presence of only side vents forced the ventilation during periods of wind movement outside. Instead, ridge vents and side vents permit the greenhouse to be vented by both wind pressure and thermal gradients. Thermal gradients generally are generated by solar energy heating the materials inside, which heat the air. Due to the heating,

density of air decreases and it rises and goes out through the ridge vents, with fresh air incoming at the same time from outside through the sidewall vents. If sidewall and ridge vents are properly sized, quite satisfactory ventilation rates can be achieved with some degree of temperature control. These aspects make clear that a natural ventilation system will not be as dependable or satisfactory as a mechanical ventilation system in terms of providing continuous, uniform greenhouse ventilation. However, some newly-designed structures naturally ventilated are capable of achieving a good standards of environmental modification for increased plant production. Anyway, for plant species that require air temperatures lower than outside air, an evaporative cooling system is needed, in which mechanical ventilation is an integral part. Mechanical ventilation permit a more effective and precise capacity on control and maintenance of internal environment. The presence of fans shows a lesser dependence from the external condition and internal buoyancy forces than natural ventilation. Thus mechanical ventilation reduces internal air stratification and vertical temperature gradients in summer. Furthermore, this system allows to treat the air flow rate before its inlet in the greenhouse (air flow mixing, heat recovery, pre-heating, etc.). If only mechanical ventilation is used the greenhouse is a closed-system. In fact, for summer ventilation are considered systems taking advantage of water evaporation:

- cooling system, which consists in fans placed on a wall and, on the other side, alveolar panels humidified.
- fog system, which consists in diffusion of sprayed water at high pressure (35-40 bar).

Any ventilation system is usually integrated with shading systems, internal and external, which act positively on the solar radiation in order to reduce the internal overheating. However, it is not possible to make definitive statements on which is the best system. Here, the focus will be on a natural ventilated glass greenhouse. These greenhouse types are usually the most common commercial cases. However, the importance of the development of a sustainable horticulture and the improvement of the energy management and the environmental impact of this productive sector have directed towards innovative ideas of greenhouses, such as **closed greenhouse** (Vadiee and Martin, 2012). This new concept of greenhouse is not widely implemented and there is no specific definition of it available in literature. It is commonly define as: "A greenhouse, which is completely closed, no windows to open to release excess humidity or to cool the house when it is too warm" (Amstrong, 2003). The closed greenhouse compared to the conventional greenhouse technology could be independent from fossil fuels, since it is design for maximizing the use of solar energy through seasonal thermal energy storage (TES) (Vadiee and Martin, 2012). In this way, the greenhouse is only slightly affected from

the weather situation and it could be a technology applicable all over the world. An important limit of this concept consists in the geology of the ground, since it affects the under ground seasonal storage which is significantly a cost-effective aspect. Other limitations could be the type of heating and ventilation systems implemented in the structure and the rate of solar radiation. In any case, this greenhouse case is not considered as possible study case for this research since it is not a commercial greenhouse type yet and also does not provide the possibility of having natural ventilation.

2.2.2 Wine cellar ventilation systems

In wine production, it is important to maintain a constant low temperature inside the room where wine is stored, in order to obtain an high-quality end product as well as to reduce wine losses (Cañas and Mazarrón, 2009). Unanimity about the optimum interval for the wine comfort does not exist. However, the majority of authors agree on the harmful effects of temperature above $18 - 20$ °C on the wines color, flavor and fragrance (Yravedra Soriano, 2003). Another issue, without unanimous opinions about the specific values, is that the combination of low humidity, high temperatures and ventilation increases the loss due to evaporation, which can be as high as 9% of the stored wine per year (Ruiz De Adana et al., 2005; Togores, 2003). However, two aspects collect the unanimity of opinions which are:

- High temperatures above 18 20 °C make the wine age more rapidly, with the consequent loss of quality;
- Very low temperatures, below 4 5 °C, sustained over long periods average that the wine will age slowly:

In this way, it is possible to evaluate a range of acceptable conditions between $6-18$ °C. Considering these aspects, the construction designs can help to reduce energy consumption, decrease the costs of production without affecting quality of products (Mazarrón et al., 2013). Traditionally wine ageing and preservation have been done in underground construction because the thermal inertia of the adjacent soil helps to soften the changes in exterior temperature. However, since the last century, buildings aboveground have been the new choice for production, which require a significant energy consumption to maintain suitable conditions for the ageing. In fact, air conditioning system have to be implemented in these structures. Regarding this, Mazarrón et al. (2013) presented an example where a typical above ground winery in Spain can spend over 10.000€ per year for energy costs. In this way, it was preferred to delegate temperature and humidity control to air-conditioning systems, which provide predetermined temperature and humidity with a high degree of control and precision against an energy consumption which is in close

dependence with the surrounding environmental conditions (including the site, orientation of the building, weather conditions, architectural and plant solutions adopted, etc.) (Benni et al., 2013; Tinti et al., 2015). In Tassinari et al. (2011) it was proved, thanks to direct surveys and interviews on a representative wine production area, that the energy requirement related to the product conservation accounts for approximately the 50 % of the total demand for the production of wine. In case of end products such as the classic method sparkling wine or champagne, where the entire production is aged in the bottle for periods up to five years, the consumption due to air conditioning have a greater impact. Surveys performed on a significant Italian study case underlined that energy consumption during 10 months of the year, excluding harvest period, is on average 57% of the total, and this is due almost entirely to air conditioning of underground rooms for aging in bottle. The 43% of consumption is recorded during September and October and it is mainly attributable not only to wine-making operations, but also to the air conditioning of the premises. Therefore, the energy demand for conditioning of the room for wine storage and second fermentation in bottle, is assessed between 65 and 70% of the total (Barbaresi, 2014). It is clear that the above-ground constructive solution is highly energy consuming. Another constructive valid option could be the use of basements in agricultural-buildings, as readable in (San-Antonio-Gómez et al., 2011). This solution could be considered as compromise between underground structure, with high constructive cost but no environmental control costs, and aboveground structure, with high environmental conditioning costs. In this, the indoor temperature is fundamentally conditioned by the ground and the outside air temperatures, which enter the cellars as a result of the ventilation (Mazarrón and Cañas, 2009; Cañas and Mazarrón, 2009; Martin and Canas, 2006; De Rosis et al., 2014).

Figure 2.4: Picture of semi-basement and basement wine cellars, from (Mazarrón et al., 2013)

The basements are constructed under the winery building (fermentation facilities, etc.), so they are located below ground level and they have load-bearing walls in contact with the ground. These kind of structures usually are made of reinforced

concrete with cylindrical or rectangular pillars, as showed in figure 2.4. The semi-underground constructions have similar characteristics, but they have part of its walls in contact with the exterior conditions (Mazarrón et al., 2013). The natural ventilation is more frequent than mechanical ventilation systems, which consists generally in fans forcing incoming air flows or air conditioning systems. The natural ventilation of this kind of structure depends on the environment changes with seasons. Considering spring and summer, the temperature inside the cellar is below the temperature outside and, for this reason, the heavier cold air makes it difficult for outside air to penetrate. This process significantly reduces ventilation and the moisture level is significantly increased, based on the nature of the phenomenon. Consequently, the temperature of the cellar is influenced predominantly by the surrounding soil temperature. In autumn and winter however, the temperature inside the cave is higher than outside, and the cold air outside can penetrate through the ventilation points. The increased ventilation causes a temperature drop and a reduction in humidity, though the surrounding soil temperature remains the predominant influence of internal temperature. A case of basement cellar is taken into consideration to evaluate a the improvement of the conditions around the barriques

2.2.3 Advantages and disadvantages of ventilation systems

The differences between the two systems can be significant and consistent. The underlying difference is that the natural ventilation system behavior is unpredictable due to the dependence on weather conditions. In fact, the flow rate through a vent depends on the following factors: wind speed, wind direction, temperature differences between indoor and outdoor and opening areas. Each of these parameters is time-dependent and leads to the variation of flow rate magnitude and also to unwanted changes of direction. Instead, the mechanical system can provide a constant flow rate in direction and magnitude. However, heat transfer at solid surfaces (i.e. lighting devices, surfaces of electronic devices, walls and windows), which is the major source of buoyancy, is a variable, which interests both kind of systems. Firstly, one of the positive aspect of natural ventilation is that contributes to a sustainable building environment. Moreover, natural ventilation does not need electrical energy for fans, which often consists in the 25% of the energy consumption in a mechanically ventilated structure. However, this could be compensate by considering to use heat recovery in a balanced mechanical system, but with a very tight envelope. A disadvantage of natural ventilation is that has several limitation such as the cooling capability in hot climates, particularly in the humid ones (Etheridge D., 2012) . As possible solution in these situations, could be added some sustainable (low-energy) cooling system to the natural ventilation system. Moreover, if there are errors in the project of natural ventilation systems, they

can difficultly be fixed. Overall mechanical ventilation system has an important energy consume, compared to the natural ventilation system, which consumes energy only for automatized control of openings. The main difference between the two is certainly the level of control reachable with mechanical systems, which is not obtainable with natural ventilation systems, despite a good design and an optimized control management of these systems. Anyway, this could not be a problem for the occupant of a building or for some kind of production in agricultural sector. Definitive statements about advantages or disadvantages of natural ventilation compared to mechanical systems are not possible, partially because they depend on the specific use of a building and also on the climate characteristic of the building location.

2.3 Literature overview

2.3.1 Greenhouse sector

In this section, are shortly reported several aspects of research studies in greenhouses sector, with a particular focus on ventilation and CFD application studies. Greenhouse plant production is one of the most intensive part of the agricultural production (Djevic and Dimitrijevic, 2009). In fact, it can be considered intensive in terms of yield (production) and whole year production, but also in terms of energy consumption, investments and costs (Djevic and Dimitrijevic, 2009; Canakci et al., 2005). In order to reduce costs and save energy, several construction types and different covering materials are available for the farmers, depending on the needs and the cultivated crop (Nelson, 2003). For example, Djevic and Dimitrijevic (2009) compared the energy consumption of different greenhouse constructions and demonstrated that the specific energy demand presented different values for the different cases studied. Moreover, the results showed that an higher greenhouse specific volume can bring to a lower energy input per kg of product. Considering the operative condition of crop cultivation, the management of micro-climatic variables in a greenhouse is one of the most important tasks to maximize quantity and quality of crops production. The main interest is to design facilities with the objective of suitable climatic conditions, with a reduced energy consumption and optimized control systems (Campiotti et al., 2016). Generally, the improvements on climatic conditions are focused in developing new or optimized control systems for climate variables. For example, Maher et al. (2016) validated a physical model of a greenhouse in order to propose a fuzzy-based controller to manage the indoor climate of a greenhouse using some actuators for ventilation, heating, humidifying, and dehumidifying purposes. Moreover, Ramírez López et al. (2018) focused on improving a control system for climate variables and proposed a sorting network

technique with predefined, compare and interchange operations and designed to order data very efficiently.
In fact, a key role in modifying climate inside greenhouses is played by ventilation, which can be used to control all the important parameters involved, as temperature, humidity, oxygen concentration (Bartzanas et al., 2004). A non-uniform distribution of these variables inside the greenhouse can lower the growth of the plants and can give issues with pests and diseases (Piscia et al., 2012). The ventilation can be obtained by means of forced airflow inlet systems or by proper vents in the building walls, to achieve natural aeration. From a constructive point of view, the efficiency of natural ventilation depends on the disposition of vents and on their opening timing during the day. Such action, however, should be designed in an optimal way: for example, Bartzanas et al. (2004) underlined that the optimal timing could be effective in reducing the indoor temperatures and the type of opening (roll up or side opening) could directly affect the airflow. Boulard et al. (2002) studied airflow distribution obtained by side openings, roof vents, or both, in Mediterranean climate. In this regard, the natural airflow is a key factor which directly affects the transport of heat and mass between the inside and the outside environment (Rico-García, E., 2011; Teitel et al., 2015). In fact, the goals of a ventilation system are to eliminate the excess of heat, besides to assure the exchange of CO_2 and O_2, necessary for crop efficiency and to establish acceptable levels of humidity and temperature (Fidaros et al., 2010; Teitel and Wenger, 2014). In most cases, aeration management is diversified upon the seasonal basis: in winter, it permits to eliminate the excess of humidity and to obtain appropriate climatic conditions for the plant growth, while in summer it is needed also to cool the air inside (Bournet and Boulard, 2010). Sase (2006) proved that in a mild climate appropriate design and control of ventilation are required to ensure effective cooling and uniformity of environment. It could be possible to obtain an optimal greenhouse by estimating the area, volume and area of the openings, as well as choosing appropriate materials (Impron et al., 2007). In fact, there are several studies that underline the importance of the geometry. Rico-Garcia et al. (2006) compared two different geometries and evaluated which was better between the ventilation rate of a greenhouse with large vertical roof and windows and a multi-span greenhouse. Moreover, Baeza and Montero (2008) found out that various design changes, such as size and shape of vents, can improve air movement in the area of crops. (Bakker and Montero, 2008) investigated energy balance, determining that an appropriate environmental control can reduce energy consumption and improve efficiency of agricultural production. Energy consumption has been also investigated by Fabrizio (2012), focusing on the energy performance of some of the recent envelope and systems technologies that best can contribute to a great reduction of the energy demand for the climatic control of a greenhouse for

intensive crop production. Instead, (Bournet and Boulard, 2010) gave an extensive review of experimental and numerical studies on the ventilation processes inside the greenhouses. They showed the differences between natural ventilation induced by buoyancy forces and wind-driven ventilation inside the greenhouse and the influence of the geometry of the greenhouse on the ventilation process. (Teitel and Wenger, 2014) studied the effect of cross-openings in mono-span greenhouses and they examined the effect of wind velocity on the air exchange and ventilation efficiency inside the greenhouse. (Mistriotis et al., 1997) compared no-wind and low wind speed conditions on natural ventilation processes inside greenhouses by means of CFD, focusing on the importance of side-wall vents. (Molina-Aiz et al., 2004) showed the differences between Finite Element Methods (FEM) and Finite Volume Methods (FVM) in the airflow in naturally ventilated greenhouses. They found that both methods give results in a good agreement with experiments, but FEM require much more computing time per cell and more memory storage than FVM. Only recently, (He et al., 2014) and (Montero et al., 2013) investigated the influence of horizontal shading screens on the temperature and airflow patterns, using 2D models. The numerical study of the effects of shading screens within a 3D model of a greenhouse involves the challenge of studying a complex geometry and to determine the fluid-dynamics properties of the screen, such as porosity and pressure drop across the screen. In fact, in a natural ventilation configuration, the global air-dynamics within the greenhouse may change drastically if screens are set in proximity of vents, depending on their horizontal or vertical arrangement inside the structure (Kittas et al., 2002; Teitel, 2001). Therefore, the scientific literature points out the importance of further improving management and design criteria to optimize natural ventilation in greenhouses also through in-depth analyses of the effects of shading screens. In fact, they are widespread in greenhouses and have important functions for the control of indoor temperature, but at the same time they remarkably affect natural ventilation air flows. These was just a way to give an idea of the multiple and various application of CFD in this sector.

2.3.2 Wine production sector

As presented for the greenhouse sector, in this section is reported a short state of the art about research studies in wine cellar.
First of all, as already underlined before, the importance of internal environmental conditions in a wine cellar is well known and investigated. The process of wine preparation consists in several steps, where temperature and humidity play a fundamental role, since the quality of the final products is strongly affected by constant and suitable environmental conditions (Boulton et al., 1999). Since the past centuries, the research has been devoted to the definition of ideal room conditions for wine-aging process performed in wooden barrels. In literature, on this topic, it is

possible to assess that the wine should be kept at a temperature ranging from $9°C$ to $20°C$ (Troost, 1953) and Vogt (1971) defined that an optimal thermal excursions smaller than $6°C$ and Togores (2003) considered that the relative humidity should be higher than 70 %, in order to ensure a quality aging and to prevent excessive wine loss due to evaporation. The wine losses has been considered as a function of air temperature and humidity. Negrè and Françot (1965) showed how high temperatures, as for example $18°C$, and low relative humidities, 45 %, could affect wine conservation, with losses of 7:4 % in volume per year. Ruiz De Adana et al. (2005) developed a mathematical model that correlates wine losses to the ambient conditions, thus quantifying how the air velocity, temperature and humidity can affect wine evaporation. This model considers the air velocity over the barrels, which could modify the wood surface emission coefficient (Avramidis and Siau, 1987) and then the evaporation through the barrel stave. Moreover, it is suggested that low air velocity values, limited under 1 m/s, could prevent excessive wine losses. Furthermore, Simeray et al. (2001) explained that relative humidity could favor mold and other fungi formation, which may potentially contaminate products or also affect wine quality and organoleptic properties (Picco and Rodolfi, 204). Regarding this, (Ocon et al., 2011) showed that the ventilation could be identified as a fundamental factor to reduce the mold presence in the air, considering to reduce the possibility of mold proliferation on both walls and wooden surface of the barrels. Then, besides temperature and humidity, the scientific literature highlights the relevant role of the air velocity in the wine-aging process. However, it is not clear stated which are the optimal values of air velocities close to the barriques but usually the natural ventilation leads to air velocity measured around $0.3 - 0.4$ m/s (Geyrhofer et al., 2011). Furthermore, generally it is recommended to maintain an air velocity under 1 m/s. Nevertheless, only few researches addressed issues concerning the air velocity (Ruiz De Adana et al., 2005).
In spite of the significant role of ventilation in the environmental condition in wine cellar, the application of CFD in this sector is really rare. Recently, De Rosis et al. (2014) conducted a numerical study of air flows in a wine aging-room, using a Lattice-Boltzamann method. The study underlines how barrels are differently involved in air flows and consequently the identification of the most emblematic points for air measurements. CFD could be applied more with the prospects of useful and interesting results in this sector, considering all the aspects that have been presented.

2.4 Fluid mechanics assumptions

The fluid motion is governed by three fundamental laws: principles of conservation of mass, energy and momentum. In some cases, are necessary other equations for taking in account other phenomena, such as entropy transport or electromagnetic field. The concept of *continuous* media is the starting point of view , composed by elementary volumes that are infinitesimal from macroscopic point of view but big enough compared to molecule distances, in order to consider them as continua. These volumes are called *fluid elements* in a fluid flow and they can move, rotate and deform under the action of forces. All the equations must be satisfied by any elements. The mathematical expressions of these can be done in two ways: Largangian approach and Eulerian approach. In the first one, the equations are formulated as properties of an element moving in space, which is not common in CFD. The second approach, frequent in CFD, considers the conservation principles applied to a volume, reformulated as distributed properties considered as vector or scalar depending on space, x, and time, t (Ziganov, O., 2010) . Considering a fluid volume that moves in the fluid, is possible to introduce the concept of *material derivative*. The volume moves with a velocity $\mathbf{V}(x, y, z, t)$ and a density $\rho(x, y, z, t)$, as visible in figure 2.5.

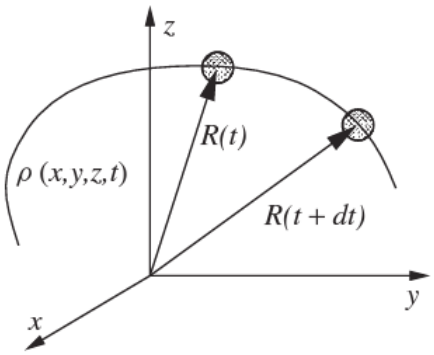

Figure 2.5: Fluid element moving in the fluid with variable density.

In the figure 2.5, it is also presented the position of the element in two different time step, with vector position $\mathbf{R}(x(t), y(t), z(t))$. By the differentiation of ρ over time, it is possible to obtain the expression of rate of change of density within the element, as shown in equation (2.1):

$$\frac{\partial \rho}{\partial t} + \frac{\partial \rho}{\partial x}\frac{dx(t)}{dt} + \frac{\partial \rho}{\partial y}\frac{dy(t)}{dt} + \frac{\partial \rho}{\partial z}\frac{dz(t)}{dt} = \frac{\partial \rho}{\partial t} + u\frac{\partial \rho}{\partial x} + v\frac{\partial \rho}{\partial y} + w\frac{\partial \rho}{\partial z}, \tag{2.1}$$

where the time derivatives of the components of vector position has been identified as correspondent components of velocity, $\mathbf{V} = \mathrm{u}i$, $\mathrm{v}j$, $\mathrm{w}k$. The right part of equation takes the name of *material derivative* and is expressed with the common expression:

$$\frac{D\rho}{Dt} \equiv \frac{\partial \rho}{\partial t} + u\frac{\partial \rho}{\partial x} + v\frac{\partial \rho}{\partial y} + w\frac{\partial \rho}{\partial z} = \frac{\partial \rho}{\partial t} + V \cdot \nabla \rho. \tag{2.2}$$

In the same way, can be expressed the rate of change of temperature or also of a velocity component, as presented below:

$$\frac{D\rho}{Dt} \equiv \frac{\partial T}{\partial t} + V \cdot \nabla T. \tag{2.3}$$

and

$$\frac{D\rho}{Dt} \equiv \frac{\partial u}{\partial t} + V \cdot \nabla u. \tag{2.4}$$

In fact, the rate of change of any distributed property is constituted by two parts: one considers the time variation of the property and the other one takes in count the element in a spatially variable field of the property. However, the mass is constant but the volume continuously changes as it moves in the flow. That can be considered caused by the velocity field that is space-dependent. In fact, based on a volume fluid the velocity at opposite side is different. Figure 2.6 shows a 2D element of size dx and high L, with a volume $\delta\ V = Ldx$. The velocity field is

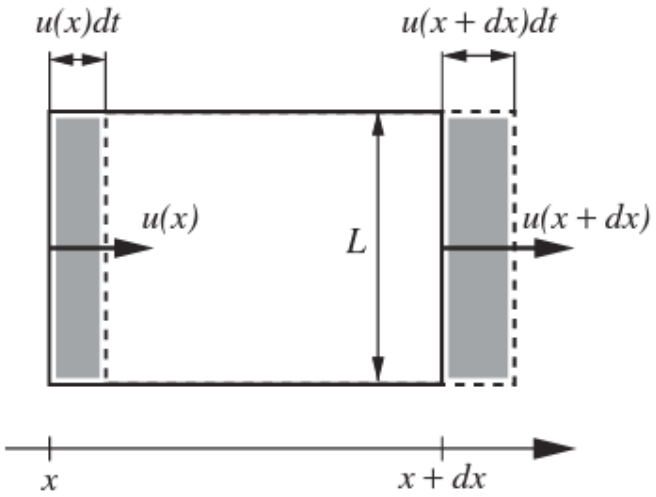

Figure 2.6: Illustration of change of volume due to the spatial variability of velocity.

simplified as monodimensional. Considering a time interval dt, the volume increases

of the quantity *Ldtu(x+dx)* and, at the same time, decreases of a quantity *Ldtu(x)*. From this, the time rate of volume change is

$$\frac{1}{\delta V}\frac{d(\delta V)}{dt} = \frac{1}{Ldx}\lim_{dt\to 0}\frac{Lu(x+dx)dt - Lu(x)dt}{dt} = \frac{Lu(x+dx) - Lu(x)}{Ldx} = \frac{u(x+dx) - u(x)}{dx}, \tag{2.5}$$

which for an infinitely small volume assumes this expression :

$$\frac{1}{\delta V}\frac{d(\delta V)}{dt} = \frac{du}{dx}. \tag{2.6}$$

If this case is extended to a three dimensional case with velocity field $\mathbf{V}$ = (U, V, W), this formula is generalized to

$$\frac{1}{\delta V}\frac{d(\delta V)}{dt} = \frac{\partial u}{\partial x} + \frac{\partial v}{\partial y} + \frac{\partial w}{\partial z} = \nabla \cdot V. \tag{2.7}$$

Starting from this concepts, it is possible to formulate the fundamental equations of fluid dynamics.

2.4.1 Mass conservation equation

The equation of mass conservation can be expressed as

$$\frac{d(\rho\delta V)}{dt} = \delta V\frac{D\rho}{Dt} + \rho\frac{d(\delta V)}{dt} = 0 \tag{2.8}$$

Moreover, dividing by $\delta\ V$ and considering equation (2.9), the relation can be as in equation (2.10) (continuity equation):

$$\frac{1}{\delta V}\frac{d(\delta V)}{dt} = \nabla \cdot V \tag{2.9}$$

$$\frac{D\rho}{Dt} + \rho\nabla \cdot V = 0 \tag{2.10}$$

This is unsteady, three-dimensional mass conservation or continuity equation at a point in a compressible fluid.
In several cases, the compressibility of a fluid can be neglected and so the density can be considered as a constant, obtaining this expression from equation (2.10):

$$\rho\nabla \cdot V = 0 \tag{2.11}$$

2.4.2 Conservation of momentum

The conservation of momentum equation is based on Newton's second law, which states that the rate of change of momentum of a body is equal to the net forces acting on it:

$$\frac{d(mV)}{dt} = F \tag{2.12}$$

Considering a fluid volume moving in the flow, the first part of the expression of eq.(2.12) can be replaced by the material derivative:

$$\rho\frac{D}{Dt}(V) = \rho[\frac{\partial}{\partial t}(V) + (V \cdot \nabla)V]. \tag{2.13}$$

Two different type of forces can affect a fluid element: body forces and surface forces. The first ones act on the mass of the fluid and come from a remote source. Examples are the gravity, electric and magnetic forces. This kind of forces are proportional to the fluid element mass. The second ones consists in pressure and friction forces acting between adjacent fluid elements and between fluid elements and a close wall. The vector field of this kind of forces can be represented as divergence of a symmetric 3×3 tensor called the *stress tensor* τ. The diagonal elements, τ, cause the contraction or extension of the fluid element, while the off-diagonal elements produce the deformation by the shear, as showed in figure 2.7 (Linden, 1999).

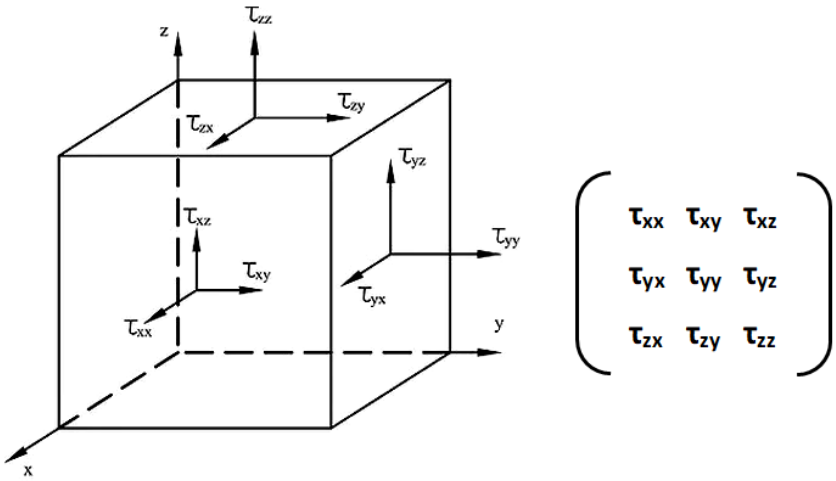

Figure 2.7: Representation of normal and shear stresses acting on the fluid element.

According to this, the momentum conservation equations can be written, based

on these two forces.

$$\rho\frac{D}{Dt}(V) = \rho\mathbf{f} + \nabla\cdot\tau. \tag{2.14}$$

The stress tensor is divided in the isotropic pressure part that is always present and the viscous or friction component, which exist only with a flowing fluid and it is zero for a still fluid:

$$\tau_{ij} = -p\delta_{ij} + \sigma_{ij}, \tag{2.15}$$

when δ_{ij} is 1 for i = j and is 0 for i $\neq$ j, is the case of Kroneker delta-tensor. In order to be able to fully describe the flow, should be introduced a model for the viscous stress, σ_{ij}. Newton was the first to suppose that it could have been proportional to the velocity gradient. Later, this was developed by Stokes in the linear model for stress tensor:

$$\sigma_{ij} = \lambda\delta_{ij}(\nabla\cdot V) + \mu(\frac{\partial u_i}{\partial x_j} + \frac{\partial u_j}{\partial x_i}), \tag{2.16}$$

where μ and λ are viscosity coefficients and u_i for the velocity components *u,v,w*. For incompressible fluid,

$$\nabla\cdot V = 0 \tag{2.17}$$

and, for compressible fluid, it is considered

$$\lambda = -\frac{2}{3}\mu, \tag{2.18}$$

which is an approximation generally valid, except for shock waves in hypersonic flows or for adsorption and attenuation of acoustic flows (Schlichting and Gersten, 2017). The model presented in equation(2.16) had been validated in experiments and also in the usual application of resulting equations. Moreover, this model is satisfied by that fluids categorized as Newtonian. Thanks to the combination of (2.16) and (2.14), can be obtained the final form of the momentum equation of Navier-Stokes, reported here only for a component:

$$\rho\frac{Du}{Dt} = \rho f_x - \frac{\partial p}{\partial x} + \frac{\partial}{\partial x}[\mu(-\frac{2}{3}\nabla\cdot V + 2\frac{\partial u}{\partial x})] + \frac{\partial}{\partial y}[\mu(\frac{\partial v}{\partial x} + \frac{\partial u}{\partial y})] + \frac{\partial}{\partial z}[\mu(\frac{\partial w}{\partial x} + \frac{\partial u}{\partial z})]. \tag{2.19}$$

The equation can be written in a shorter form by introducing the rate of strain tensor and using the Einstein summation convention, according to which repeated

indexes in a term imply summation over the possible values, as shown in equation (2.20):

$$\rho\frac{Du_i}{Dt} = \rho f_i - \frac{\partial p}{\partial x_i} + \frac{\partial}{\partial x_j}[-\frac{2}{3}\mu(\nabla \cdot V)\delta_{ij} + 2\mu S_{ij}]. \tag{2.20}$$

2.4.3 Energy conservation

The formulation of the conservation of energy, for a fluid element, can be done in a similar way such as for mass and momentum conservation, as presented in equation (2.20),

$$\rho\frac{De}{Dt} = -\nabla \cdot q - p(\nabla \cdot V) + \dot{Q}, \tag{2.21}$$

where *e(x,t)* is the internal energy per unit mass, *q(x,t)* is the vector field of heat flux by thermal conduction and $\dot{Q}$ is the rate of internal heat generation, for example, due to viscous friction or radiation. The conduction heat flux can be expressed by the Fourier conduction law

$$q = -k\nabla T, \tag{2.22}$$

where *T(x,t)* is the temperature field and k is the thermal conductivity coefficient. Another possible way to write it is the equation for total energy E (mechanical plus internal)

$$\rho\frac{DE}{Dt} = -\nabla \cdot q - \nabla \cdot (pV) + \dot{Q} + \rho f \cdot V, \tag{2.23}$$

The energy relation assumes a more complex form if other effects as chemical reactions, radiation heat transfer or Joule dissipation, are involved. They could be insert explicitly in the right-part. However, the form could also be simplified, when the internal heat generation can be neglected and the fluid can be assumed incompressible (Boussinesq approximation). In this case, the internal energy is $e = CT$, where $C = C_v = C_p$ is the specific heat, and the relation can be written as

$$\rho C\frac{DT}{Dt} = -\nabla \cdot q, \tag{2.24}$$

which lead to the formulation of the equation of convection heat transfer

$$\rho C\frac{DT}{Dt} = \rho C(\frac{\partial T}{\partial t} + V \cdot \nabla T) = \nabla \cdot (k\nabla T), \tag{2.25}$$

which takes the form of the classical heat conduction equation, in case of quiescent fluid and constant conduction coefficient, k, as visible below:

$$\rho C \frac{\partial T}{\partial t} = k \nabla^2 T. \tag{2.26}$$

In this way, the three conservation equations have been shown. In order to close the system of governing equation, it has to be added another equation, the state equation, which link the thermodynamic variables p, ρ and T. In fact, it is needed an expression of internal energy in terms of thermodynamic variables. The most used relations are the ideal gas model

$$\frac{p}{\rho} = RT, \;\; e = e(T), \tag{2.27}$$

and the model of incompressible fluid

$$\rho = constant, e = CT, \tag{2.28}$$

but other models could be used and are often necessary. Moreover, when viscosity μ and conductivity k are not considered as constants, are needed formulas describing these parameters as dependent on temperatures and other variables.
As visible in these paragraphs, there are several commonalities between equations. Considering the possibility to introduce a general variable, ϕ, the conservative form of all fluid flow equations can be written in this useful way:

$$\frac{\partial(\rho\phi)}{\partial t} + \nabla \cdot (\rho\phi u) = \nabla \cdot (\Gamma \nabla \phi) + S_\phi. \tag{2.29}$$

The terms of the equations represent:

Rate of increase of Φ of fluid element	+	Net of rate of flow of Φ out of fluid element	=	Rate of increase of Φ due to diffusion	+	Rate of increase of Φ due to sources

Figure 2.8: Diagram showing the hierarchy of ventilation systems.

The equation (2.29) is the commonly called transport equation, for property ϕ. In the left part are present the rate of change and the convective term. Instead, at the right part there are the diffusive term (Γ is the diffusive coefficient) and the source term. In the source term, the not shared terms between equations should be considered part of the source term to obtain the common features.

2.4.4 Type of fluid flow in Ventilation

The range of flows that can characterize ventilation are of various types: laminar, transitional, turbulent, steady or unsteady and several combinations of these. To be able to appreciate the differences, must be considered the Reynolds number.

Reynolds Number

A classification of the fluid flow is possible thanks to the Reynolds number, which has different range of values associated to different flow. The general form of this number is

$$Re = \frac{\rho\ d\ u}{\mu}, \tag{2.30}$$

where d and u are respectively a velocity and length of the flow, under consideration. This number can be interpreted as an indication of the ratio of dynamic to viscous forces or the ratio between diffusion by turbulence and molecular diffusion. The value of Re depends on the choice of u and d, so this can be an indicator of the importance of the viscosity. In case of low values of Re, the viscous effects can be considered important, which is certainly valid for flows through some kind of envelope openings. Moreover, there are some cases of internal air motion, where the flow can not be defined entirely or only in part fully turbulent. This could be important for modeling flows in room with CFD, because the relations for turbulence chosen could not be totally appropriate. However, in this section will be presented a brief presentation of each flow type.

Laminar flow

The laminar flow is characterized by a velocity field without random component, except for the ones caused by the boundary conditions. In a laminar flow, the instantaneous velocity is deterministic. For example, this could be calculated by N-S equations, with known boundary conditions to the system, including the initial velocity at $t = 0$. In ventilation, for example, the flow in a small envelope opening due to the action generated by buoyancy forces can be considered as a steady laminar flow. Considering the pressures generated by the wind, the laminar flow is unsteady and for this not exactly classifiable as a turbulent flow as the usual meaning of the term, because the unsteadiness doesn't depend on the transition within the vent.

Transition flow

The transition flow is identified as a phase of the development of a turbulent flow starting from a laminar flow. In the present context, a transitional flow takes place

when part of the flow field is not laminar and not fully turbulent. This distinction is not clear in a room flow, maybe hidden by the recirculating nature of the flow, but it can be easily applied in a flow with a dominant direction (Davidson, 2004). This flow can be presented as based on instability of flow equation that leads to chaotic motion. There are basically two types of transition, both relevant to ventilation. One type characterize streamline bodies, as exemplified by a flat plate in a uniform flow with velocity, U, as showed in figure 2.9. A boundary layer takes place in which the velocity increases from zero at the surface to a value close to U .

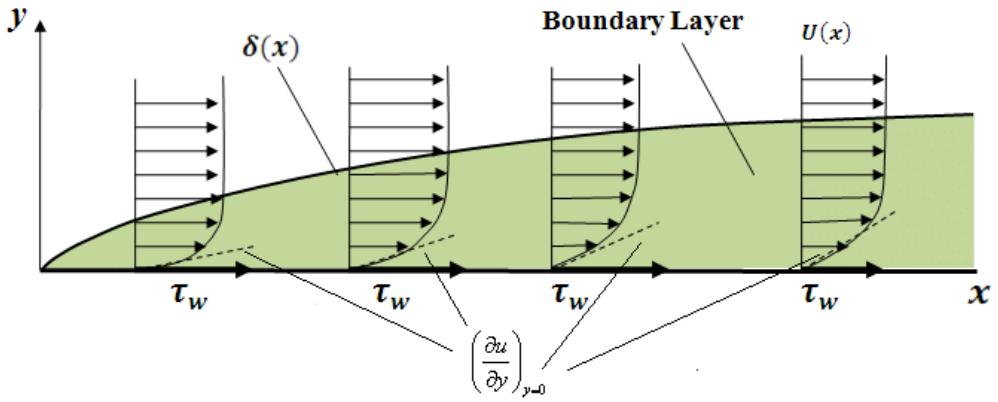

Figure 2.9: Representation of laminar flow on a plate and modification of the velocity profile.

This is definable as shear layer, which has a characteristic velocity profile (i.e. the variation of velocity through the layer) and a thickness of the layer, δ (known as boundary layer). The thickness of layer rises up in the downstream direction, x , due to molecular diffusion of velocity (momentum). The disturbances can be amplified or softened depending not only on the nature of them, but also on shape and dimensions of velocity profile and on viscosity. These factors can be summarized in two: the shape of the profile and the magnitude of the Reynolds number, based on distance from the base point, x:

$$Re_x = \frac{\rho\ x\ u}{\mu}, \tag{2.31}$$

This means that, at high values of x, the disturbances are augmented until a full developed turbulent flow is established at the end of the process. For example in a long smoothed duct, Re_x associated to an established turbulence is around 10^5. In this way, it is clear that this process (transitional flow) characterized a finite length or period. In specific, the criterion for a transition definition commonly used is the Reynolds number based on hydraulic diameter. As example, a value of 2300 is commonly stated as value at which happen the transition in a pipe. In

ventilation, it depends on the type of openings, case by case. In fact, a case could be characterized by a Re higher than 2300 but the vent length can be such that the flow is laminar. Instead, in case of a sharped opening the flow is separated and jet is formed, which can generate a velocity profile that leads to an important amplification of disturbances.
The other type is related to the instabilities derived from fluid flow separations, which, for example, could be due to bluff bodies, like objects in rooms. This kind of separation are frequent in ventilation cases. If the flow is at low velocity, the separation generates ordered vortices. At increasing velocities, the flow starts being much more chaotic up to eventually have downstream flow ruled by a turbulent random motion. This usually happens in indoor spaces, so that the air flow is turbulent. In fact, indoor air flow can be assumed turbulent. However, only with low velocities the turbulence modeling could be difficult and a laminar flow assumption can be more appropriate.

Turbulent flow

A turbulent flow is a type of flow, where the velocity, like pressure, at a pint has a random fluctuating component and a non-random component. The velocity components can be written in this form

$$u(x,t) = \bar{u}(x) + u'(x,t), \tag{2.32}$$

where $\bar{u}$ is the steady component and u′ is the random fluctuation. Turbulent flows are considered unsteady but they could be treated as steady, if the non-random components are constant. An example of steady turbulent flow can be the one generated around a building by the wind with velocity magnitude and direction constants. Another example can be the internal flow in a room crated from strong wind through a large opening. Instead, an unsteady turbulent flow would happen when a vent is gradually closed and the flow moves from a steady state to another. Anyway, a turbulent flow can be described by the unsteady form of the Navier-Stokes equations. This means that it is possible to calculate the temporal variation of velocity at a point, u(t), of a real flow, when the cause of the random part is known, in order to be specified as time-dependent form boundary condition. Unfortunately, this information can not be measured for a real flow, except in case of very small disturbances. In principles, it is possible to calculate *u(x,t)* using N-S equations, with sufficient boundary conditions, and statistical calculations of *u'(x,t)* should be close to the reality (not the actual variation with time), even though the instantaneous values would not be predictable (Etheridge D., 2012) . However, in ventilation sector the main interest is on time-averaged values of quantities, partially because humans, animal, plants and buildings respond slowly, compared to the timescales of turbulence related to wind and internal air motion.

Chapter 3

Material and methods: CFD approach

Computational fluid dynamics (CFD) is the part of fluid mechanics that uses numerical analysis and data structures to solve and analyze problems that involve fluid flows. It can be used to perform the calculations required to simulate the interaction between liquids and gases with surfaces defined by boundary conditions. Moreover, can be applied in cases of sonic or turbulent flows, which are still complex scenarios. In fact, ongoing research yields software that improves the accuracy and speed of complex simulation such these ones. Initial experimental validation of simulations is performed using a wind tunnel and the final validation coming in full-scale testing, e.g. flight tests. In this chapter, the aim is to introduce some useful concepts of computational fluid dynamics. The first part is focused on the generic topics about the computational fluid dynamic approach and its applications. Moreover, are presented its possible models. Finally, it starts the main part of the software characterization and application in CFD study cases. These aspects are the methods applied for the further studies, presented in Chapter 4.

3.1 Computational fluid dynamic

The definition of computational fluid dynamics is:
CFD is set of numerical methods applied to obtain approximate solutions of problems of fluid dynamics and heat transfer.
The basic idea was to calculate approximate solutions of differential equations describing fluid flow and heat transfer. The evolution of computational power of computers pushed the efforts to develop and apply methods of numerical simulations. The CFD started to be applied on the military field, but in the last 20 to 30 years the computer revolution had extended the field of CFD application. Nowadays, CFD

has the role of an everyday engineering tool for design, optimization and analysis. CFD is related to numerical solution of N-S equations, based on treating the fluid as a continuum, but it is possible to consider the fluid at molecular level. The study of individual behavior of molecules is called as molecular dynamics (Koplik and Banavar, 1995). Instead, the treatment of molecules groups, that are forced to move within a lattice, is known as Lattice Boltzmann methods (LBM). Both of these approaches are rarely applied in ventilation, however can have potential advantages fo simulations of fluid close to surfaces.

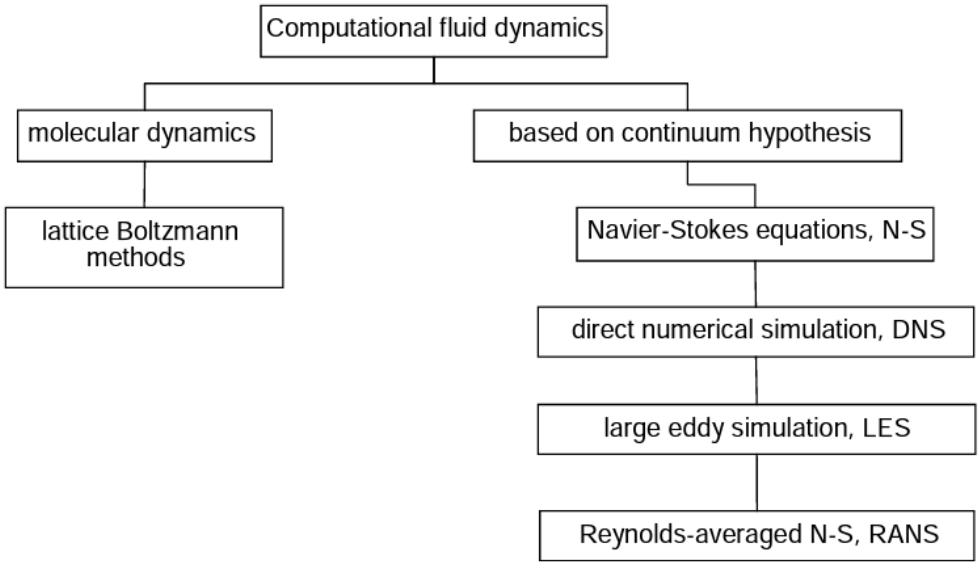

Figure 3.1: Types of CFD, from (Etheridge D., 2012).

Considering the methods based on N-S equations, they goes from the direct numerical solution of equations (DNS), to time-averaged form of them, so called Reynolds Averaged Navier-Stokes equations (RANS). In the middle of these two, can be considered the Large Eddy Simulation method (LES). In figure 3.1, a summary is presented (Etheridge D., 2012). In this work, the methods considered is the RANS.
In order to obtain an appropriate numerical solution, the discretization methods have to be used to approximate differential equations by algebraic equation, solvable on computer. Approximations are applied to small spatial and/or time domains, then numerical solution gives result only in discrete point of time and space. By the comparison of simulated physical quantities with eventual measurements, can be appreciated errors. Errors can derive from several causes, which the most common ones are:

- Differential equations include approximation and idealization;

- Some approximations could be created in discretization process;
- During solution of discretized equations, methods are applied, which don't produce exact solution, due to the fact that they should run for a infinite time.

Unfortunately, the only way to reduce error related to differential equations is rethinking the set of equations used. However, discretization errors can be reduced by applying approximation to smaller domains. As regards errors caused by iterative methods, the only option possible is to augment iterations number. This alternatives however increase solution time and cost, and for these reasons a compromise is necessary. Once obtained a solution, errors should be identified. A good way to evaluate errors is to validate solutions calculated against experimental results, using a proper statistical method.

3.1.1 Applications in natural ventilation

The application of CFD to design of natural ventilation in buildings are (Etheridge D., 2012):

1. calculation of velocity and temperature fields in rooms;
2. calculation of envelope building, such as heat exchange air and envelope or either air exchange through leakages;
3. calculation of wind pressures distributions;
4. global combination of others;
5. calculation of flow characteristics of vents.

CFD can be also applied to optimize the management and the environmental indoor conditions of already existing buildings. It can be used to predict the quality of building performance, the ventilation system activity and eventually energy demands. Talking about mechanical ventilation, the first one is the main application, with the envelope flows defined as boundary conditions. Instead, for natural ventilation, a whole-field calculation is more common. Practically in this case, 1 2 and 3 are part of the same calculation. In figure 3.2 are illustrated a schematic representation of the different types of interests.

Usually the external wind flow is considered turbulent and with uniform temperature (heat exchange between wind and building surfaces is ignored). Internal flows can involve a wide range of flow types in different parts of the space: laminar, transitional and turbulent shear layers, positively and negatively buoyant plumes,

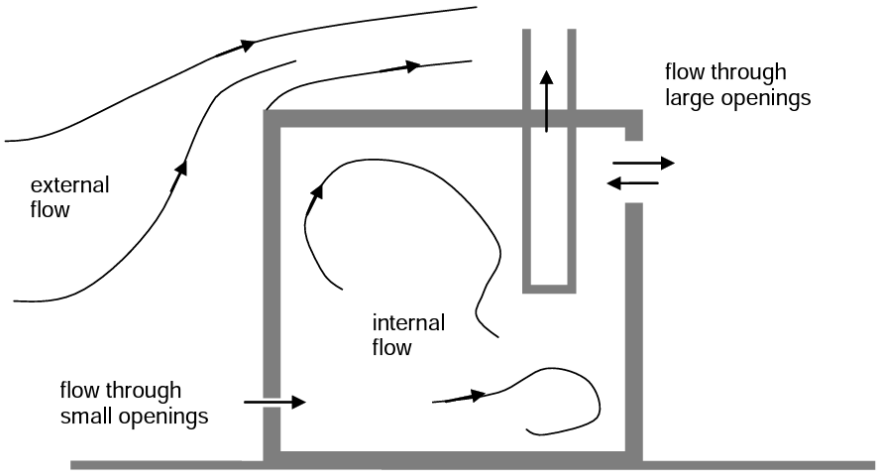

Figure 3.2: Flows of interests in ventilation, from (Etheridge D., 2012).

flow separation and vortex shedding from bluff bodies; high streamline curvature, low velocities and correspondingly low Reynolds numbers. These are all challenging situation to be simulated in CFD.

3.1.2 Components of a numerical solution

The process of numerical solution requires the definition of several aspects and each of them leads to a final solution in a unique way. The steps can be identified in the list below:

1. **Model**: definition of equations describing the situation under examination. In fact, a choice can be made among the momentum equation, the Turbulent Kinetic and Dissipation equations. It is also possible just to calculate mean physical quantities, or to limit the analysis to a certain scales or to obtain all quantities throughout time. This choice corresponds to a specific class of models: RANS, LES and DNS, which have been shortly presented in section 3.1.

2. **Numerical grid**: step in which are defined points for solution calculation. The domain is divided into sub-domains, such as elements, control volumes etc. The grids are usually classified as structured, where grid lines intersect just once, and unstructured, where the grid can assume any shape.

3. **Discretization method**: decision of points where the equations derived from previously chosen model have to be computed. Among three-dimensional approaches, one is the Finite Differences, in which the approximation of partial

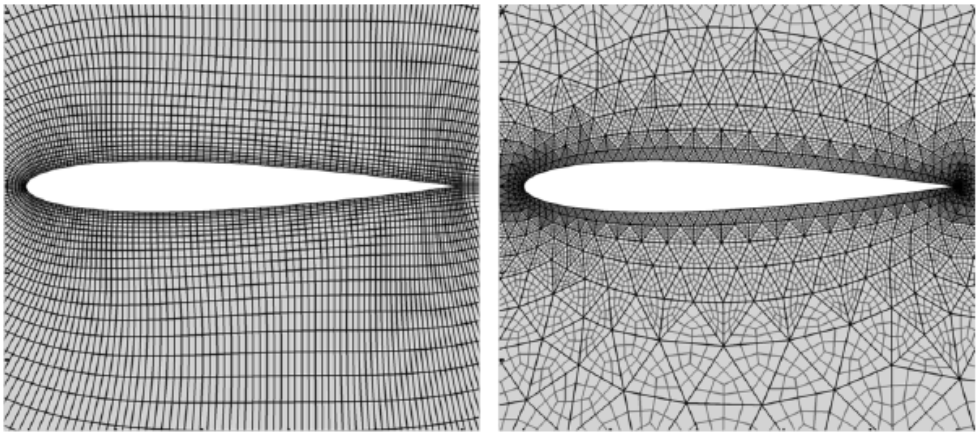

Figure 3.3: Examples of the two different grid type (Jung et al., 2016)

derivatives is based on value in nodal points. A second one is the Finite Volumes method, in which domain is subdivided into volumes and physical quantities are calculated in their geometric centroids. The third method is the Finite Elements method, which is similar to the previous one but have an important difference, which is the fact that the equations are weighted with functions before integration.

4. **Approximation**: choice of approximations for partial derivatives, or for volume or surface, for integrals and weigh functions. For our cases, this step is directly coupled with the model.

5. **Solution method**: decision of resolution method for equations in grid options. In fact, this uses time-space points, which permit to CFD to compute values and there are various methods, such as upwind scheme, Eulero etc.

6. **Convergence criteria**: last step for deciding when the solution are satisfying and so for stopping iterative method.

3.1.3 Properties of numerical resolution method

A numerical method produces a solution, which needs to have particular features to be considered acceptable. The most important ones are:

Consistence : it consists in a truncation error as difference between value from a discretized equation and the real one, evaluated in a nodal grid point. A method

to be consistent must have truncation error becoming zero when Δt tends to 0 and/or Δx tends to 0. Usually it's proportional to spatial and/or time Δ.

Stability : a numerical solution is stable if it does not amplify errors during numerical resolution process. For example, an iterative method is stable if it does not increase during iterations.

Convergence : in a convergent method, the solution of discretized equations tends to solution of differential equations when grid spacing tends to zero. For non-linear problems, that are strongly influenced by boundary condition, convergence is checked repeating the calculation on a series of successively refined grids.

Conservation : Since the model follows the conservation law, numerical resolution have to do it too. This means that, at steady state and in the absence of sources and sinks, the amount of conserved quantity leaving a closed volume is equal to the amount entering that volume.

Boundedness : Numerical limits are defined for a numerical solution, in which it should lie in between, that are often imposed by Physics itself. Some quantities such as density, kinetic turbulent energy must be positive. In some other times, other quantities may have to lay between 0% and 100%.

3.2 Modeling and simulation

As presented in the beginning of the chapter, there are several approaches for resolution of the N-S equations. In fact, focusing on the chaotic nature of flow, it is evident the impossibility of developing an accurate theory or model. This is mainly due to the nature of velocity field, which is three-dimensional, time-dependent and random.

Considering the scale of motion, the largest one has comparable dimension to boundary geometry but it can not be universal. In fact, there is a large range of timescales and lengthscales which are differently linked to the Reynold Number. Mathematically, the nonlinear convective term in the N-S equation raises the difficulties, such as the pressure-gradient term, which becomes non-linear and non-local, if expressed as a function of velocity. This is presented in the right part of this equation,

$$\frac{Du_i}{Dt} = -\frac{1}{\rho}\frac{\partial p}{\partial x_i} + \epsilon_{ij3} f u_j + \nu \frac{\partial^2 u_j}{\partial x_j \partial x_i} - \delta_{i3} g, \tag{3.1}$$

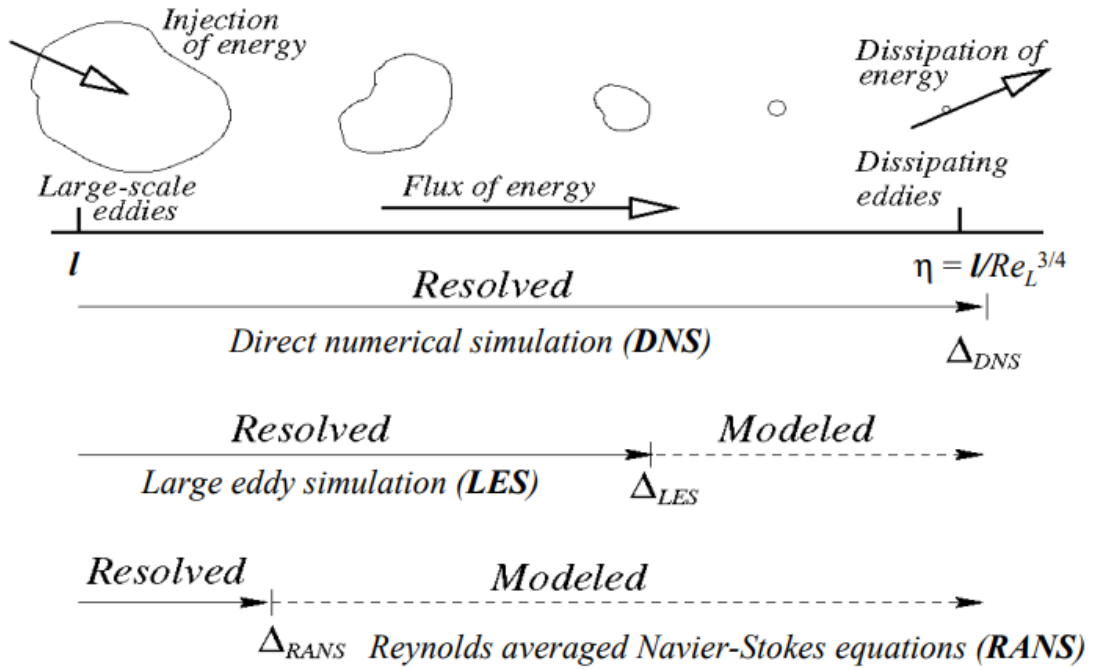

Figure 3.4: Comparison of lengthscales, solved or not, in different model.

where f is the Coriolis force and ν is the kinematic viscosity. There are two significant groups of turbulent flow simulations and turbulence models. In turbulent flow equations, the equations are solved for time-dependent velocity field, such as for examples in simulations conducted using direct numerical simulation (DNS) or large-eddy simulation (LES). On the contrary, turbulence models solve equations for some main quantities, e.g. U , $\bar{u}_i u_j$ or ϵ. Reynolds-averaged Navier-Stokes (RANS) are part of this family, since they involve the solution of the Reynolds equation to determine the mean velocity field.

3.2.1 RANS models

The Reynolds-averaged form of basic equations is obtained when the instantaneous value of a quantity is expressed into two components: a time-averaged component, independent from time, and a time-varying component, for which the time average is equal to zero (Etheridge D., 2012). In this models, the mean field of physical quantities is calculated, leaving to a parametrization term of upper order. An expression, named enclosure, for the Reynolds stress term is required in the Navier-Stokes equation. A distinction in two main types of models can be done. The

first one is based on the concept of an equivalent turbulent viscosity, μ_t, or eddy diffusivity, $\epsilon_m = \mu_t/\rho$, which links the turbulent stresses to mean velocity gradients such as the molecular viscosity. For example, the equations below

$$\rho\overline{u'^2} = -\mu_t\frac{\partial\bar{u}}{\partial x}, \quad \rho\overline{u'v'} = -\mu_t\frac{\partial\bar{u}}{\partial y}, \quad \rho\overline{u'w'} = -\mu_t\frac{\partial\bar{u}}{\partial z}, \tag{3.2}$$

can be inserted in the N-S equations. In this way, they can be written, for x direction and with Boussinesq approximation, as

$$\rho(\bar{u}\frac{\partial\bar{u}}{\partial x} + \bar{v}\frac{\partial\bar{u}}{\partial y} + \bar{w}\frac{\partial\bar{u}}{\partial z}) = -\frac{\partial\bar{p}}{\partial x} + (\mu + \mu_t)(\frac{\partial^2\bar{u}}{\partial x^2} + \frac{\partial^2\bar{u}}{\partial y^2} + \frac{\partial^2\bar{u}}{\partial z^2}) \tag{3.3}$$

Usually the molecular viscosity is littler than turbulent viscosity, by several orders of magnitude, hence turbulent flows tend to be barely dependent on Reynolds number. One of the most used between these model is the k-ϵ model, with several variants. The k is the kinetic energy per unit mass of the turbulent fluctuations and ϵ is the dissipation rate. A weakness assumption of this model is the assumption of μ_t as isotropic.
The second type of models use transport equations for the individual turbulent stresses and are known as Reynolds Stresses Models (RSM). These are more realistic but implicate the resolution of a larger number of equations. The RANS models can be also differentiated, based on equation number. For example, the **mixing length model** is a zero equation model. Instead, a one-equation model is the **Spalart-Almaras** model and two equations model are **k-ϵ** models, **k-ω** models and ASM. Finally, the **Reynolds stress model** is a seven equations model. The number of equations denotes the number of additional partial differential equations (PDE_s) that are being solved.

3.2.2 K - epsilon model

This is a semi-empirical model, because the transport equations for k and ϵ contain empirical parameters, obtained from experiments. This means that the equations (3.2) are still valid but μ_t is calculated from an empirical relation with k and ϵ. The model consists in:

- **turbulent viscosity hypothesis**: it was postulated by Boussinesq in 1877 and it states that the momentum transfer, due to turbulent eddies, can be modeled with an eddy viscosity (Schmitt, 2007). This leads to the use of the Reynolds Stress Tensor, τ_{ij}:

$$\tau_{ij} = 2\mu_t S^*_{ij} - \frac{2}{3}\rho k\delta_{ij} \tag{3.4}$$

where S^*_{ij} represents the mean strain rate tensor and the scalar μ_t is the eddy viscosity.

- **model transport equation for k**: it describes the variation along time of turbulent viscosity, k, caused by effects of dissipation, buoyancy, turbulence, velocity/pressure coupling and wind shear. The equation can be derived from the momentum equation, where

$$q^2 = \overline{u_i' u_j'}, \qquad \frac{D}{Dt}(\frac{1}{2}k^2) = -\overline{u_i' u_j'}\frac{\partial u_i}{x_j} - \frac{\partial}{\partial x_j}\left(\frac{\overline{p' u_j'}}{\rho} + \overline{u_i' u_i' u_j'}\right) - \frac{g}{\rho}\overline{\rho' u_3'} - \epsilon. \tag{3.5}$$

  First term on the right represent wind shear, the two terms between parenthesis stand for pressure-velocity coupling and for the turbulence, second to last term represent buoyancy force and the last one indicates dissipation.

- **model transport equation for ϵ**: it can be derived in the same way but it is not a useful starting point. This is because ϵ can be easily seen as the energy-flow rate in the cascade of energy, and it is defined by the large-scale eddies, independently from viscosity. Moreover, exact equation for ϵ is related to processes involved in the dissipative range. For this, the empirical equation for ϵ is the most used,

$$\frac{D\epsilon}{Dt} = -C_{\epsilon 1}\overline{u_i' u_j'}\frac{\partial u_i}{\partial x_j}\frac{\epsilon}{k^2/2} - -C_{\epsilon 2}\frac{\epsilon^2}{k/2} + \frac{\partial}{\partial x_j}(\frac{\nu_T}{\sigma_\epsilon} + \frac{\partial \epsilon}{\partial x_j}). \tag{3.6}$$

  The constants of the model are

$$C_{\epsilon 1} = 1.44 \;\; C_{\epsilon 2} = 1.92 \;\; \sigma_\epsilon = 1.3. \tag{3.7}$$

- **Turbulent viscosity**: represents the transfer of momentum caused by the turbulent eddies. It is specified as

$$\nu_T = C_\mu \frac{k^2}{\epsilon} \tag{3.8}$$

  C_μ is another constant of the model, equal to 0.009.

Through these are calculated also other characteristics of the flow, such as length-scale ($L{=}k^{2/3}/\epsilon$) or timescale ($\tau = k\epsilon$).
This approach is one of most economic, at least in terms of computational resources. It is also the first one to be put into practice, since it does not need to solve Navier-Stokes equations, thanks to implementation of specific parametrizing models.

The basic k - ϵ model had undergone two developments that are called RNG and SST models. In these models, the coefficients in transport equations are not constant but evaluated locally. This has been demonstrated to be to offer better accuracy for flows with low Reynolds number, verifiable in room air movement.

3.2.3 Other models

Direct Numerical Simulation

Also referred as DNS, direct numerical simulation consists in solving the Navier-Stokes equations, resolving all scales of motion. In the flow, can be considered that there is a passage of kinetic energy from the largest eddies to the smaller ones. Practically, the mesh size should be enough fine to describe the process. This means that the whole range of spatial and time scale are resolved, which means no turbulence model is needed. In a simulation, are needed small time steps and cell dimensions. In fact, the physical quantities are calculated in N finite points, divided into intervals of length h. In specific, to satisfy the resolution requirements, a model have to contain integral length scale, L, and the Kolmogorov scale η, which is the appropriate length scale for dissipation rate. From this, $\mathbf{NH} > \mathbf{L}$ and $\boldsymbol{h} \leq \eta$. Moreover, the number of points for each direction in a simulation has to be equal to

$$N \geq \frac{Re^3}{2}. \tag{3.9}$$

So it is easy to understand why this technique requires a large memory storage for analysis of turbulent flows, which implies great Re number values. This approach is extremely computational power consuming. In Hirsch (2007), it is presented a flow over a simple geometry and the relative time of solution by DNS is estimated around 6 moths on a super computer of 2100 processors. On the other hand, considering the empowering of calculators, studies are starting adopting it due to the fact DNS offers the most precise results. However, until now is rarely applied in ventilation studies.

Large Eddy Scales

This approach provides a filter in dimension of eddies. In fact, LES modeling directly solves only the largest eddies and the smaller ones are modeled in a semi-empirical way. LES can be seen as going through four conceptual steps, listed below:

- Firstly, there is the **filtration of variables**, starting from the velocity. The velocity is separated in a filtered part and a residual part. The first one is the random variable, $u_f\mathbf{(x,t)}$, representing the large eddies motion. The

second one, u'_f**(x,t)**, is the one that need to be modeled. In an ideal case, the filter width should be somewhat smaller than l_{EI}, smallest energy containing motions.

- The further step is the **filtration of equations**. Having the filtered velocity field, can be filtered the velocity gradient form $\frac{\partial u_f}{\partial x_j}$ and the residual stress tensor τ_{ij}:

$$\tau_{ij} = \frac{1}{2}\left(\frac{\partial u_{if}}{\partial x_i} + \frac{\partial u_{jf}}{\partial x_j}\right) \tag{3.10}$$

- Then it is possible to apply the **closure** to the residual stress tensor τ_{Sij}. For this purpose, several models can be chosen like the Smagorinsky, which relates residual stress to the filtered rate of strain and model eddy viscosity, in analogy with mixing-length hypothesis. The relation is $\nu_T = l_M^2$ **S** with l_M is the length-scale and S is the rate of strain.

- Finally, the filtered equation can be **solved**, providing an approximation to the large scale motion in one realization of turbulent flow.

In terms of computational cost, it is clear that costs increases for LES compared to RANS models. While RANS doesn't resolve the Navier-Stokes equations, LES takes into account at least the first order of variables and solves the unsteady equations, for that more computing power is required. Moreover, LES is more computational demanding due to the fact that boundary conditions should be specified in unsteady form.

3.3 Applied Software

In this work, the software adopted to numerical computation was Ansys Fluent. The first version used was Fluent 6.3, coupled with Gambit for the geometrical modeling of the case and grid creation. Gambit permits users to create simulation of a virtual environment for example pipes, ship hulls and an buildings. It is possible to use volumes, faces, edges and to mesh them, that means to subdivide domain into smaller elements over which the equations can be approximated. After a preliminary use of these two software, the release of the software was updated to Ansys Fluent 17.2. This release does not allow to employ Gambit. For this reason, Autodesk Inventor was applied for geometrical modeling and ICEM CFD as grid generator. In fact, the models were prepared in Autodesk Inventor and then imported in ICEM CFD, which permit to mesh the cases by a structured or unstructured grid, based on user choice.
However, in any version, ANSYS Fluent is the real computational fluid dynamic

software (CFD), used to simulate fluid flows in a virtual environment. Through this, users can choose and manipulate fluid dynamic models, set surroundings conditions and study resulting configuration. The next pages are focused on this last software, in order to describe how CFD simulation are computed.

3.4 Behind calculations

In order to understand processes behind calculation of physical quantity, it is necessary to analyze the set of equation defining the model of conducted simulations. If not differently specified every equation is referred to Fluent Inc (2006) and ANSYS (2013). Of interests are the Navier-Stokes equations calculated by Fluent, presented previously in chapter 2. For all type of flow, the momentum equation is ANSYS (2013),

$$\frac{\partial}{\partial t}(\rho\vec{v}) + \nabla \cdot (\rho\vec{v}\vec{v}) = -\nabla p + \nabla \cdot (\overline{\overline{\tau}}) + \rho\vec{g} + \vec{F}, \tag{3.11}$$

where p is the static pressure, $\vec{g}$ is the gravitational force, $\vec{F}$ are gravitational body forces and external forces. Moreover, it can contain other model-dependent source, like a porous-media. $\overline{\overline{\tau}}$ is the stress tensor, expressed as

$$(\overline{\overline{\tau}}) = \mu[(\nabla\vec{v} + \nabla\vec{v}^T) - \frac{2}{3}\nabla \cdot \vec{v}I], \tag{3.12}$$

where μ is the molecular viscosity, $(\nabla\vec{v} + \nabla\vec{v}^T)$ is the term that describes the volume dilatation and I is a unit tensor. Moreover, the mass conservation expression from the manual is

$$\frac{\partial\rho}{\partial t} + \nabla(\rho\vec{v}) = S_m \tag{3.13}$$

where S_m is a mass source. For flows involving heat transfer, an additional equation for energy conservation is solved. Additional transport equations are also solved when the flow is turbulent. These equations are the starting point for the turbulence modeling.

3.4.1 k-ϵ standard model

As underlined in the previous section 3.2.1, in RANS models the solution variables of N-S equations are separated in mean and fluctuating components. This leads to the necessity of a proper modeling of the term, so called Reynolds stresses, $-\rho\overline{u_i'u_j'}$. A solution is the application of the Boussinesq hypothesis that link the

Reynolds stresses to the mean velocity gradients. In the derivation of this model, the assumption is that the flow is fully turbulent, and the effects of molecular viscosity are negligible, and it is therefore valid only for fully turbulent flows (eq. 3.14).

$$-\rho\overline{u_i'u_j'} = \mu_t\left(\frac{\partial u_i}{\partial x_j}+\frac{\partial u_j}{\partial x_i}\right)-\frac{2}{3}\left(\rho k+\mu_t\frac{\partial u_k}{\partial x_k}\right)\delta_{ij} \tag{3.14}$$

The Boussinesq hypothesis is used in the Spalart-Allmaras model, the k-ϵ models, and the k-ω models. The advantage of this approach is the relatively low computational cost associated with the computation of the turbulent viscosity, μ_t. In particular, in ANSYS Fluent, k-ϵ model falls within this class of models and has become the workhorse of practical engineering flow calculations in the time since it was proposed by **?**. The standard k-epsilon model is based on model transport equations, which consider the turbulence kinetic energy (k) and its dissipation rate (ϵ). The kinetic energy and its dissipation rate are derived from these transport equation, (ANSYS, 2013)

$$\frac{\partial}{\partial t}(\rho k)+\frac{\partial}{\partial x_i}(\rho k u_j)=\frac{\partial}{\partial x_j}[(\mu+\frac{\mu_t}{\sigma_k}\frac{\partial k}{\partial x_j})]+G_k+G_b-\rho\epsilon-Y_M+S_k \tag{3.15}$$

and

$$\frac{\partial}{\partial \epsilon}(\rho \epsilon)+\frac{\partial}{\partial x_i}(\rho \epsilon u_j)=\frac{\partial}{\partial x_j}[(\mu+\frac{\mu_t}{\sigma_\epsilon}\frac{\partial \epsilon}{\partial x_j})]+C_{1\epsilon}\frac{\epsilon}{k}(G_k+C_{3\epsilon}G_b)-C_{2\epsilon}\rho\frac{\epsilon^2}{k}+S_\epsilon \tag{3.16}$$

where G_k represents the generation of turbulence kinetic energy due to the mean velocity gradients, G_b is the generation of turbulence kinetic energy due to buoyancy and Y_M represents the contribution of the fluctuating b dilatation in compressible turbulence to the overall dissipation rate. Moreover, $C_{1\epsilon}$ $C_{2\epsilon}$ $C_{3\epsilon}$ are constants (values reported in section 2.2.2) and $\sigma_{epsilon}$ σ_k are the Prandtl numbers for ϵ and k respectively. In particular G_k is calculated through the formula below.

$$G_k=-\rho\overline{u_i'u_j'}\frac{\partial u_j}{\partial x_i}, \tag{3.17}$$

Considering a non-zero gravity field and temperature gradient simultaneously present, Ansys Fluent in k-epsilon model takes into account the generation of k due to buoyancy and the related contribution to ϵ production. In specific, the generation of turbulence due to buoyancy is given by

$$G_b=\beta g_i\frac{\mu_t}{Pr_t}\frac{\partial T}{\partial x_i}, \tag{3.18}$$

where β is the coefficient of thermal expansion, g_i is the component in ith direction of gravitational vector and Pr_t where is the turbulent Prandtl number for energy. In this model, Pr_t is equal to 0.85 as default value.

Moreover, Ansys fluent considers the dilatation dissipation term, Y_M, which is related to the compressibility affecting the turbulence for high-Mach number flows. In facts, Y_M takes into account the fluctuating dilatation in compressible turbulence to the overall dissipation rate, as showed in (3.19):

$$Y_M = 2\rho\epsilon M_t^2 \tag{3.19}$$

where M_t is the turbulent Mach number, $M_t = \sqrt{\frac{k}{a^2}}$, where a is the speed of sound. This parameter can be defined as $a = \sqrt{\gamma RT}$, where γ is the adiabatic index, representing of specific heats of a gas at a constant pressure to a gas at a constant volume, C_p/C_v. The eddy viscosity is computed by the combination of k and ϵ, obtaining the following form:

$$\mu_t = \rho C_\mu \frac{k^2}{\epsilon}. \tag{3.20}$$

In this way, has been presented the formulation of k-ϵ model in Ansys Fluent.

3.4.2 k-ϵ realizable model

It is a semi-empirical model, and the derivation of the model equations relies on phenomenological considerations and empiricism. K-ϵ realizable model is another possible turbulence model between the class of RANS methods. It is different from the k-ϵ standard model in two way, (Shih et al., 1995):

- it contains an alternative formulation for the turbulent viscosity;
- it considers a modified transport formulation for the dissipation rate, ϵ, which has been derived from an exact equation for the transport of the mean-square vorticity fluctuation (eq. 3.21 and eq.3.22):

$$\frac{\partial}{\partial t}(\rho k) + \frac{\partial}{\partial x_i}(\rho k u_j) = \frac{\partial}{\partial x_j}[(\mu + \frac{\mu_t}{\sigma_k}\frac{\partial k}{\partial x_j})] + G_k + G_b - \rho\epsilon - Y_M + S_k \tag{3.21}$$

and

$$\frac{\partial}{\partial t}(\rho\epsilon) + \frac{\partial}{\partial x_i}(\rho\epsilon u_j) = \frac{\partial}{\partial x_j}[(\mu + \frac{\mu_t}{\sigma_\epsilon})\frac{\partial \epsilon}{\partial x_j})] + \rho C_1 S_\epsilon - \rho C_2 \frac{\epsilon^2}{k + \sqrt{\nu\epsilon}} + C_{1\epsilon}\frac{\epsilon}{k} C_{3\epsilon} G_b + S_\epsilon \tag{3.22}$$

where $C_1 = max[0.43, \frac{\eta}{\eta+5}]$, $\eta = S\frac{k}{\epsilon}$ and $S = \sqrt{S_{ij}S_{ij}}$.

In particular, it is defined *"realizable"* because the model satisfies certain mathematical constraints on the Reynolds stresses, consistent with the physics of turbulent flows. For the k-ϵ standard, this definition is not applicable. An significant benefit of the realizable k-ϵ model is that it more accurately predicts the spreading rate of both planar and round jets. It is also likely to provide greater performance for flows involving rotation, boundary layers under strong adverse pressure gradients, separation, and re-circulation. In fact, this model would be used in wine cellar case, which consists, in few words, in a flow through a pipe by a fan. Considering to combine the Boussinesq relationship (Eq. 3.14) and the eddy viscosity definition (Eq. 3.20) to obtain the following expression for the normal Reynolds stress in an incompressible strained mean flow:

$$\overline{u^2} = \frac{2}{3}k - 2v_t\frac{\partial U}{\partial x} \tag{3.23}$$

Using equation 3.20, $\overline{u^2}$, which is for definition a positive quantity, could become negative, that is, non-realizable, when the strain is large enough to satisfy:

$$\frac{k\partial U}{\epsilon\partial x} > \frac{1}{3C_\mu} \approx 3.7. \tag{3.24}$$

Moreover, the Schwartz inequality for shear stresses, $(\overline{u_\alpha u_\beta})^2 \leq \overline{u_\alpha^2 u_\beta^2}$, could be violated when the mean strain rate is large. The most straightforward way to ensure the realizability, which means positive value of normal stresses and Schwarz inequality for shear stresses, is to make C_μ variable by sensitizing it to the mean flow (mean deformation) and the turbulence (k,ϵ). The definition of C_μ is sustained by experimental evidence and it is found to be around 0.09 in the logarithmic layer of equilibrium boundary layers, and 0.05 in a strong homogeneous shear flow.

Equation 3.21 can be considered the same as that in the standard k-ϵ model, except for the model constants. However, the form of equation 3.22 is quite different from that one in the standard model. One of the noteworthy features is that the production term in the equation (the second term on the right-hand side of equation 3.22) does not involve the production of k. This is because it doesn't contain G_k term such as equation 3.16.It is believed that the present form better represents the spectral energy transfer. Instead, considering the eddy viscosity, the parameter C_μ is no longer a constant, but it is computed by this form:

$$C_\mu = \frac{1}{A_0 + A_s\frac{kU*}{\epsilon}}, \tag{3.25}$$

where $U* = \sqrt{S_{ij}S_{ij} + Q_{ij}\vec{Q}_{ij}}$, $A_0 = 4.04$ and $A_s = \sqrt{6}\cos\phi$. In specific, $\vec{Q_{ij}}$ depends on the mean rate-of-rotation tensor viewed in a moving reference frame

with the angular velocity ω_k. Moreover, $\phi = 1/3\cos^{-1}(\sqrt{6W})$, with $W = \frac{S_{ij}S_{jk}S_{ki}}{\vec{S}^3}$, $\vec{S} = \sqrt{S_{ij}S_{ij}}$and $S_{ij} = \left(\frac{\partial u_j}{\partial x_i} + \frac{\partial u_i}{\partial x_j}\right)$ In synthesis, C_μ is a function of the mean strain and rotation rates, the angular velocity of the system rotation, and the turbulence fields.
The realizable k-ϵ model has shown substantial improvements over the standard k-ϵ model where the flow features include strong streamline curvature, vortices, and rotation. However, initial studies have shown that the realizable model provides the best performance of all the k-ϵ model versions for several validations of separated flows and flows with complex secondary flow features.

3.4.3 Porous media model

The porous media model can be applied in a wide variety of problems, and in specif in greenhouse studies, it can be used to model plants present inside the structure but also insect and shading screens if they are present. To use this model, a cell zone has to defined in which this model is applied. For the case of insect screens for example, a mono-dimensional simplification of the porous media model, named "porous jump". In fact, usually it can be used to model a thin membrane with known velocity/pressure-drop characteristics. The porous jump model is applied to a face zone, not to a cell zone, and should be used whenever possible because it is more robust and yields better convergence. However, practically the porous media model is nothing more than an added momentum source in the governing momentum equations. The source term is composed by two parts: a viscous loss term and an inertial loss term (equation (3.26)).

$$S_i = -(\sum_{j=1}^{3} D_{ij}\mu v_j + \sum_{j=1}^{3} C_{ij}\frac{1}{2}\rho|v|v_j) \tag{3.26}$$

where S_i is source term for ith momentum equation, $|v|$ is the velocity magnitude and D and C are both matrix. These terms contribute to the pressure gradient in the porous cell, creating a pressure drop that is proportional to the fluid velocity in the cells.

The simplest case is an homogeneous porous media, for which the (3.26) can be written as

$$S_i = -\left(\frac{\mu}{\alpha}v_i + C_2\frac{1}{2}\rho|v|v_i\right) \tag{3.27}$$

where α is the permeability and C_2 is the inertial resistance factor. This expression can be obtain from eq. (3.26) by expressing D and C as diagonal

matrices with $\frac{1}{\alpha}$ and C_2 on the diagonals, respectively, and other elements are zeros. This expression is also known as Darcy-Forchheimer's law.

Darcy's law and inertial loss coefficient

The first term in the equation (3.27) is known as Darcy's law, and describes the pressure drop caused by a laminar flow through a porous media. In fact, it ignores the convective and diffusion contributes and the form of the problem is

$$\nabla p = \frac{\mu}{\alpha}\vec{v}. \tag{3.28}$$

Considering the ith component of velocity field, the equation (3.28) becomes

$$\Delta p_i = -\sum_{j=1}^{3} \frac{\mu}{\alpha_{xj}} v_j \Delta n_i. \tag{3.29}$$

where Δn_i is the thickness of the porous medium in ith direction.

The Inertial loss coefficient is present in the second part of (3.27). It is reffed to high velocities flows and can be considered as a loss coefficient per unit length along the flow direction, thereby allowing the pressure drop to be specified as a function of dynamic head, $[1/m]$. If the flow is turbulent and the contribution of inertial loss predominates, the equation (3.27) can be written for the ith direction as

$$\Delta p_i = -\sum_{j=1}^{3} C_{2ij} \left(\frac{1}{2} \rho v_j |v| \Delta n_i \right), \tag{3.30}$$

in the same way as the Darcy's law. Inertial coefficient is also known as Forchheimer coefficient, $\beta = \frac{1}{2}C_2$ The applicability of only the Darcy's law is

related to Reynolds number. The limit of application for this law is not well identified, in fact several authors have given different values of limit Reynolds number. For example, Sukop et al. (2013) and Alabi (2011) have established a Re = 10 and Re = 1 respectively as upper limit of Darcy's law application.

However, permeability ans Forchheimer coefficient can be calculated through several formulas available in literature, based on such parameters of porous media as porosity or tortuosity, but the formulas are usually empirical and not universal (Sobieski and Trykozko, 2014a). In fact, different formulas computed with a fixed set of parameters can lead to totally different values of β coefficients, ranging even over several orders of magnitude, as showed in Sobieski and Trykozko (2011). Insights about the determination of these parameters will be conducted later in this study.

Energy Equation in Porous Media

Considering the energy equation, Fluent solves the standard energy transport equation with changes to the conduction flux and the transient term only. The modification to the conduction flux uses an effective conductivity and includes the thermal inertia of the solid region in the transient term.

$$\frac{\partial}{\partial t}(\gamma\rho_f E_f + (1-\gamma)\rho_s E_s) + \nabla\cdot(\vec{v}(\rho_f E_f + p)) = \nabla\cdot[k_{eff}\nabla T - (\sum_i h_i J_i) + (\overline{\overline{\tau}}\cdot\vec{v})] + S_f^h \tag{3.31}$$

where:
E_f is total fluid energy
E_s is total solid energy
γ is the porosity of medium
k_{eff} is effective thermal conductivity of the medium
S_f^h is fluid enthalpy source term Effective.

The last term is defined as the sum of the internal energy of the fluid and the product of the pressure and its volume:

$$S_f^h = E_f^h + pV. \tag{3.32}$$

Moreover, the effective thermal conductivity, k_{eff}, is computed by Fluent as the volume average of the fluid conductivity and the solid conductivity:

$$k_{eff} = \gamma k_f + (1-\gamma)k_s, \tag{3.33}$$

where k_f represents thermal conductivity and k_s is the solid thermal conductivity. About porous media influence on turbulence, it is possible to notice that turbulence in the medium is treated as though the solid medium, it has no effect on the turbulence or dissipation rates. Therefore, inside this media, turbulence is computed just as in the bulk fluid flow. In conclusion, for all scalars, when the effect of porosity is taken into account, for all scalars the time derivative term becomes $\frac{\partial}{\partial t}(\gamma\rho\phi)$ where ϕ is the scalar quantity and γ is again the porosity.

3.4.4 Boundary conditions

Boundary conditions are essential for the accuracy of CFD calculations. In the long term, the uncertainty of CFD solutions for ventilation design may be determined by the accuracy with which the boundary conditions can be specified. (Etheridge D., 2012)
Boundary conditions have to be specified at domain surfaces and at solid surfaces

in the domain. In fact, they impose limits to the physical quantities and dictate behavior of simulation near spatial limits. The boundary types in Fluent are dived in:

- Flow inlet and exit boundaries: pressure inlet, velocity inlet, mass flow inlet, inlet-vent, intake fan, pressure outlet, pressure far-field, outflow, outlet vent, and exhaust fan;
- Wall, repeating, and pole boundaries: wall, symmetry, periodic, and axis;
- Internal cell zones: fluid, and solid (porous is a type of fluid zone);
- Internal face boundaries: fan, radiator, porous jump, wall, and interior.

Notice that the internal face boundary conditions are defined on cell faces, which means that they do not have a finite thickness and provide a means of introducing a change in flow properties. These boundary conditions are used to implement physical models representing fans, thin porous membranes, which are two cases treated in this study.

The inlet and exit boundary conditions

In Fluent are available several options, here are reported the ones considered in the case studies:

- Velocity inlet used to define the velocity and scalar properties of the flow at inlet boundaries.
- Pressure inlet used to define the total pressure and other scalar quantities at flow inlets.
- Pressure outlet is considered to define the static pressure at flow outlets (and also other scalar variables, in case of backflow). The use of this instead of an outflow condition often results in a better rate of convergence when backflow occurs during iteration.
- Outflow used to model flow exits where the details of the flow velocity and pressure are not known prior to solution of the flow problem. It is appropriate where the exit flow is close to a fully developed condition, as the outflow boundary condition assumes a zero normal gradient for all flow variables except for pressure.
- Intake fan boundary conditions are used to model an external intake fan with a specified pressure jump, flow direction, and ambient (intake) total pressure and temperature.

- Exhaust fan boundary conditions are used to model an external exhaust fan with a specified pressure jump and ambient (discharge) static pressure.

Moreover, the software at flow inlet to the domain considers the specification of transported turbulence quantities. In specific in $k-\epsilon$ model is possible to specify the turbulent kinetic energy and the dissipation rate. In alternative, there are other parameters that can be specified:

Turbulent Intensity is obtained as the ratio of the root-mean-square of the velocity fluctuations, u', to the mean flow velocity, u_{avg}. This parameter is usually expressed in percentage, considering a range that goes from low intensity, 1%, to high values, such as 10%. The turbulence intensity at the inlets totally depends on the upstream history of the flow. If the flow can be considered fully-developed, this parameter can be estimated from the following formula derived from an empirical correlation for pipe flows:

$$I = \frac{u'}{u_{avg}} = 0.16(Re_{DH})^{(} - 1/8), \tag{3.34}$$

where Reynolds number is calculated based on the duct height (Re_{DH}).

Turbulence Length Scale is a physical quantity related to the size of the large eddies that contain the energy in turbulent flows. In fully-developed duct flows,$\boldsymbol{l}$ is restricted by the size of the duct, or in ventilation case to opening size, since the turbulent eddies cannot be larger than the duct. An approximate relationship between l and the physical size of the duct is $\boldsymbol{l} = 0.07L$, where L is the relevant dimension of the duct. The value of L can be associated to other dimensions depending on the case studied. For example, if it is studied a flow with an obstacle, the length of the obstacle could be more appropriated to calculate the turbulence length.

Hydraulic Diameter is understandable from the name that is related to the diameter of the duct. In specific cases, like for the turbulence length scale, it can be considered another dimension more influential on the characteristics of the flow.

These parameters are also related to kinetic energy and dissipation rate and can be used to calculate them. In fact the turbulent kinetic energy is directly related to the turbulent intensity and the dissipation rate to the turbulence length scale, in these forms:

$$k = \frac{3}{2}(u_{avg}I)^2 \tag{3.35}$$

and

$$\epsilon = C_{\mu}^{\frac{3}{4}} \frac{k^{\frac{3}{2}}}{l}. \tag{3.36}$$

There other ways to determine these two turbulence parameters but this topic will be explored in the case studies presentation.

Wall boundary condition

It could be useful to explain a bit more about wall boundary condition. This is used to bound fluid and solid regions. By default it is defined as a stationary wall and a no-slip condition is applied to it. In particular, this predicts that flow at a solid boundary must have zero velocity relative to the boundary. At the wall boundary, the shear stress is defined as

$$\tau_w = \mu \frac{\partial v_{\perp}}{\partial n} \tag{3.37}$$

where $v_{\perp}$ is the component of velocity perpendicular to the wall (fig. (3.5)). However, turbulent flows are significantly affected by the presence of walls, even though respects the no-slip conditions. Near walls, viscous influxes reduces the tangential velocity fluctuations and kinematic blocking reduces the perpendicular fluctuations.

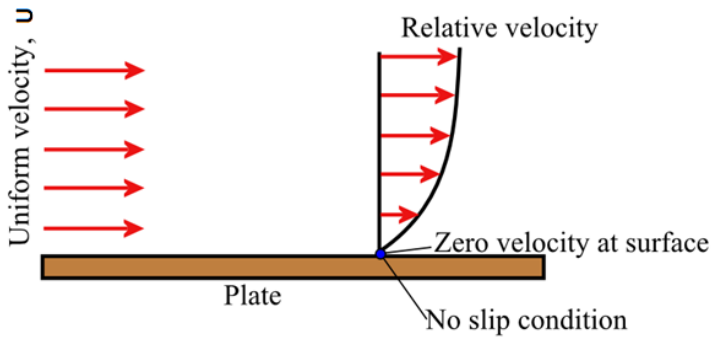

Figure 3.5: Representation of no-slip condition

Considering the outer part, turbulence increases by the production of turbulent kinetic energy caused by the large gradients in mean velocity. By default in the software, the viscous region closer to walls is not resolved. Instead, it is possible to use semi-empirical functions called wall function. For this reason, it is not necessary to modify the turbulence models to account for the presence of the wall. However, in case of k-ϵ model, Fluent applies Standard Wall Functions.

Momentum

Near-wall velocity follows a linear law due to the viscous effects

$$U^* = \frac{1}{k}\ln(Ey^*) \tag{3.38}$$

and

$$U^* \equiv \frac{U_P C_\mu^{1/4} k_P^{1/2}}{\tau_w/\ rho} \tag{3.39}$$

and

$$y^* \equiv \frac{\rho C_\mu^{1/4} k_P^{1/2} y_P}{\mu} \tag{3.40}$$

where k is the von Karman constant, E=9.8 is an empirical constant, U_P k_P are the mean velocity and the turbulence kinetic energy at point P, y_P defines the distance from P to the wall and μ is the dynamic viscosity of the fluid.

Turbulence

In the cells close to the wall, the energy production term G_k in equations 3.4 and 3.5 is considered in equilibrium with dissipation rate, ϵ. Under these conditions and independently from the model applied, terms are computed as:

$$G_k = \tau_w \frac{\tau_w}{k\rho C_\mu^{1/4} k_P^{1/2} y_P} \tag{3.41}$$

$$\epsilon = \frac{C_\mu^{3/4} k_p^{3/2}}{k y_P} \tag{3.42}$$

3.5 Numerical grid and discretization method

For all the studies, considering the geometries, structured grids have been chosen. Is possible to have a variable density of subdivisions and different models may have different meshes. The choice of calculation domain and the associated grid (or mesh) has been recognized as being very important to the results of the calculations. It is not just a matter of the size of the individual cells that comprise the grid, but also their shape and orientation. Generally speaking, the density of the grid needs to be larger in regions of high spatial gradients and in regions of particular interest. The orientation of the cells relative to the local flow direction is important, because it can lead to spurious numerical diffusion. An important parameter is the number of cells in the domain. This impacts directly on the memory required

and on the CPU time. For a given domain size, the number of cells determines the grid sizes (i.e. the distances over which spatial gradients are evaluated), which is important for convergence and accuracy. However, for simplicity the most regular has been adopted and, moreover the finite volume method, which implies that scalar quantities are calculated and stored in the middle of cells volume. Face values ϕ_f are required for the convection terms and must be interpolated from the cell center values. In order to accomplish this, has been used the second order upwind scheme. This method is based on approximating the derivatives appearing in the partial differential equations by a Taylor expansion up to second order. Generally, this method can be seen as a scheme, which states that the scalar at the downwind node ϕ_i^{n+1} depends on value of scalar in upwind nodes ϕ_i^n, on time step ∂t and on spacial step ∂x. Applied to one dimensional motion equation,

$$\frac{\partial u}{\partial t} = a\frac{\partial u}{\partial x} \tag{3.43}$$

and this scheme becomes

$$u_i^{n+1} = u_i^n - \Delta T(a^+ u_x^- + a^- u_x^+). \tag{3.44}$$

The parameters, u_x^- and u_x^+, are defined as

$$u_x^- = \frac{3u_i^n - 4u_{i-1}^n + u_{i-2}^n}{2\Delta x} \tag{3.45}$$

$$u_x^+ = \frac{4u_{i+1}^n + u_{i+2}^n - 3u_i^n}{2\Delta x}. \tag{3.46}$$

The software stores discrete values of scalar, ϕ, at cell centers, and also the face values, ϕ_f, are necessary for the convection term in each equation. This is possible through an upwind scheme, where upwind means that ϕ_f is derived from quantities in upstream cells, considering the direction of the normal velocity, v_n. Fluent allows the user to decide between several upwind scheme: first order upwind, second order upwind, power law, and QUICK scheme. In the cases here presented, has been chosen a second order upwind. In this approach, higher-order accuracy is achieved at cell faces through a Taylor series expansion of the cell-centered solution about the cell centroid. Thus when second-order up winding is selected, the face value ϕ_f is computed using the following expression:

$$\phi_{f,SOU} = \phi + \nabla\phi \cdot \vec{r} \tag{3.47}$$

where ϕ and $\nabla\phi$ are the cell-centered value and its gradient in the upstream cell, and $\vec{r}$ is the displacement vector from the upstream cell centroid to the face. This needs the determination of the gradient in each cells. However, the gradient $\nabla\phi$ is limited so that no new maximum or minimum are introduced. The methods used in this software to estimate the gradient are Green-Gauss Cell-Based, Green-Gauss Node-Based and Least Squares Cell-Based. The last one is the one applied to the subsequent simulations.

Least Squares Cell-Based

In this method the solution is assumed to vary linearly. Referring to figure 3.6, is possible to formulate the variation in cell values between two cells along $\partial\vec{r_i}$, from the centroid of one to the centroid of the other one, in this way:

$$(\nabla\phi)_{c0} \cdot \Delta r_i = (\phi_{ci} - \phi_{c0}) \tag{3.48}$$

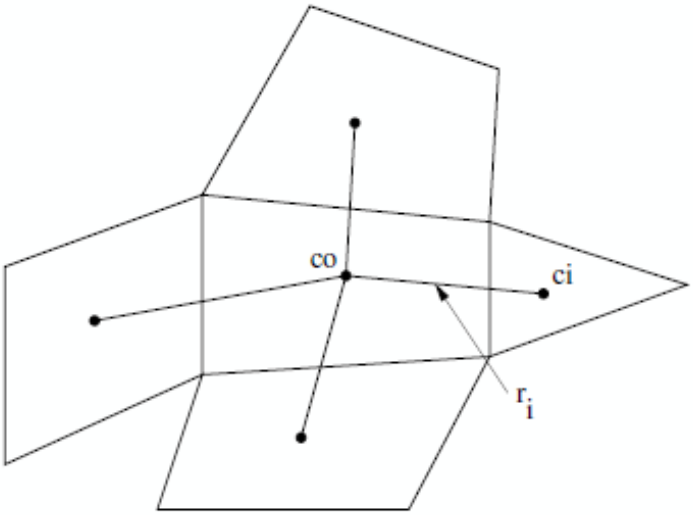

Figure 3.6: Cell centroid evaluation (Fluent Inc, 2006)

Considering the same equations (3.48), it is possible to write the same for all the cells in figure 3.6, obtaining the form, written in a compact form,

$$[J](\nabla\phi)_{c0} = \Delta\phi, \tag{3.49}$$

where [J] is the coefficient matrix which is purely a function of geometry. The interest is to determine the cell gradient by solving the minimization problem

for the system of the non-square coefficient matrix in a leastsquares sense. The linear system of equations is over determined and can be solved by decomposing the coefficient matrix using Gram-Schmidt process. The decomposition takes into account a matrix of weights for each cell. Referring to the cell-centered scheme, this means that the three components of the weights (W_{i0}^{x}; W_{i0}^{y}; W_{i0}^{z}) are produced for each of the faces of cell c_0. Then the gradient can be calculated by multiplying the weight factors by the difference vector $\Delta\phi = (\phi_{ci} - \phi_{c0})$. When a flow solution is solved on polyhedral meshes the cell-based least squares gradients are recommended for use over the default cell-based gradients. Although, it is better to use the node-based gradients in case of triangular and tetrahedral meshes since they are known to be more stable.

3.6 Convergence Criteria

Unfortunately, there are no universal parameters for judging the convergence of a case. It is possible in Fluent to monitor the convergence dynamically by checking several parameters, such as residuals, statistics and force values. In the study cases, the main focus was on the residuals. The software, at each solver iteration, computes and stores the residual sum for each of the scalar, both in scaled and in unscaled form. On a computer with infinite precision, these residuals will go to zero as the solution converges, but a normal pc generates inevitably some errors and then they can not be end up as zero. In fact, the residuals decay to some small values, defined as round-out, and then stop changing, known as level out. For single precision computations, residuals could decries as many as six orders of magnitude before hitting round out. Double precision residuals can drop to twelve orders of magnitude. Referring to a scalar ϕ, the conservation equation at a cell P can be written as

$$a_P \phi_P = \sum_{nb} a_{nb} \phi_{nb} + b, \tag{3.50}$$

where a_P is the center coefficient, a_{nb} are influence coefficients for closest cells, and b is the contribution of the constant part of the source term and boundary conditions. The residual R_ϕ computed by Fluent is the sum over all the computational cell of P, defined as unscaled, with this form

$$R_\phi = \sum_{cells P} |\sum_{nb} a_{nb} \phi_{nb} + b - a_P \phi_P|. \tag{3.51}$$

However, it is not simple to judge the convergence by the unscaled form and is

better to use the scaled residuals, computed by pressure-based solver, defined as

$$\bar{R}_{\phi} = \frac{\sum_{cellsP} |\sum_{nb} a_{nb}\phi_{nb} + b - a_P\phi_P|}{\sum_{cellsP} |a_P\phi_P|}. \tag{3.52}$$

The software plots scaled residuals for all relevant scalars of simulations, letting the users to monitor changing in scalar residuals.

$$R_{\phi} = \frac{R^{\phi}_{iterationN}}{R^{\phi}_{iterationM}}, \tag{3.53}$$

In addition, can be set a residual cut off letting to stop iterating if residuals become smaller than this value. The software permit to normalize the residual by dividing by the maximum residual value after M iterations, where M is set by user (M = 5 by default).

Chapter 4

Case studies and results

The topics presented in the previous chapters have served to introduce and develop theoretical and research aspects that will be published in the following chapter. In fact, in this chapter several cases of ventilation in different structures will be presented and developed. In specific, a natural ventilation study of a glass greenhouse has been conducted, with a specific interest on the evaluation of the effect of shading screens on the air flow inside the structure. Moreover, the results of this research led to a deepening on the shading screens item in agriculture sector. Finally, the last case involved the ventilation of a cellar. In specific, considering the internal environmental condition of a particular wine cellar, it was hypothesized the application of an optimized designed ventilation system.

4.1 Greenhouse study

As outlined in the section 2.3, the control of indoor climate condition can have a significant role in plant growing in greenhouses. The parameters involved are temperature, humidity, air velocity and CO_2 or O_2 concentration. In this chapter, a case study of natural ventilation of an experimental greenhouse of the University of Bologna, placed in Imola district, is presented.

4.1.1 Case presentation

The greehouses usually are controlled by automated systems, frequently based on temperature values. As explained in chaper 1, in mediterrenean climate cooling of greenhouses is a problematic aspect but also has a key role to improve crop production and quality. There are several approach to obtain the decrease of temperature and humidity. For example, in natural ventilation, the most applied way is the manegement of opening vents, the placement of shading screens for the

solar radiation and the choice of different materials for the cover. Many numerical studies of natural ventilation inside a greenhouse are available in literature and they try to consider all the possible influences. In fact, the natural ventilation at zero or low wind velocity was investigated by Mistriotis et al. (1997). Instead, Baxevanou et al. (2010) used the CFD for studying the effect of solar radiation, taking into account the thickness of the cover, its spectral optical and thermal properties by a 2D model. These were just two examples of CFD approach applied in greenhouse climate studies, aspect already disclosed in section 2.3.1. In fact, the scientific literature points out the importance of further improving management and design criteria to optimize natural ventilation in greenhouses also through in-depth analyses of specific aspects such as the choice of covering materials or the effects of shading screens. Therefore, the aim of this case study is to numerically investigate the natural ventilation of a glass greenhouse, under different wind velocity, adopting a 3D modeling approach. Moreover, a focus on how internal sun-shading screens can affect the ventilation was carried out, trying to understand what changes between the two configurations (without and with screens). For doing this, it has been necessary also to find a methodology for measuring mechanical properties, related to fluid-dynamics, of this screens type.

Greenhouse description

The greenhouse considered for this study consists in a three spans greenhouse of the Department of Agricultural and Food Sciences of the University of Bologna, placed in Imola. Precisely it is located 44.337340 °N latitude, 11.718647 °E longitude and 72 m altitude, about 30 km east of Bologna. The layout of the greenhouse is shown in figure 4.1. The axes of the Cartesian coordinate system was set parallel to the sides of the greenhouse plant. Three access doors are located on the NE wall of the building. The greenhouse covers an area of 304.8 m^2 and each span is 8 m wide, 12.7 m long, and 4 m high at eave, with 5.5 m maximum height (pitch slope is 40%). The pavement is in concrete, the structure in steel with a cover of 4 mm tempered glass. In each span, there are two roof vents (B) and (C) with opening angle of 25° and length of 1.5 m. Besides, there are two lateral openings (A), of the same size, on the SE and NW walls. These vents are continuous for all the length of the greenhouse. The area of each vent is 8.1 m^2, for a global opened area of 24.2 m^2. The dimensions of the vents, related to the ones of the structure, are important for an optimal design of a greenhouse. For mild climates, a significant parameter is the ratio between the openings area and greenhouse floor area, which, from literature, should be recommended between 0.18 and 0.29 but from experiences the ratio suggested is 0.18 0.25 (von Zabeltitz, 2011). In this case, the ratio is equal to 0.21 for the global structure and 0.21 for the studied span, both within the more restrictive range for a sufficient ventilation in a greenhouse. The spans are indoor areas

separated by glass walls and connected through internal doors. The investigations have been focused on the South-Est span, highlighted in Fig. 4.1. This span, the first shown by Fig. 4.2, is provided with three benches with an aluminum structure. This area is arranged to experimental and educational activities related to propagation, protection, nutrition, and programming of phenological phases of potted and soil less ornamental plants. Furthermore, it is applied to directly investigate the micro-climate management in a protected environment, to test the interactions between climate parameters and plants growth and for the validation of CFD models (Benni et al., 2016, 2017). In fact, the equipment allows to regulate independently the indoor conditions of the spans by means of a computer, which controls heating and cooling systems, vent opening, and shading curtains.

As introduced before, this study focuses on a case of wind-driven natural ventilation, i.e. an internal ventilation induced by the external wind entering from the openings. Indoor temperature and relative humidity are monitored in each span with 10 min acquisition time; outdoor meteorological data of illuminance, temperature, wind speed and direction are collected with the same frequency. Data of wind direction, related to a period of 2 months (May and June), have been observed in order to evaluate the probability of SE wind, in specific $270° \pm 30°$ direction. It has been noticed that the wind was coming from SE for more than 50% of the data recorded. Moreover, the data recorded during the measurements campaign showed an 84% of wind direction values in the desired range, during the time of measurements, and a 52% during the entire day.

4.1.2 Case modeling

The first step of the modeling has been the definition of the geometrical domain of the case. A geometrical model through gambit of the greenhouse inside a bigger domain was carried out through Gambit. In particular, the global dimensions were decided based on several studies from literature (Gromke et al., 2008; Rong et al., 2015; Boulard et al., 2002; Bournet et al., 2007). Considering the greenhouse height as reference (H), the dimensions of the domain are presented in figure 4.3 (161.5 m $\times$ 63.5 m $\times$ 27.5 m).

However, due to the computational power available for this study, it was decided to create an alternative model with reduced dimensions, in specific 76 m $\times$ 50.7 m $\times$ 22 m. This was obtain considering the height of the gutter(4 m) as reference for deciding the distances of inlet and outlet from the structure. After the creation of similar grids, a comparison between the results obtained, for a simple case of constant velocity incoming from the inlet, was carries out with the two different domains. As expected, the air flow velocity close to the buildings and, mainly, inside the first span were considerable the same.

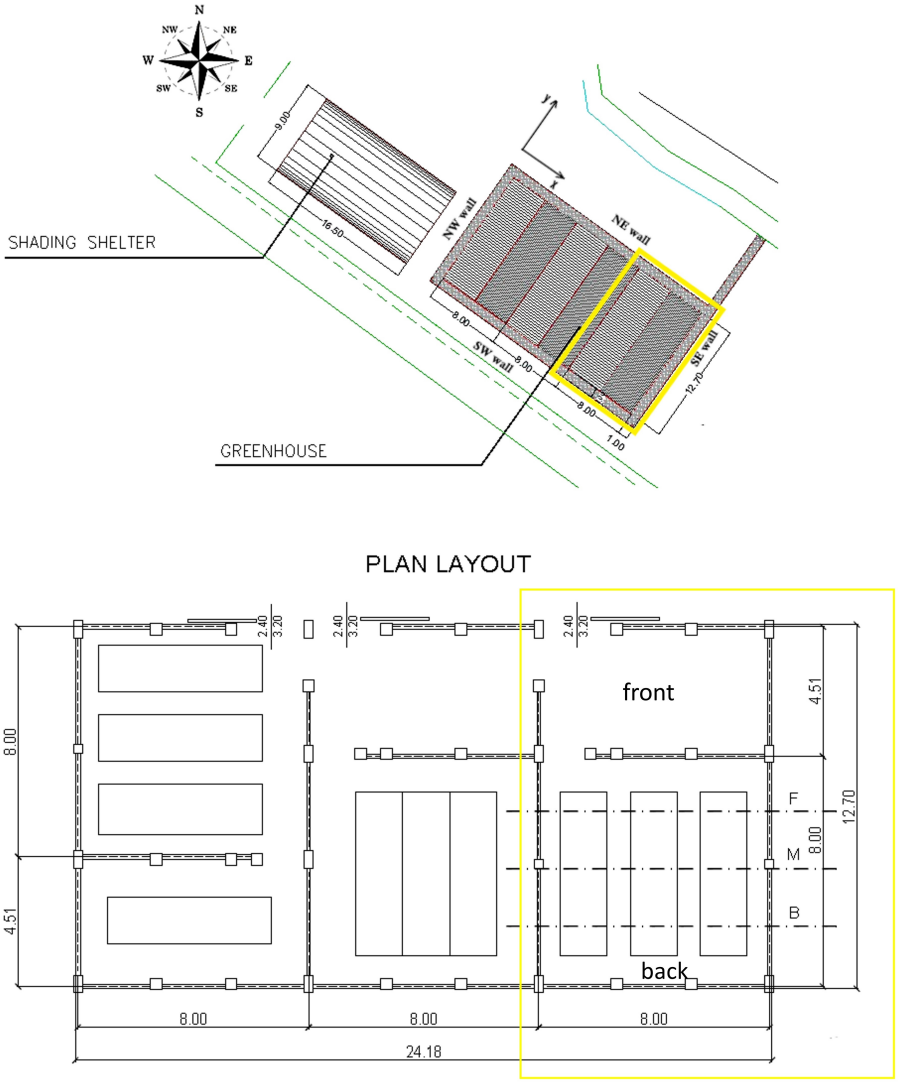

Figure 4.1: Overall layout of the greenhouse (top) and detailed drawing of the section marked in the yellow frame (bottom), in both cases.

In both cases, the greenhouse numerical domain is adherent to the real geometry, in which there is a separation wall, dividing the spans in two, called front and back, as shown in Fig. 4.1. The benches located in the first span in the cultivation zone have been modeled as parallelepipeds, with a distance of 1 m from the back wall, 1.49 m from the separation wall, at a high of 0.65 m. The greenhouse has been modeled as an empty building, in order to obtain results independently from the quantity or type of plants inside the structure, and on their arrangement.

Figure 4.2: Picture of the greenhouse studied.

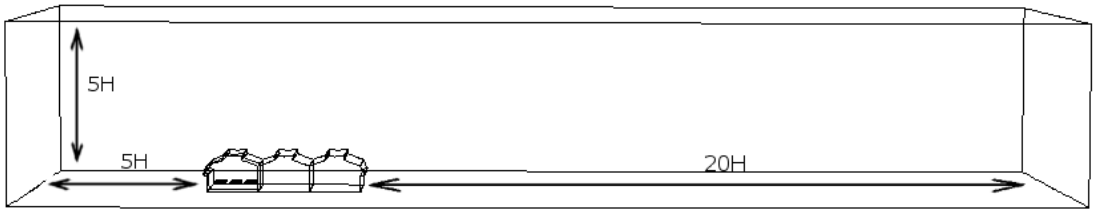

Figure 4.3: 3D model of the complete domain considered in the simulations, with the specified dimension of the model and the wind direction and profile.

The benches have been modeled as obstacles for the fluid flow with the shape of parallelepipeds. Moreover, in the model considering the presence of the screens, these were created as surfaces. They were placed vertically close to the lateral vent side and horizontally at gutter level.

Boundary condition details

As regards the boundary conditions, a *Symmetry* boundary conditions have been considered on the top and lateral sides of the computational domain, to enforce a parallel flow. At the boundary downwind of the greenhouse, where the fluid leaves the computational domain, an *outflow* boundary condition has been used, to force all derivatives of the flow variables to vanish, corresponding to a fully developed flow (Gromke et al., 2008; Di Sabatino et al., 2007). All the surfaces composing the greenhouse are defined as walls, excluding vents imposed as interiors and the screens as porous jump. Moreover, it was decided to model the wind velocity as a

neutral atmospheric boundary layer, with the following velocity profile:

$$u(z) = \frac{u_*}{\kappa} \log\left(\frac{z + z_0}{z_0}\right) \tag{4.1}$$

where $u(z)$ is the average wind speed at the height z above the ground, z_0 is the surface roughness, u_* is the friction velocity and κ (0.40) is the von Karman's constant. The standard $k - \epsilon$ turbulence model has been used, with inlet turbulent kinetic energy and dissipation rate profiles specified as:

$$k = \frac{u_*^2}{\sqrt{C_\mu}}\left(1 - \frac{z}{\delta}\right) \tag{4.2}$$

and

$$\varepsilon = \frac{u_*^3}{\kappa z}\left(1 - \frac{z}{\delta}\right) \tag{4.3}$$

respectively, where δ is the atmospheric boundary layer depth and C_μ is a coefficient used to define the eddy viscosity in $k - \epsilon$ models. A standard value of C_μ=0.09 has been chosen, according to (Di Sabatino et al., 2007). The definition of z_0 follows the *Norme tecniche per le costruzioni del 2008*. In this code, it is possible to derive these parameters defining the class of exposition of a site based on geographical location and the roughness of the terrain. In specific, we are located in agricultural area without obstacles, and z_0 can be considered 0.10 and also the wind could be constant for the first five meters.

With these values we verified that logarithmic velocity profile is maintained very well throughout the length of the computational domain, as well as the profiles of k and ε (Di Sabatino et al., 2007). An example of this condition obtained for the case studied is showed in figure 4.4.

Fluent used the turbulence quantities specified in equations (4.2) and (4.3) to derive the Reynolds stresses at the inlet from the assumption of isotropy of turbulence. A standard discretization scheme was used for pressure and second order upwind discretization schemes were used for momentum, k and ϵ to increase the accuracy and reduce numerical diffusion. The SIMPLE scheme was used for the pressure-velocity coupling. FLUENT used an iterative method to solve the algebraic system of equations. A termination criterion of 10^{-6} was used for all field variables (Gromke et al., 2008). All the simulations were run in steady-state conditions. The simulations were performed considering several cases with inlet wind velocity magnitudes: $v_{ref} = 1$; 2; 4; 8 m/s at 5 m high from the ground with south-est direction as showed in figure 4.5.

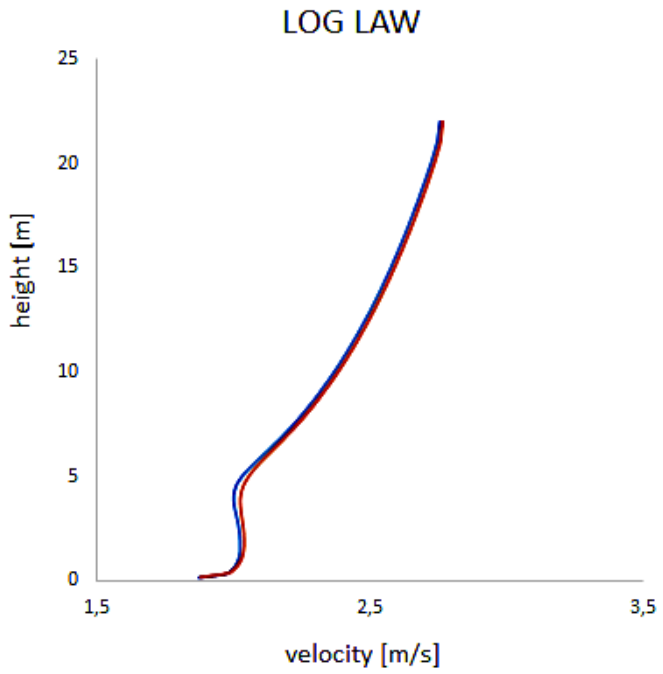

Figure 4.4: Logarithmic wind profile in two different positions, at 4 m from inlet (blue curve) and outlet (red curve) respectively.

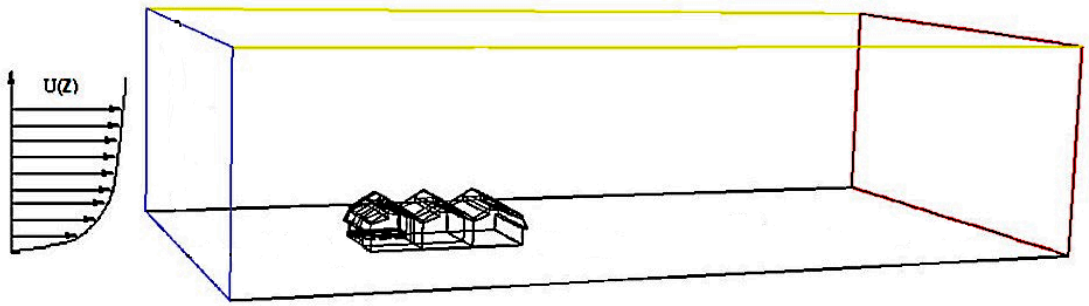

Figure 4.5: 3D domain with wind direction from SE.

Grid convergence

The mesh was built with structured hexahedral elements with a finer resolution close to the ground and within the greenhouse. A grid convergence study was been conducted in order to identify the independence of the results from mesh dimensions. The study was achieved by running simulations on five different structured meshes, with the same set up. In order to differentiate zones of interest, the meshes was

divided into 2 different parts, with specific cells dimensions. In fact, each mesh had elements with dimensions d_1 inside the greenhouse, and dimensions starting from d_2 and growing to d_3 outside the greenhouse, with a growth factor of 1/3. Table 4.1 shows the values of the mesh dimensions and total number of elements N for all the grids considered.

Table 4.1: Size of the meshes used for convergence study

Mesh n.	d_1(m)	d_2(m)	d_3(m)	N
1	0.5	0.6	1	2×10^5
2	0.4	0.5	1	4×10^5
3	0.3	0.4	1	6×10^5
4	0.2	0.3	1	1×10^6
5	0.1	0.2	1	3×10^6

For studying the grid convergence, vertical velocity profiles were extracted and compared. In order to estimate the variations between the results obtained, the progressive differences of the resultant profiles, obtained with each grid, were calculated by the $\|L\|_\infty$ norm and by the $\|L\|_2$ norm. Before computing these values, it was necessary to interpolate the velocity values (vector of n dimension depending on the number of cells) obtained from the software elaborations, because they had a different length. After this first step, it was possible to calculate $\|L\|_\infty$ by:

$$\|L\|_\infty = max(|v_a - v_b|) \tag{4.4}$$

where v_a and v_b are velocity values referring to two different meshes. Usually, this is calculated between two meshes, starting from the coarsest to finest progressively. Instead, the expression of $\|L\|_2$ is reported in equation 4.5,

$$\|L\|_2 = \sqrt{\sum_1^n |v_a^2 - v_b^2|} \tag{4.5}$$

where n is resulting dimension after the interpolation. These calculations were conducted for each profile and then they were averaged in order to have an only value of $\|L\|_2$ and $\|L\|_\infty$ for each mesh difference. Both approaches gave similar results, for this reason only the results of $\|L\|_\infty$ norm were reported. Figure 4.6

shows the convergence results, *i.e.* a plot of $\|L\|_\infty$ norm as a function of the number of mesh elements.

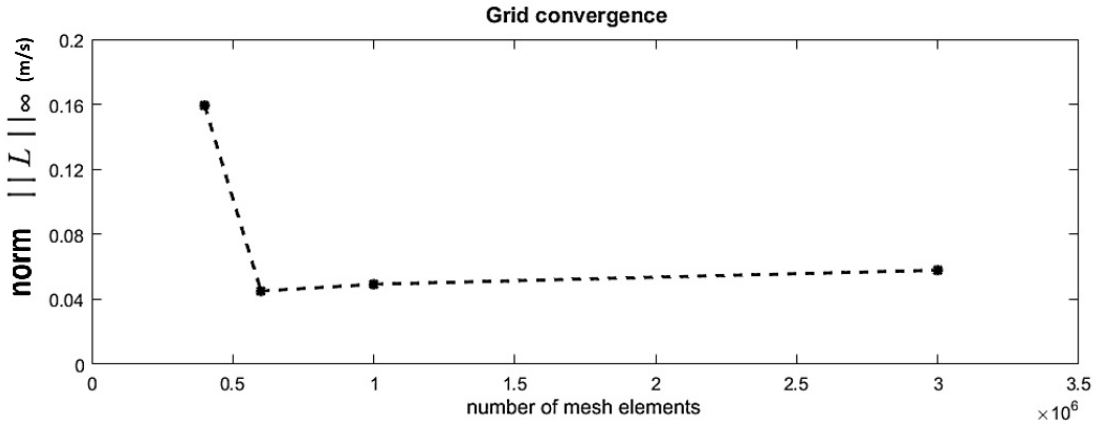

Figure 4.6: Results of infinity norm for grid convergence study.

The curve rapidly decreases, in the first section, to reach the horizontality, with an error of around 0.04 m/s. This means that the convergence was reached between the third grid and the last one, at the last two differences values. For this reason and for caution, the fourth grid (N = 1×10^6) was selected for the subsequent simulations, as a compromise between the accuracy of the results and the computational burden.

4.1.3 Screens characterization

Until now, specific information has been omitted about the screens inside the greenhouse. The screens placed in the structure are shading screens, specifically *XLS-16 firebreak*, for the protection from solar radiation. In particular, three screens have been placed inside the cultivation room. Two internal screens are parallel to the external walls, one to the lateral wall and the other to the back wall; while the third is placed horizontally, between the cultivation room and the roof, at eaves height. The lateral and the back screens are located about 20 cm from the respective walls. Instead, the third screen has a distance of about 15 cm from the back wall and has a separation in the middle of the room of about 15 cm, as represented in fig. 4.7. Moreover, black shading and anti-hail screens are present above the roof, as it is shown in Figure 4.2.

For the screens simulation a porous jump modeling approach has been used in the CFD code, already presented in section 3.2.2. In fact, the screens are modeled as a thin porous surface with a finite thickness δ over which the pressure change

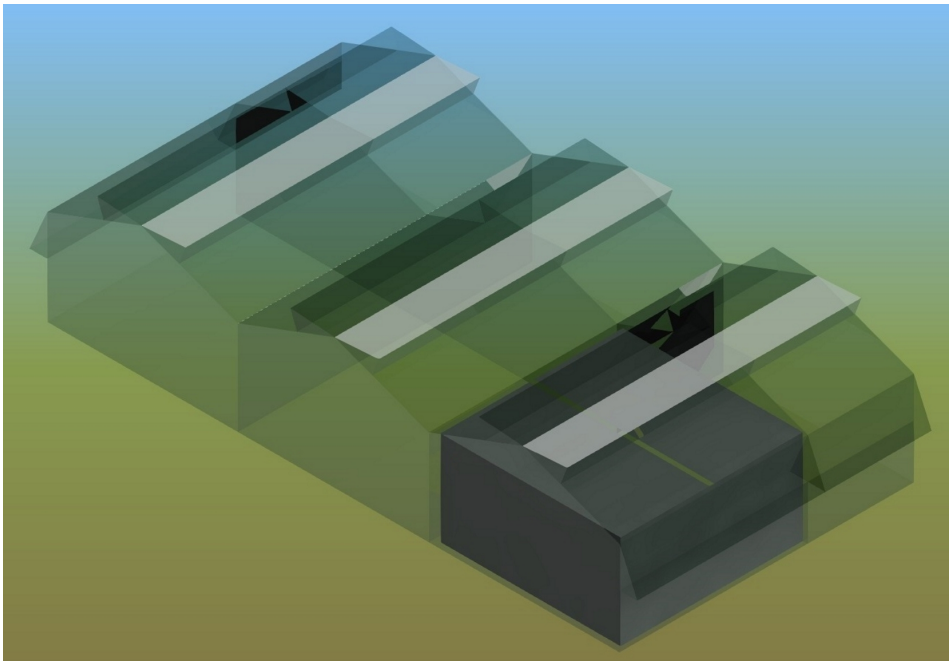

Figure 4.7: 3D sketch of the screens configuration within the greenhouse.

Δp is defined as a combination of Darcy's law and an additional inertial loss term:

$$\Delta p = -\left(\frac{\mu}{\beta} v + C_2 \frac{1}{2} \rho v^2\right) \delta \tag{4.6}$$

where μ is the air viscosity, ρ is the density of air, v is the air velocity, β is the screen permeability and C_2 is the pressure-jump coefficient. These parameters were unknown for this type of screen, since they are not reported in the data sheet.

Porosity measurements

In order to describe the aerodynamic characteristics of the screens, the airflow resistances and the permeability of different textures were evaluated experimentally, according to the ISO9053:1991. According to this, the specific airflow resistance (R_s) and the permeability (α) are given by

$$R_s = \frac{\Delta p \, A}{q_v}, \tag{4.7}$$

and

$$\alpha = \frac{v\,\mu\,\delta}{\Delta p}, \tag{4.8}$$

in which q_v is the volumetric air flow rate through specimens and A is the cross sectional area of test specimen, perpendicular to the flow. These parameters were obtained by testing three different samples of each net, following the protocol, determining airflow resistance, resistivity and permeability ISO9053:1991. In particular, the difference between samples of a net is mainly the deterioration degree that can affect their characteristics. The tests were conducted using the experimental apparatus , shown in figure 4.8, which follows the guidelines and the scheme of the International Standard ISO9053:1991. The test-specimen was placed in a cylindrical tube which was crossed by a flow rate of air pumped by compressor. The mass flow rate of air was measured by means of a flow-meter Sensirion SFC4000 (with uncertainty 0.005 l/min) and the pressure difference across the test specimen was measured by means of a Sensirion pressure gauge sensor (with uncertainty 0.01 Pa).

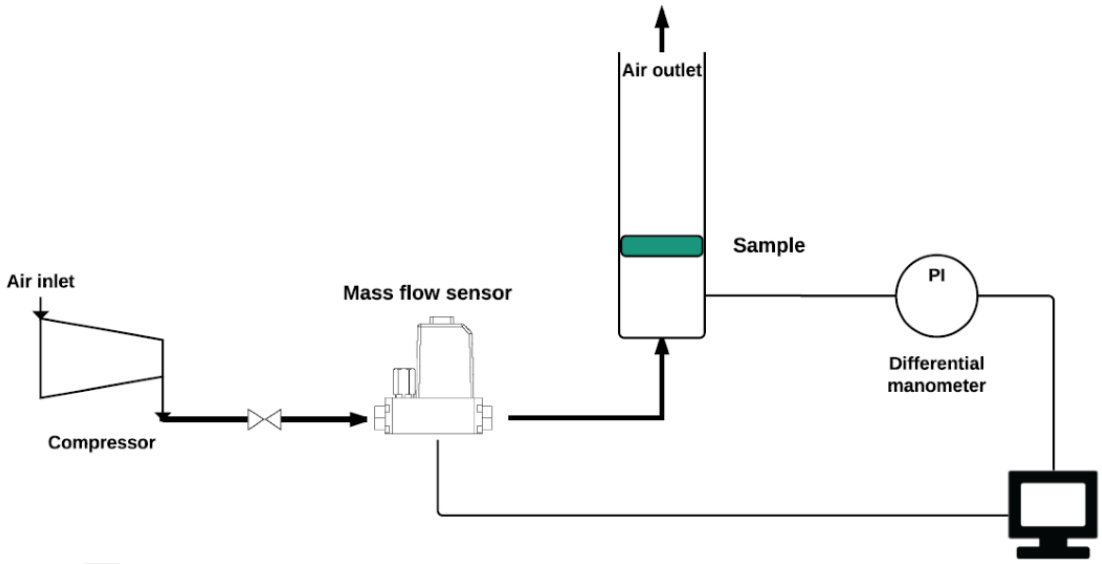

Figure 4.8: Block diagram of the experimental apparatus for air resistance measurements.

On one hand, the samples of the external screens had not showed an appreciable resistivity to the airflow, on the other hand the samples of internal screens have demonstrated a not negligible responses in the tests. For these reasons, the results on the tests on internal screens were reported as follows. Table 4.2 shows the

measured values of Δp as a function of the average air velocity $v = q_v/A$, for three different screens. These materials are used as internal screens in the greenhouse. Table 4.2 also shows the specific resistance R_s and permeability α.

Table 4.2: Results of test, following ISO9053:1991

	Δp (Pa)	v (m/s)	R_s (Pa s/m)	β (m^2)
sample 1	0.19	0.002	80.64	9.81×10^{-11}
	0.54	0.005	112.02	7.06×10^{-11}
	0.90	0.007	124.92	6.33×10^{-11}
	1.28	0.010	133.24	5.94×10^{-11}
	1.66	0.012	138.30	5.72×10^{-11}
sample 2	0.08	0.002	33.59	2.36×10^{-10}
	0.31	0.005	64.33	1.23×10^{-10}
	0.56	0.007	77.68	1.02×10^{-10}
	0.81	0.010	83.97	9.42×10^{-11}
	1.08	0.012	89.94	8.80×10^{-11}
sample 3	0.03	0.002	10.51	7.53×10^{-10}
	0.07	0.005	15.13	5.23×10^{-10}
	0.19	0.007	26.37	3.00×10^{-10}
	0.29	0.010	30.36	2.61×10^{-10}
	0.40	0.012	33.53	2.36×10^{-10}

The first test-specimen shows the highest values of specific resistance. The specific resistances of the three samples, shown by Table 4.2, were plotted in Figure 4.9 as a function of v. The figure shows an asymptotic behavior of R_s for all the three specimens, where the maximum is reached for velocities of bout 0.012 m/s. The results of the specimen with greatest resistance ($R_s = 138.3$ Pa s/m and $\beta = 5.72 \times 10^{-11}$ m^2) were adopted as input for material properties in the simulations, in order to account for the most conservative case of screen effects on airflow dynamics.

Due to a restrict range of velocity reachable from this apparatus, the transition from laminar to turbulent flow was not completely reached. For this reason, in a conservative approach, was assumed to consider equal the contributes of the components of the Darcy-Forchheimer equation. Then, the value of the inertial

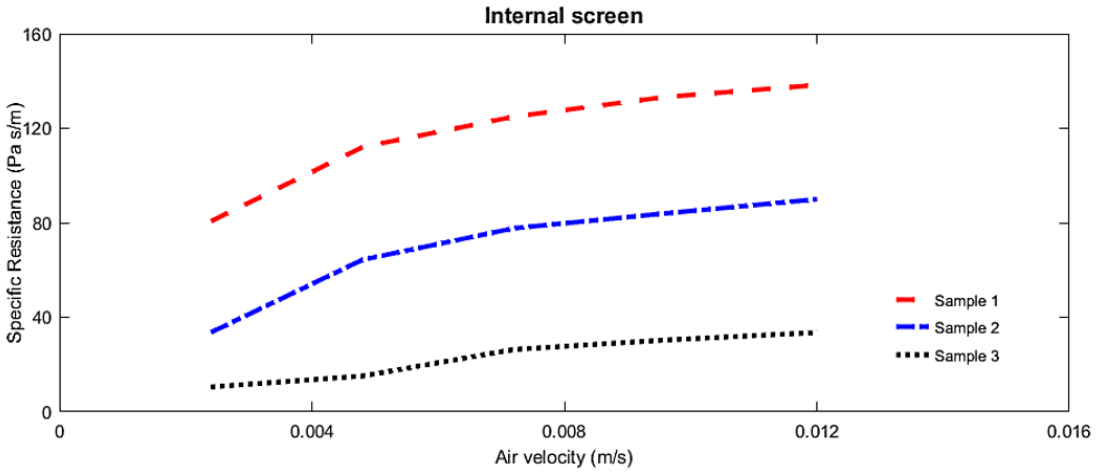

Figure 4.9: Specific resistance of samples, depending on the air flow velocity.

coefficient C_2 was obtained, as

$$C_2 = \frac{\Delta p}{1/2\, v^2\, \rho\, \delta} = 4.37282 \times 10^7\, \mathrm{m}^{-1} \tag{4.9}$$

where $\delta = 0.43$ mm ρ=1.25 kg/m^3.

This was a preliminary approach adopted for the screens characterization, in this study. After several researches and insights on the topic, new developments and advances have been obtained. These will be presented in Chapter 5.

4.1.4 Validation Process

The model needs to be validated to be considered reliable for the simulations. The validation can be obtained trough a comparison with measurements in situ. In this case it has been carried out through the comparison of air velocity data measured inside the structure, in a day with wind velocity from SE.

Measurements and instruments descriptions

The measurements were performed in different positions inside the greenhouse (M1-M5), shown by Figure 4.10. The velocity has been measured under controlled environmental conditions, in absence of plants inside the structure.

The measurements have been performed with the screens with the characteristics measured and the positions, presented in section 4.2.1. Our experiments were performed during the morning of a cloudy day with presence of wind blowing from

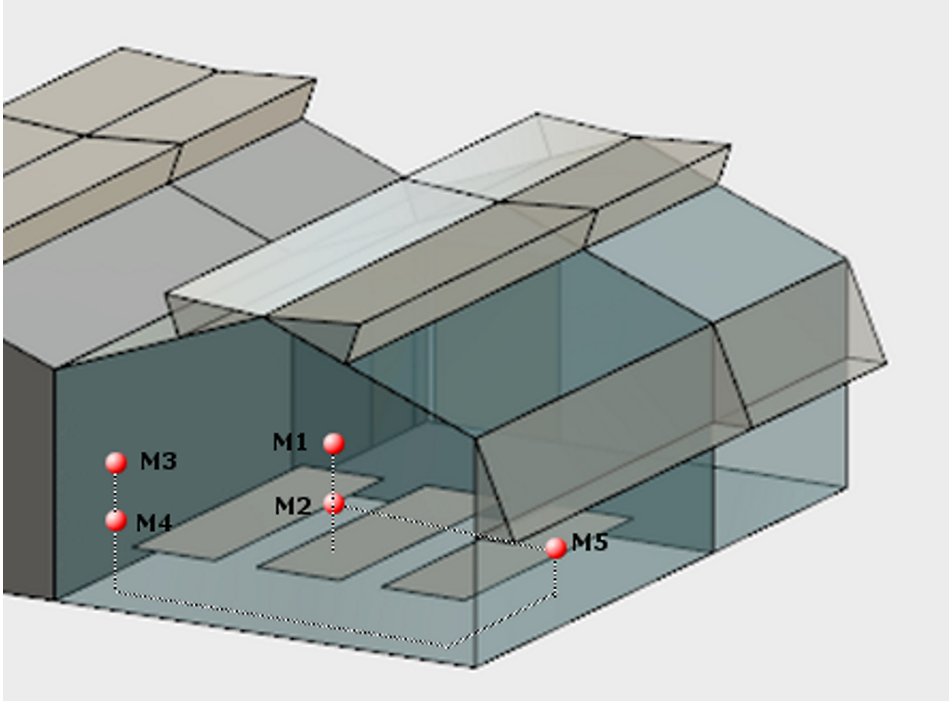

Figure 4.10: 3D representation of measurement points.

SE (July, 20th, 2016). In this way, solar radiation effect, such as the buoyancy forces in the ventilation was considered negligible (Baxevanou et al., 2010). For each measuring position, a data set was collected with 60 measurements, with 1 s sampling step. The velocities have been measured by an hot-wire anemometer (Delta Ohm, with an uncertainty of 0.01 m/s).

Model validation

The measures of velocity collected were compared with the values extrapolated from the simulation. The resulting velocity value was obtained as the average of the data collected, and the respective error was estimated as the standard deviation.

The uncertainty due to the measurements of sensors position was assessed equal to 0.05 m, by considering the uncertainty of the instruments and of the operators. These results were compared to the velocity profiles obtained by the simulations. Figure 4.11 shows that the experimental data are in a good agreement with the respective simulated profiles.

The measured and numerical velocities obtained in the positions are shown by Table 4.3. The biggest difference is about 0.02 m/s, corresponding to the position M4. This point is located at 2 m height, between the first bench and the internal wall. In the other measurement positions, the difference between measured and

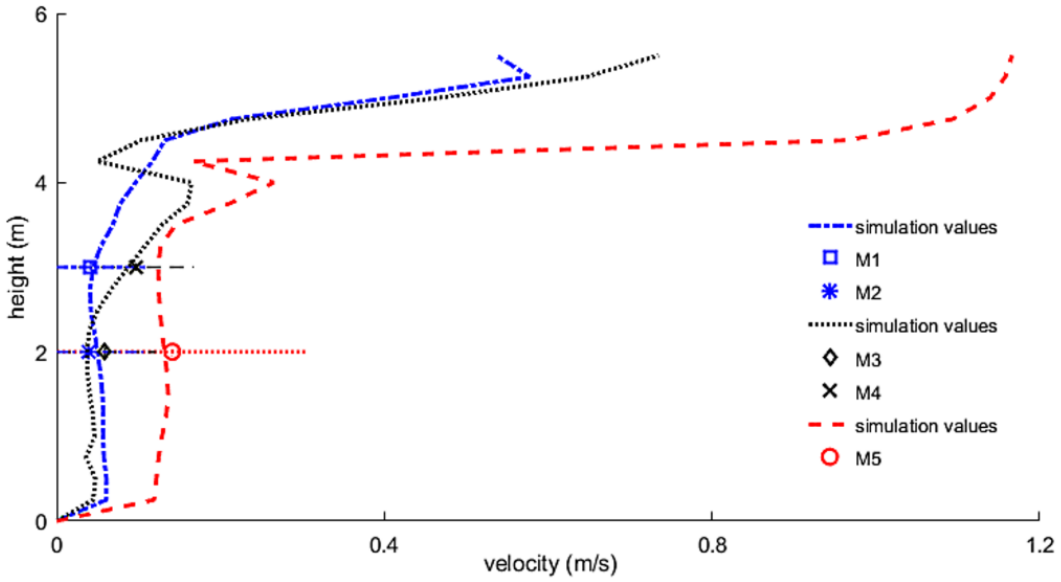

Figure 4.11: Comparison between simulated profile and punctual data obtained by measurements

Table 4.3: Comparison between measurements and simulations

Measurements	Measured velocity (m/s)	Simulated velocity (m/s)	Error %
M1	0.04	0.044	10
M2	0.04	0.049	22.5
M3	0.10	0.074	26
M4	0.06	0.039	35
M5	0.14	0.136	2.8

numerical velocities are lower than 30%. The model was considered validated and used for the simulations with different v_{ref}.

4.1.5 Simulation results

The effects of the shading screens on the air velocity distribution inside the greenhouse have been studied under the following wind speeds: 1, 2, 4, 8 m s^{-1}. The results are shown on three vertical planes M (middle), F (front) and B (back). Plane F and B have been defined, starting from the central plane M, two meters

towards the front and two meters towards the back of the greenhouse respectively, as represented in Figure 4.1. Figure 4.12 shows the vectors of velocity colored depending on magnitude on the plane F, for the case of 4 m/s.

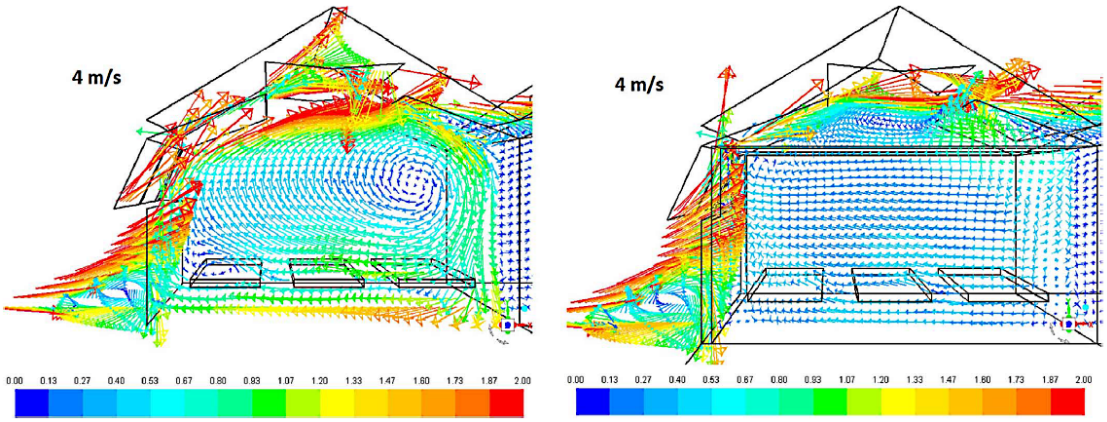

Figure 4.12: Vectors distribution in plane F, exemplified by the case with wind speed of 4 m/s. The vector maps in the left column correspond to the configuration without screens, while the vector maps in the right column correspond to the configuration with shading screens.

This case is representative of the simulations conducted, as the pattern is substantially the same for the other cases of wind speed considered, albeit with different magnitudes. It can be observed a difference in the flow configuration between the cases with and without shading screens. In the case without screens, a vortex is present at height about $3/4H$, closed to the downwind wall. The dimension of the section of the vortex is approximately half of the area between the floor and roof. In the case with screens, a narrow vortex is present between the screen and the roof, while no vortex is present in the region below. A uniform velocity field, with uniform vectors oriented in the same direction of the wind, is found in the case with screens. Similarly to the case of plane F, figure 4.13 shows the vectors of velocity colored, depending on magnitude on the plane B, for the case with wind speed of 4 m/s.

A difference in the flow configuration between the cases with and without shading screens can be noticed. In the case with screens, a narrow vortex is present between the screen and the roof, while no vortex and a uniform velocity field are present in the region below. In the case without screens, the velocity distribution differs from that one of plane F, as a vortex is present at height about $1/2H$, centrally located, affecting approximately all the area between the floor and roof. Figure 4.14 shows horizontal profiles of velocity magnitude on planes B and M, at a height of the vortex center, *i.e.* at 2.5 m and 3 m respectively, for the case

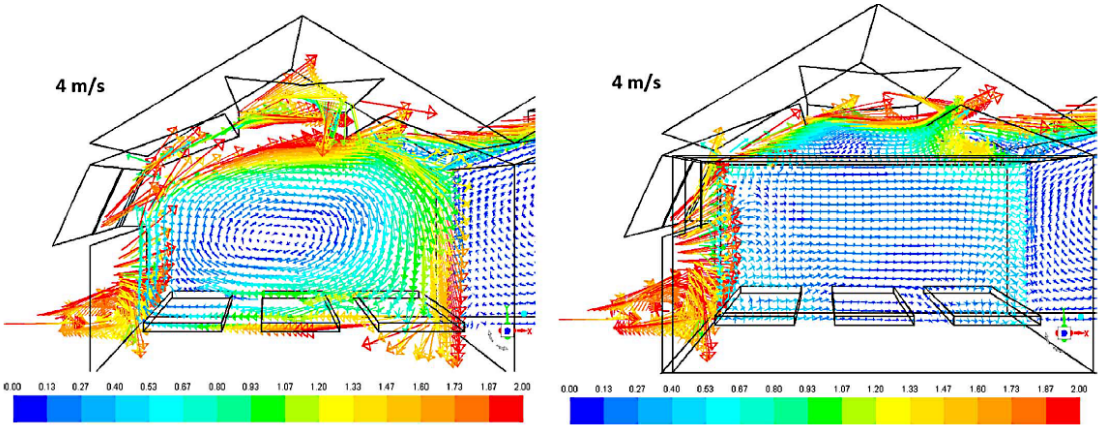

Figure 4.13: Vectors distribution in plane B, exemplified by the case of 4 m/s. The vector maps in the left column correspond to the configuration without screens, while the vector maps in the right column correspond to the configuration with shading screens.

without screens.

In the middle plane, velocity peaks near the walls are higher for all the velocities as well as in the middle plane the region with the minimum of the velocity is larger, in correspondence of the center of the vortex. Moreover, the maximum of the two peaks is reversed in the two planes, and that means that the vortex has a light swirl. These is visible in Figure 4.15 where the pathlines entering from the middle line of the lateral vent A are shown.

The figure shows that the vortex with the same dimensions of the cultivation room is present only in the case without screens. Figure 4.16 shows horizontal profiles of velocity magnitude on plane M, at a height of 4.5 m (*i.e.* above the top screen), for the case with screens, where there is only one vortex in the region above the top screen.

The figure shows that velocities peaks near the walls have a more complex shape than those obtained in the case without screens, such as the vortex in this case is confined between the top screen and the roof.

In figure 4.17, the sections above the gutter height (4.1 m) (a. and b.) and above the benches (0.90 m) (c. and d.) are compared in both cases. In both sections without screens, it is clear that the vortex has a light swirl, from the back section to the front section of the cultivation area, as outlined before. Instead, the sections with screens show the presence of an horizontal vortex that interests all the area. Thus, the presence of screens completely modifies the airflow patterns. In addiction, comparing the cases at gutter level, is clearly visible the interference of the screens on natural air circulation, entering from the lateral vent. In fact, the air

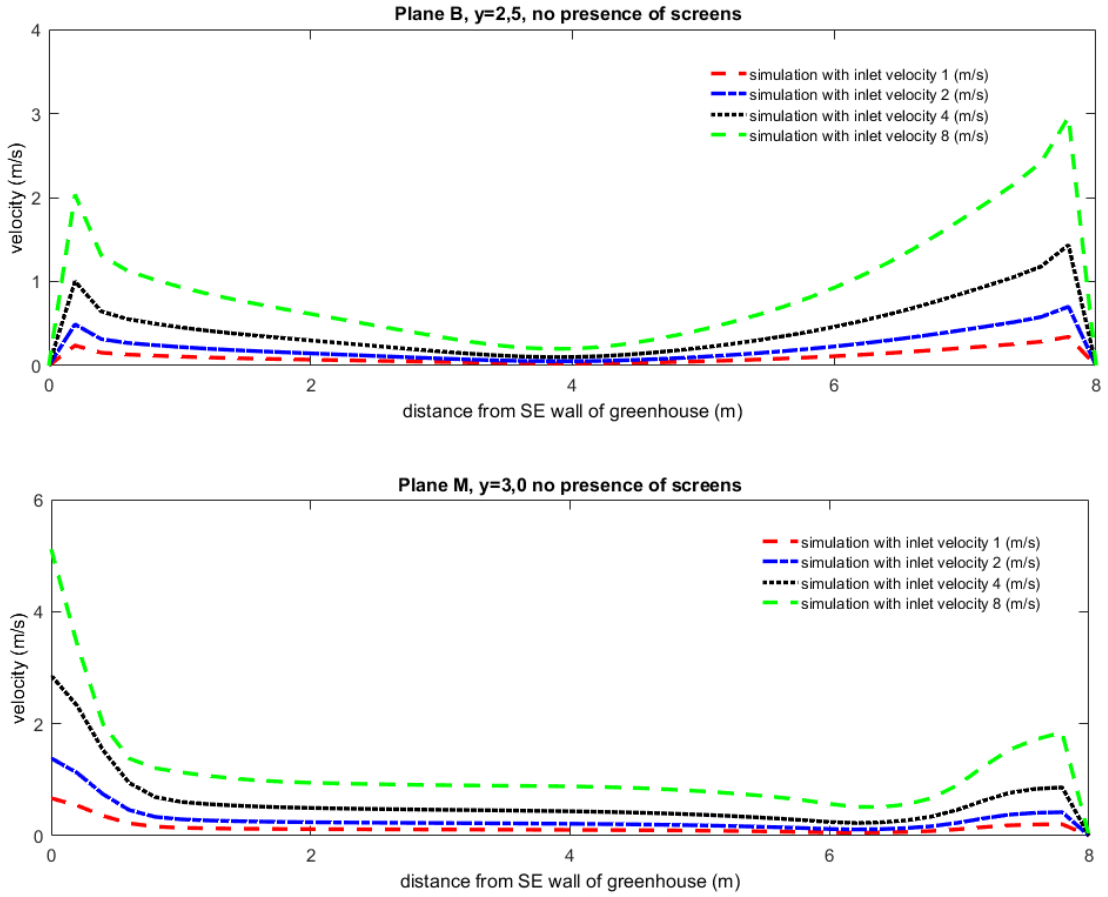

Figure 4.14: Horizontal profiles of air velocities in the middle of planes M and B, without screens

flows incoming from the lateral opening deviate the pattern and, passing through the screens, decrease their velocity. As delineated above, the main differences between the cases with and without screens are related to the range of velocity and to the dimension of the areas occupied by the vortex. The range of the velocity inside the greenhouse increases with the increasing of the inlet velocity, as shown in Table 4.4, both for the case with and without screens. However, for the cases with screens the average velocity inside the greenhouse is about the half of the velocity obtained without the screens for all the inlet velocities, with exception of the case $v_{in} = 1$ m/s.

The highest values of velocity, for plane B, are found near the floor, under the benches for case without screens, visible also in Figure 4.18. On the contrary, in the case with screens the highest values of velocity are found near to the top screens.

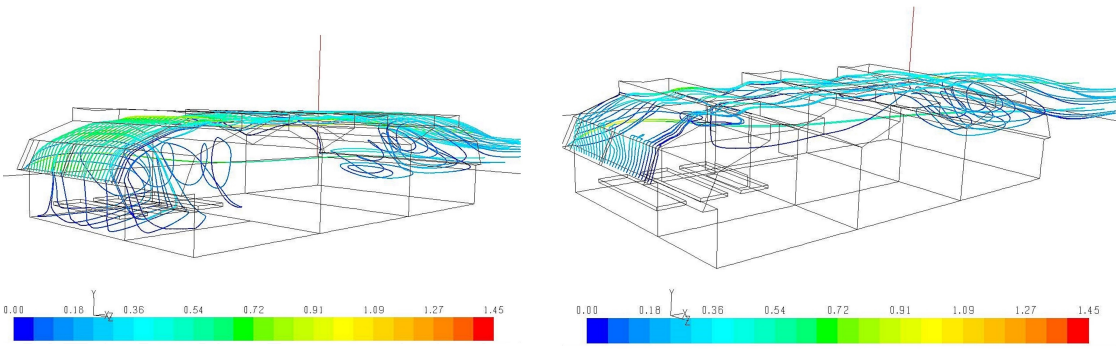

Figure 4.15: Pathlines from the middle of lateral vent, in cases without (left) and with screens (right)

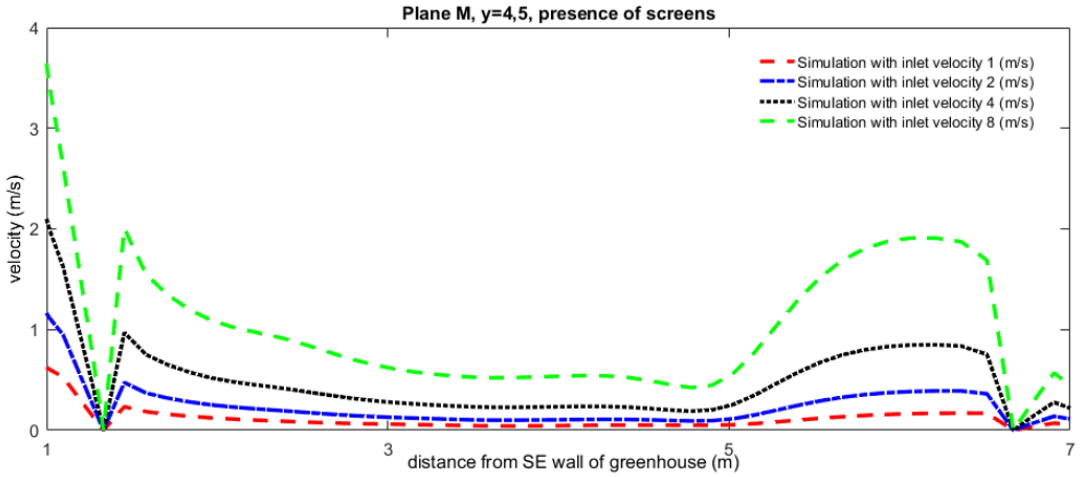

Figure 4.16: Horizontal profiles of air velocities on the plane M, with screens

A similar situation has been noticed in plane F, with comparable velocity values, as shown in Table 4.5.

As it is predictable, the same behavior has been found on plane M, where the velocity map is similar to the one obtained on plane B and F. In order to have a global look of the situations in all, planes, figure 4.18 shows a comparison of the velocity magnitude obtained for the cases with and without screens, on the planes B, M and F, for an inlet wind velocity $v_{ref} = 1$ m/s. The figure shows that, for the case without screens, the area with a velocity in the range $[0.05 - 0.1]$ m/s is smaller than that obtained with screens and reaches the first row of benches, while near the walls the velocity is higher, in the range $[0.3 - 0.4]$ m/s. On the contrary, for the case with screens, the area with a velocity in the range $[0.05 - 0.1]$ m/s covers

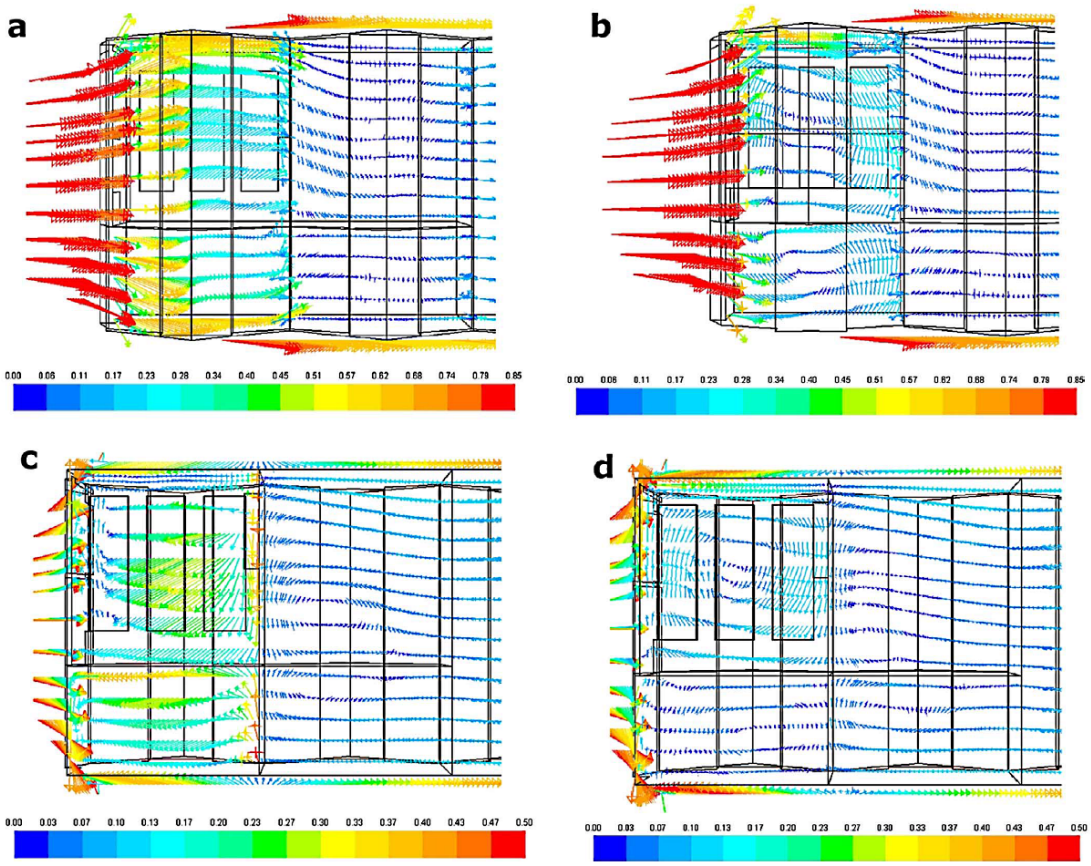

Figure 4.17: Sections along the vertical axis above the gutter height, 4.1 m, (picture a. and b.) and above the benches, 0.90 m, (pictures c. and d.) of case with $v_{ref} = 1$ m/s; in the left column cases without screens and in the right column cases with screens.

almost the entire room and no higher velocities are observed near the walls. In this case the minimum is on the central bench. In the case without screens the distance from the floor of the vortex center increases from backward to forward. From these results, it is clear that the role of the screens on the air flow distribution within the greenhouse is to reduce the magnitude of the velocity of about 50 % and to change the position and the dimensions of the vortexes. Considering the importance of optimal ventilation conditions in the cultivation area, horizontal profiles at a height of 90 cm above the floor, (*i.e.* 7 cm above the benches) have been considered, as shown by Figure 4.19 in order to compare the velocity magnitude near the benches for the cases with and without screens. The figure shows that the influence of the screens becomes more relevant with the increasing of inlet velocity. In fact, the peaks above the benches are higher by more than 50%, for the case of an inlet

Table 4.4: The maximum magnitude of air velocity relative to the plane B. v_{ref} is the characteristic velocity of the simulation, and v_{max} is the maximum velocity found in section B.

v_{ref} (m/s)	v_{max} without screens (m/s)	v_{max} with screens (m/s)
1	$0.30< v <0.35$	$0.30< v <0.35$
2	$0.70< v <0.80$	$0.30< v <0.40$
4	$1.21< v <1.41$	$0.62< v <0.82$
8	$2.42< v <2.82$	$1.21< v <1.64$

Table 4.5: Highest values of air velocity relative to the plane F. The v_{ref} is the characteristic velocity of the simulation, and v_{max} is the maximum velocity found in section F.

v_{ref} (m/s)	v_{max} without screens (m/s)	v_{max} with screens (m/s)
1	$0.35< v <0.40$	$0.25< v <0.30$
2	$0.60< v <0.70$	$0.30< v <0.40$
4	$1.41< v <1.61$	$0.62< v <0.82$
8	$2.82< v <3.22$	$1.23< v <1.64$

velocity of 8 m/s, while for lower inlet velocities, the profiles are more similar. If we assume that the optimal value of air velocity distribution around plants should be in the range $[0.5 - 0.7]$ m/s, the screens in all cases reduce too much the velocity. In fact, in both the sections, the air velocity near the benches is within the range $[0.05 - 0.3]$ m/s for inlet velocities $v_{ref} < 4$ m/s. On the other hand, the results of the simulations without screens show that, in both the sections, the air velocity near the benches is within the range $[0.1 - 0.8]$ m/s for inlet velocities $v_{ref} < 4$ m/s. However, with low inlet velocity $v_{ref} < 2$ m/s, the velocity distribution around the benches is lower than 0.5 m/s for all the cases considered.

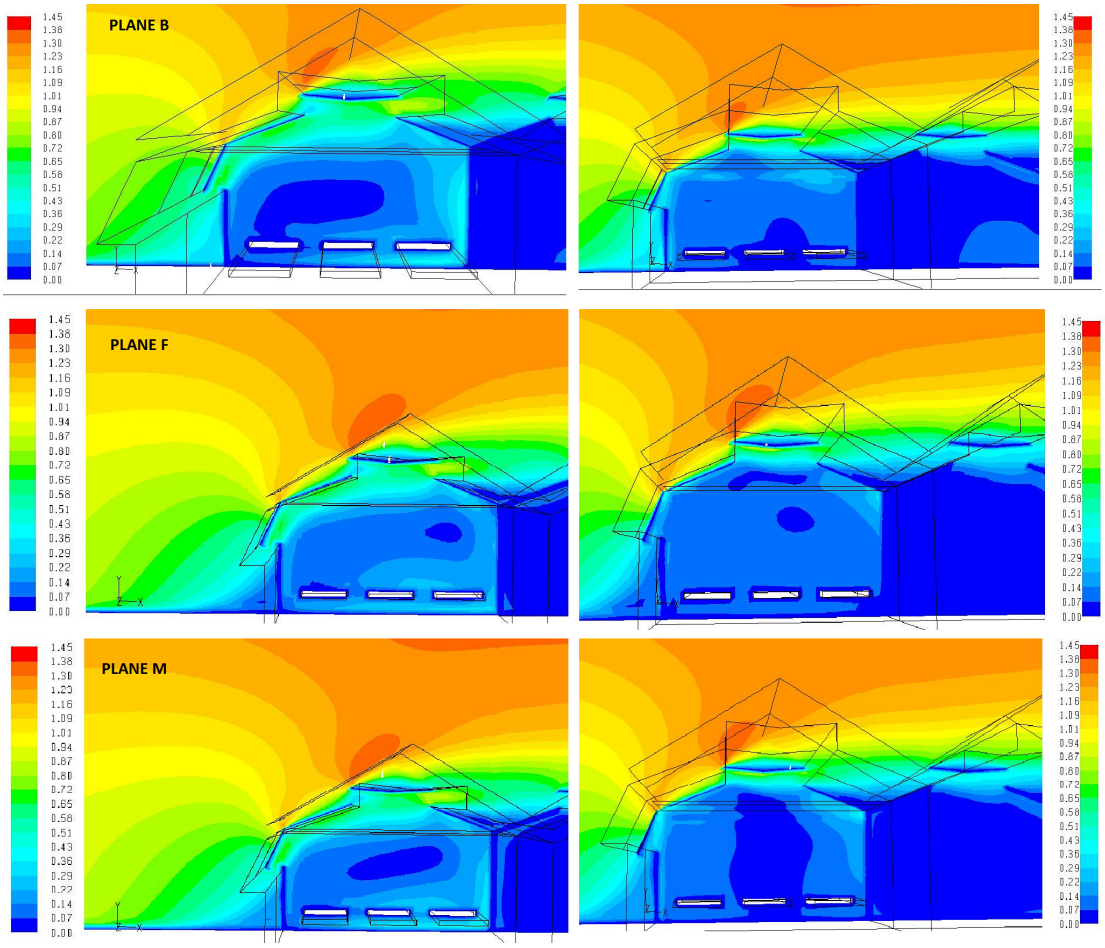

Figure 4.18: Velocity magnitude, without screens (left column) and with screens (right column) on the planes B, M and F.

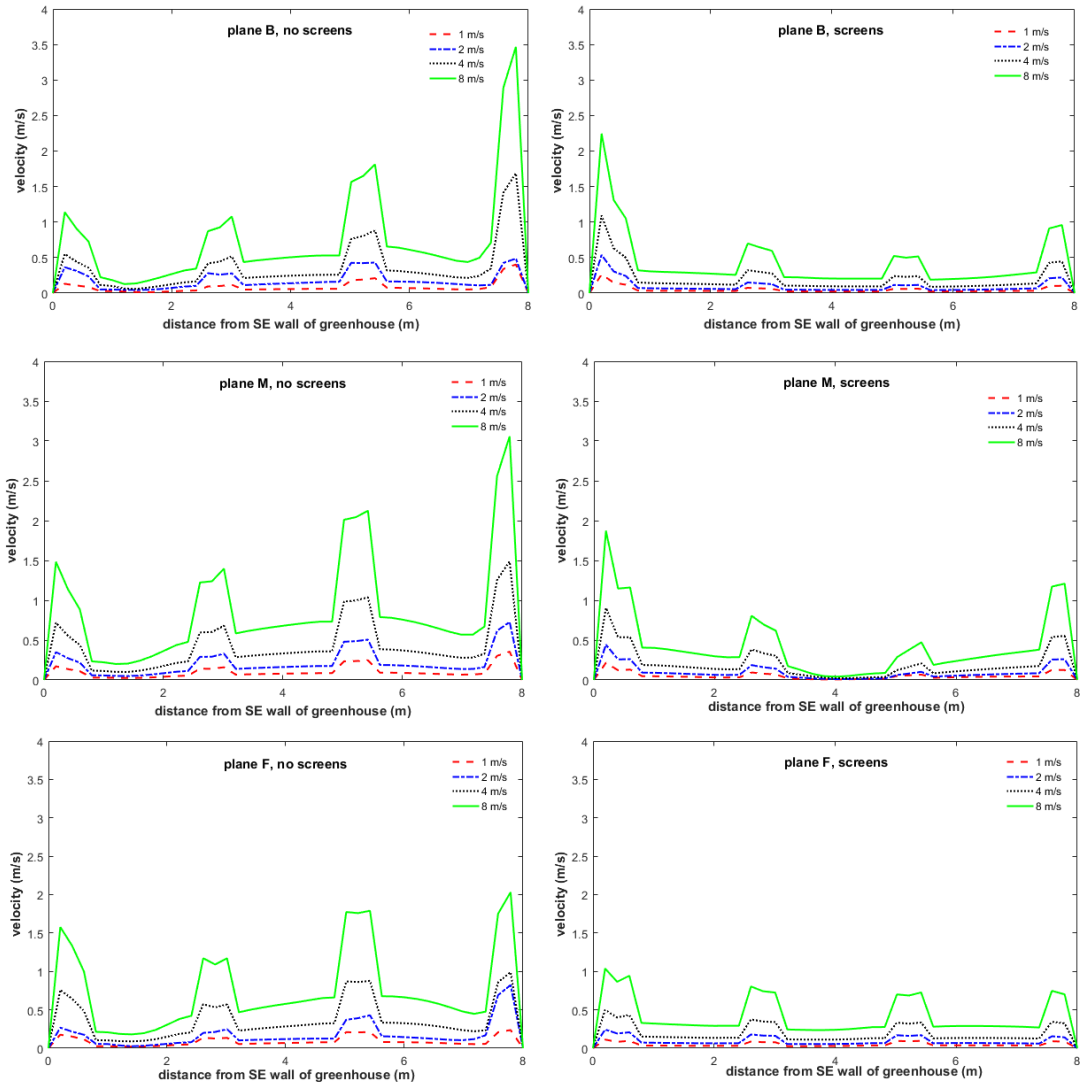

Figure 4.19: Comparison between horizontal profile of air velocity of simulations with and without screens, in the cultivation area for planes B, M and F.

4.1.6 Discussion

Considering the results obtained from the comparison between the two configuration of greenhouse, it was possible to determine that the screens clearly affect the flow patterns inside the greenhouse. They also reduce velocity magnitude to values to low respect to the optimal values for plant growth. In specific, they so significantly affect the ventilation, that optimal conditions of cultivation are not reached in any case studied with screens and the contribution of roof vents in the air mixing is negligible.
Even if these results depend on the geometry of the greenhouse and on the position of the screens, these differences point out that in the evaluation of ventilation conditions in a greenhouse the presence of shading screens can not be neglected and the CFD characterization of the air flow within greenhouses have to be performed with particular focus on their characteristics in order to provide realistic results.
Moreover, the optimization of the position and characteristics of the screens can be significant to produce a uniform air velocity distribution near the crops.
Staring from these results, has been decided to concentrate the research on a deeper study of screens, starting from a better experimental analysis to consider the definition of a methodology for their characterization. Considering also the results related to the greenhouse ventilation, the interest was also evaluate the air flow dynamic inside the greenhouse, with screens different from XLS-16. The advances obtained are presented in following sections.

4.2 Investigation of agricultural screen types

As outlined with the previous sections, the shading screens can have characteristics that could significantly affect the ventilation inside a greenhouse. For this reason, the choice of placing one specific shading screen instead of another one, at the same effect on solar radiation, can have an important role on the resulting indoor air flow. About this, the development of new materials and the advanced technologies have involved the presence on the market of a considerable number of types of screens, applicable in several fields. In particular in horticulture, screens are applied in multiple situations with specific goals. For example, thermal screens are used as a cheap and effective way of avoiding night-time heat loss; shading screens control the solar radiation inside a greenhouse, while insect screens prevent the entrance of both insects and birds (Miguel, 1998).

In particular, the use of any type of screens, mainly the application of thermal and reflective screens, in greenhouses has increased in all the countries where the radiation has an important role in cultivation, because can definitely affect the optimal climate for plants growth. One of these countries is Italy (Castellano et al., 2009). Focusing on the shading devices, the possible selection of screens is wide and depends on the application and needs of the grower. In fact, shading curtains could be placed outside of the structure, just upon the roof, or inside, close to plants. Depending on the needs, they could be colored differently, made by different material and have a specific texture.

The internal shading screens, due to their characteristics and location, can negatively affect ventilation and indoor climate because they can generate an extra resistance to mass, heat and momentum transfer, caused by their porosity (Katsoulas et al., 2006; Santolini et al., 2018). In fact, having a low porosity, they can affect the ventilation, reducing air velocity and modifying the air patterns inside the cultivation area. Consequently all this could alter the inside climate, increasing air temperature and humidity, which are unfavorable conditions for the crop.

The purpose of this chapter is to define experimentally the air flow parameters for three types of screens with a complicated texture. It has been also estimated the relative porosity by a scanning and image elaboration by Matlab, considering to also verify the goodness of equations present in literature, for this type of products. Finally was conduct a CFD model of the case of one screens in order to be able to estimate air flow parameters when is not available an experimental wind tunnel or similar apparatus. This model has been validated thanks to pressure-velocity measurements and PIV technique.

4.2.1 Theoretical background

In literature, the majority of studies evaluates the screens effects on ventilation and the related parameters, such as permeability and porosity, for screens with a simple and regular geometry, like woven or insect screens. Contrarily to these types of materials, the current shading screens have a complex texture, which impede to derive easily the parameters related to the ventilation, starting from porosity, and consequently to be able to investigate their effect on the ventilation and microclimate of a greenhouse, possibly using a CFD approach. In fact, considering the porous media approach, presented in section 3.2.2, to estimate the screen effect, the pressure drop through a porous media, depending from the fluid velocity, is expressed by the Darcy-Forchheimer's law (Sobieski and Trykozko, 2014a,b):

$$\frac{\Delta P}{\Delta x} = \frac{\mu}{K}u + \rho\beta|u|u \tag{4.10}$$

$$\beta = \frac{Y}{K^{\frac{1}{2}}}. \tag{4.11}$$

To be able to evaluate the air flow characteristics of greenhouse screens, these parameters should be known, which are intrinsically related to the porosity of the surfaces. This relation can be expressed by several equation, available in literature. For example, in (Miguel et al., 1997) and (Miguel et al., 1998), the author considered equation (4.12) as the best expression of the relationship between porosity and, respectively, permeability and inertial coefficient.

$$K = 3.44 \times 10^{-9}\alpha^{1.6} \quad and \quad Y = 4.3 \times 10^{-2}\alpha^{-2.13} \tag{4.12}$$

where α is the porosity of the samples. These relations were obtained by testing 14 different screens. Among these, some of them had an irregular mesh, made by polyethylene strips held by a threads, and the author used a microscope for the evaluation of the porosity. A similar correlation was given by Valera et al. (2005) obtained by testing eleven different screens in a wind tunnel:

$$K = 5.68 \times 10^{-8}\alpha^{3.68} \quad and \quad Y = 5.67 \times 10^{-2}\alpha^{-1.1604} \tag{4.13}$$

New relations could be found in Flores-Velazquez and Montero (2008), based on previous studies such the ones reported:

$$K = 2 \times 10^{-7}\alpha^{3.3531} \quad and \quad Y = 0.342 \times 10^{-2}\alpha^{-2.5917}. \tag{4.14}$$

Several authors have used these equations, mainly eq.(4.12), to derive the parameters necessary to conduct CFD studies of greenhouses with screens presence (Kittas et al., 2002; Campen and Bot, 2003; Fatnassi et al., 2003; Molina-Aiz et al., 2004; Campen, 2005). However, several authors, such as (Teitel, 2007) demonstrate that these relations (Eq.(4.12),eq.(4.13) and eq.(4.14)) could lead to an overestimation of the parameters, between 5 and 1.5 times bigger. Considering the fact that is not always possible to obtain the data of porosity of a screens due to his complexity, a CFD approach could be use to simulate the flow through a porous surface, overtaking this complication (Teitel, 2010). Teitel (2010) proposed two different approaches studying woven screens. In the first approach, the realistic models of studied screens were simulated. Moreover, in the second approach, each screen was simulated as an 8-mm thick porous slab. The study found that for woven screens with mono-filament threads, method I can be recommended to obtain K and Y. This method treats each screen individually rather than finding out a global correlation to relate K and Y to alpha, based on tests of screens with differing porosity. Nevertheless, in literature has not be found a well identifiable methodology, which could be applied in cases different from woven or regular texture screens.

4.2.2 Experiments and CFD model

Based on the literature review,it was assumed to experimentally obtain the physical characteristics of the samples through wind tunnel experiments. However, this approach required the availability of use of a wind tunnel or any apparatus with similar operating characteristics. This could not always possible and, for that, two other approaches were considered. On one hand, through imaging processing it could be possible to estimate a porosity in order to refer to the equations 4.13, 4.14, 4.12 for further calculations. On the other hand, it was considered a CFD approach on a scaled model representing the pattern of the screens. This model has been validated through Particle Images Velocimetry (PIV) mesurements.

Screens description

For this research, three type of shading screens frequently used in Emilia-Romagna region were selected. In specific the three screens are:

- Harmony 4215 O FR;
- Harmony 5220 O FR;

- Harmony 3647 FR.

To simplify the reference to them, they will be abbreviated as: H4215, H5220 and H3647.

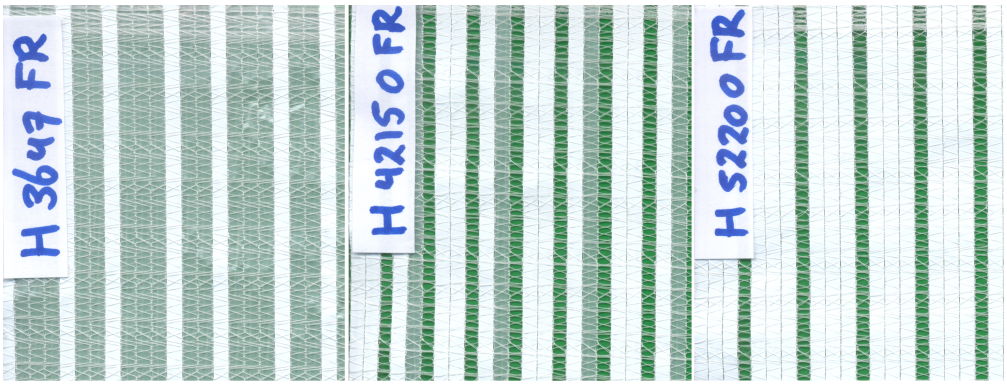

Figure 4.20: Picture of the three samples, made using a scanner of 1200 dpi.

They are three types of shading screens commonly applied in the cultivation, for strawberries, horticultural and ornamental plants. These screens are from the same family of product and they have similar characteristics in terms of direct solar radiation barriers and diffusive solar light diffusers, as readable from data sheets. Instead, they have significant diversities in terms of texture, as showed in figure 4.20 obtained through a scanning process. In fact, H4215 is composed by a pattern of strips as 1 white diffuse, 1 transparent, 1 white diffuse, 1 open, 1 white diffuse, 1 open, of 4 mm width. Instead, H5220 is composed by 3 white diffuse, 1 open, 2 white diffuse, 1 open strips and H3647 by 3 transparent diffuse, 1 white diffuse, 2 transparent diffuse, 1 white diffuse strips. The last one is the only one without any open strip.

Wind tunnel tests

The experimental tests were conducted in a wind tunnel, placed in the laboratories of the Department of Industrial Engineering of the University of Bologna.

It is a wind tunnel with a test chamber of 30 x 30 x 60 cm as dimensions. It is composed by an honeycomb of 90 cm of side, connected to a convergent conduct, which is directly connected with the test section (fig. 4.21). After the test chamber, there is a divergent conduct connected to a rectangular conduct, which lead to the fan, end of the system. In specific, in this system, the fan has a diameter of 45 cm and can reach limit frequency of 50 Hz. In the apparatus, the tests were conducted with the goal of evaluating the parameters: K, Y and β of the three screens. Before starting the experiments, was necessary to determine the calibration curve of the

Figure 4.21: Picture of the entire wind tunnel at the Department of Industrial engineering, Unibo.

Figure 4.22: Images of the test section (at left) and of the honeycomb (at right), initial part of the wind tunnel.

system in order to be able to know the relation between the frequency of the fan and the velocity of the fluid.

First of all, the wind tunnel was characterized, collecting velocities data in three different positions along the width of the test chamber, precisely 3 cm from both walls and in the middle of the section, with a Pitot probe and a micro-manometer

Figure 4.23: Image of the Pitot probe and micro-manometer used to collect data of air velocity and differential pressure.

with a sensibility of 0.01 m/s (fig.4.23). These measurements were repeated four times and for different fan frequencies. The same type of measurements were reproduced afterwards in presence of each screen sample. Was prepared a sample of 30 × 30 cm of dimension, for each screen, with a frame as support during tests. In these cases, the instrument was placed distant from the screen in order to avoid any interference, and, in addiction, all the process of measurements was repeated another time. Form the elaboration of measurements, was possible to estimate the characteristic curve of the system in each case, as showed in figure 4.24. It is clear that the presence of the screens modify the characteristic curve of the system. On one hand, the presence of H4215 and H5220 respectively increases fluid velocity among the conduct, at parity of fan frequency. In fact, due to the structure based on the polyethylene stripes alternated with an empty strips, these types of screens reduce the area where the fluid can pass through, which is forced in these way to accelerate. On the other hand, screen H3647, due to a structure of all plastic strips linked, acts significantly as an obstacle, blocking the fluid passage. After this first phase, were conducted the measurements of pressure placing the tubes of the instrument in figure 4.23 (without aluminum pitot) before and after the sample in order to obtain a pressure drop (ΔP) value. In this way, it will be possible define the relation between air velocity and pressure drop, refereed to each case, which will show in section 5.3.

Images elaboration

It is clear, since section 3.2.2, that However, in this type of screens porosity is not reported on the data sheets and it is not easy to identify and calculate it. For these reasons has been decided to define porosity by conducting an image analysis by Matlab. First of all, each screen was scanned by an Epson Scannerjet 5530, with an optical resolution of 2400 pet 4800 dpi and a selectable resolution from

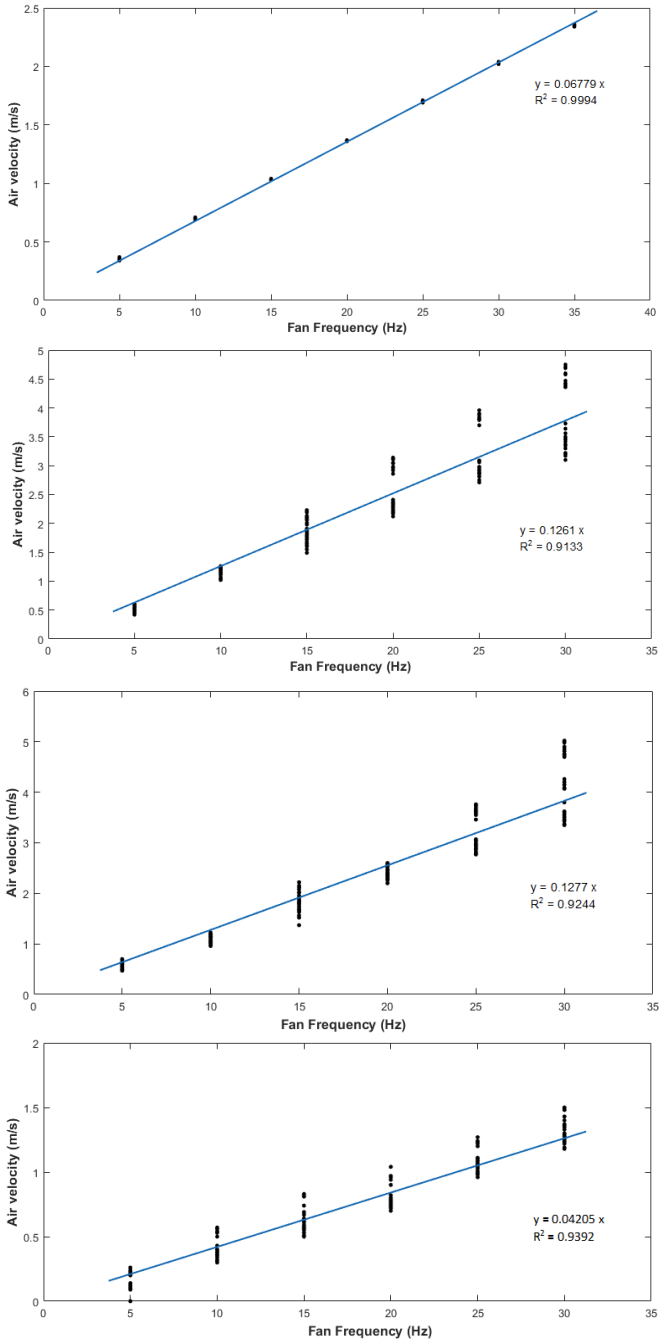

Figure 4.24: Calibration curves of different cases, from up to bottom: calibration curve of the wind tunnel, calibration curve of the case with screen H4215, the one for the case of screen H5220 and finally the on of screen H3647.

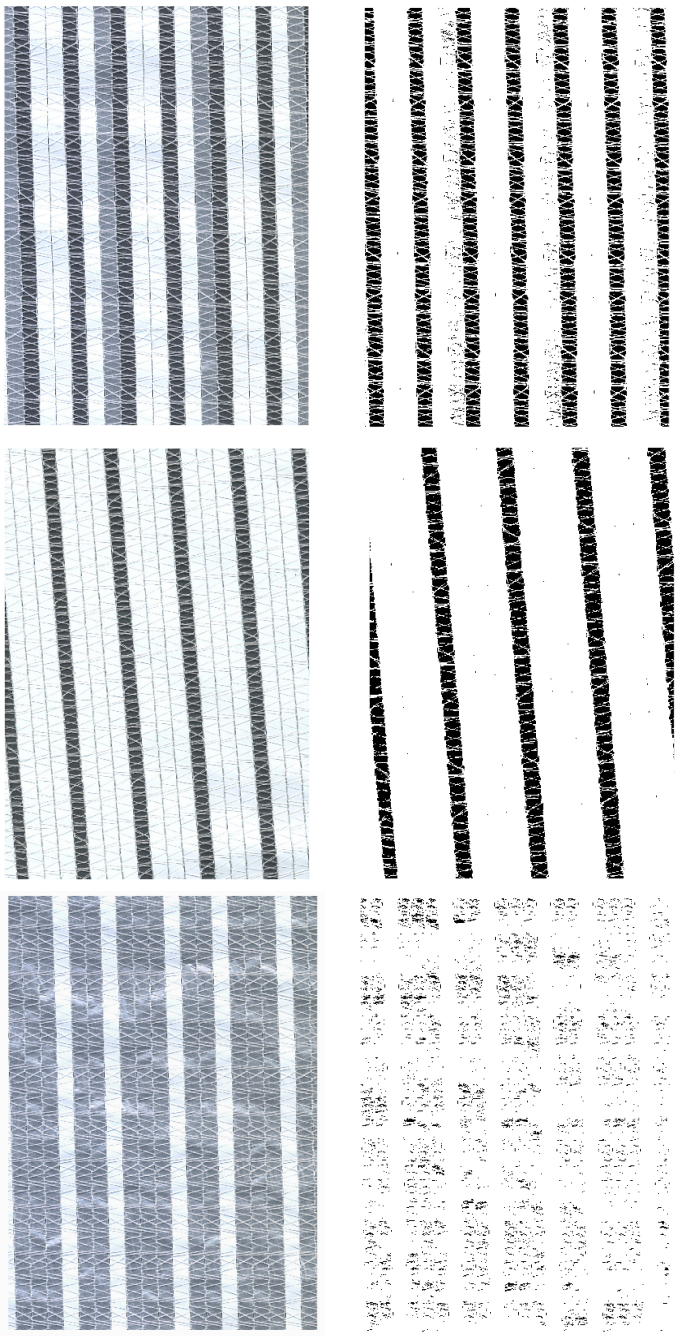

Figure 4.25: Figure representing the comparison of the scanned sample and the Matlab manipulation result. From the top there are: H4215, H5220 and H3647.

12 dpi to 999.999 dpi optimized with scale 100%. In this case, was firstly chose a resolution of 600 dpi and then raised up to 1200 dpi. Due to the dimension of

the scanner was impossible to scan the whole sample. However, observing the repetitiveness of the texture, the image obtained from the scan could be considered anyway representative for the entire sample. Moreover, each sample was scanned three times in different positions, in order to reduce the error of porosity evaluation. From these images, was possible through Matlab to obtain the dimension of pixels limited to the empty zones of the texture, and then compare them to the global pixels dimension of the image. In fact, it was possible to consider the ratio of black pixels on the whole pixels of the figure. An enlargement of the image manipulation results is visible in figure 4.25 compared to the scanned images. These type of analysis was conduct with all the three images of each screen type. These approach lead to the definition of a reliable results for two of the three cases, which will be showed in section 4.2.3.

CFD approach

For the CFD approach, was firstly decided to focus on modeling one case and was chosen the screen H5220, as study case. It was prepared a scaled model of 3 × 3 cm (1:10 of wind tunnel sample), using Autodesk Inventor. The model was created drawing a central portion of the scanned sample, emblematic of its structure, and the dimension of the total domain was 3 × 3 × 18 cm, as showed in fig. 4.26.

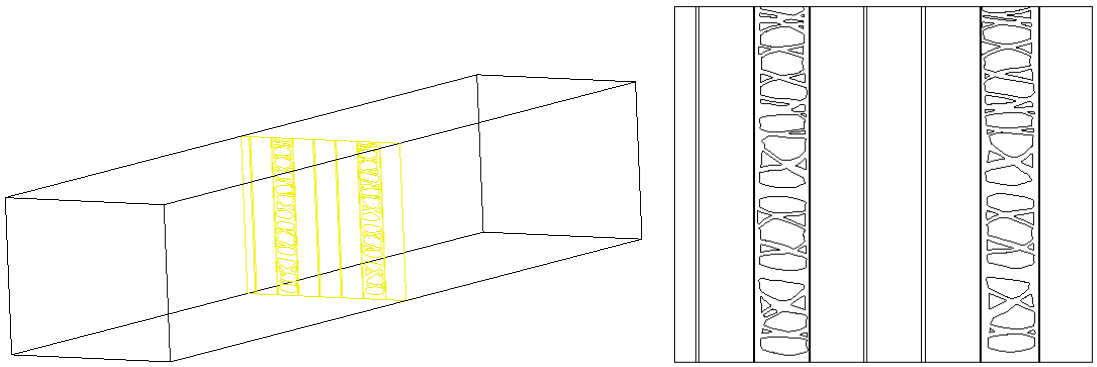

Figure 4.26: 3D model of the entire domain (at left) and a zoom of screen modeling (at right).

Grid convergence

The meshing process was performed using ICEM CFD and the simulations were conducted using Ansys-inc Fluent 17.2. The meshes were unstructured meshes of tetrahedral elements, obtained by the application of robust (Octree) method. The turbulence model applied was a standard k-epsilon model. The figure 4.27

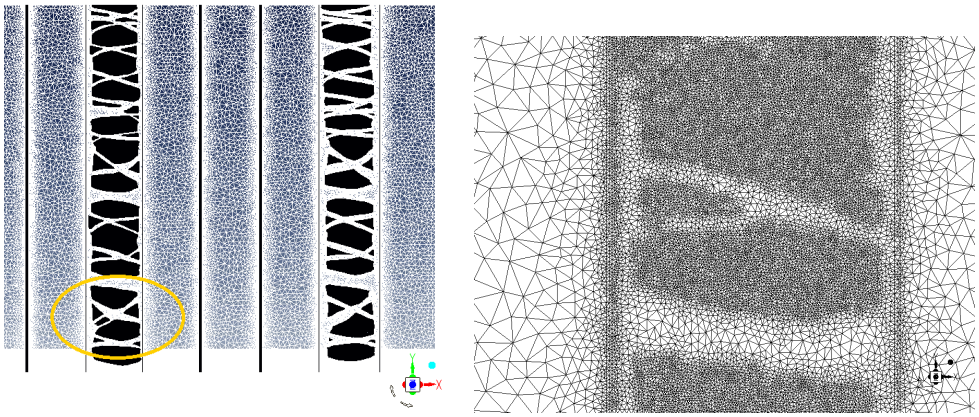

Figure 4.27: The figure shows at the left an image of the mesh of the screen and at the right a particular of the strip characterized with the presence of the thread and so free to the air flow.

shows the unstructured mesh of the screen, with a focus on a smaller area of the empty strip. The porous areas were modeled as an interior surface were the air could pass freely and the strips and thread as walls, impermeable to the fluid passage. The lateral surfaces were defined as symmetries. In addiction, was tried to approximate the spaces open to air flow flow, created by weaving thread, in form of vertical fissures of tiny dimensions. However, the sample was considered as a surface, based on its tiny thickness, as visible in figure 4.26. Moreover, were prepared seven different meshes, with different refinement of grids, from 6×10^5 to 1.4×10^7 cells, for the grid sensitivity study.

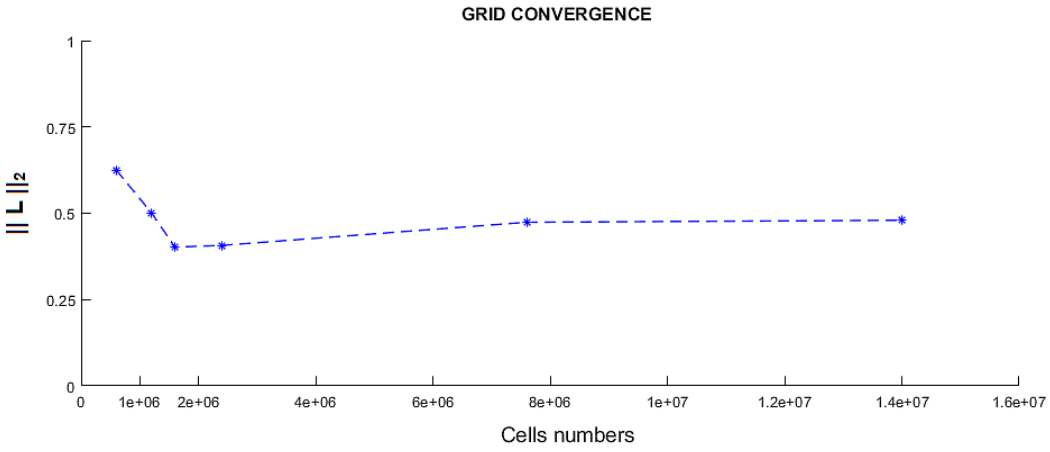

Figure 4.28: Results of the grid convergence study, calculating the $\|L\|_2$ of several velocity profiles, coming from each simulation.

The comparison was conduct between twelve different velocity profiles, considering three profiles in four different distances from the screen surface. In specific, the section chosen were at 3 and 6 cm from the screen, in both directions. Following the process presented in section 4.1.4, the results obtained had a similar trend in both cases ($\|L\|_\infty$ norm and $\|L\|_2$ norm), as happened in the previous study case, and, for this reason, has been reported only the results of $\|L\|_2$ calculation, in figure 4.28. From fig. 4.28, it is visible the stabilized trend of simulation results between fourth and sixth meshes, which lead to choose the mesh of 7.6×10^{06} for the following investigation, with cells dimensions for the screens of the order of 10^{-2}mm. It has been showed in figure 4.27 how is the resulting mesh of the screen, with a focus on a texture strip. Since this result, the simulations were performed with a convergence criteria of 10^{-5} for continuity and 10^{-6} for all others parameters. The investigation was planned on the set up of experimental measurements.

PIV measurements

In order to validate the CFD model and evaluate the realistic modeling of the phenomenon, on a physical point of view, by the CFD approach, were conducted several tests in wind tunnel, using particle image velocimetry (PIV).

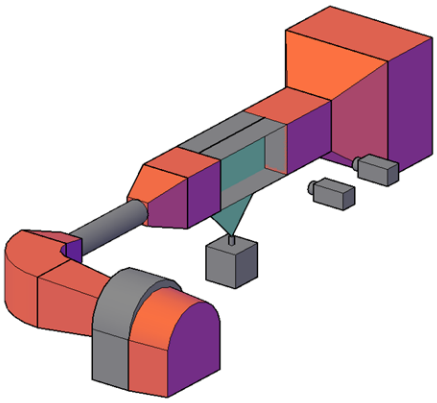

Figure 4.29: Image represents a simplified scheme of PIV set up, with cameras and laser layer visible in the test room.

The particle image velocimetry is a technique applicable in a wind tunnel, within several field, from the automotive to the atmospheric studies. This technique permits to determine the instantaneous velocity in a plan identified by a high energy pulsed laser light and related properties of fluids. Can be also applied to study the effect of an obstacle or an object on a well defined flow. In fact, it is frequently used to study the air dynamics around scaled model of cars or buildings. In this case, a sample of screen H5220 has been placed inside the test chamber. Considering

his reflection of lights, the sample had been painted in black in order to avoid any interference with the laser light. PIV apparatus consists of two cameras (Canon), a Nd:YAG laser with an optical arrangement to limit the physical region illuminated (light sheet), a synchronizing system to act as an external trigger for the control of the camera and laser, the seeding particles, product by a smoke machine, and the fluid under investigation (air).

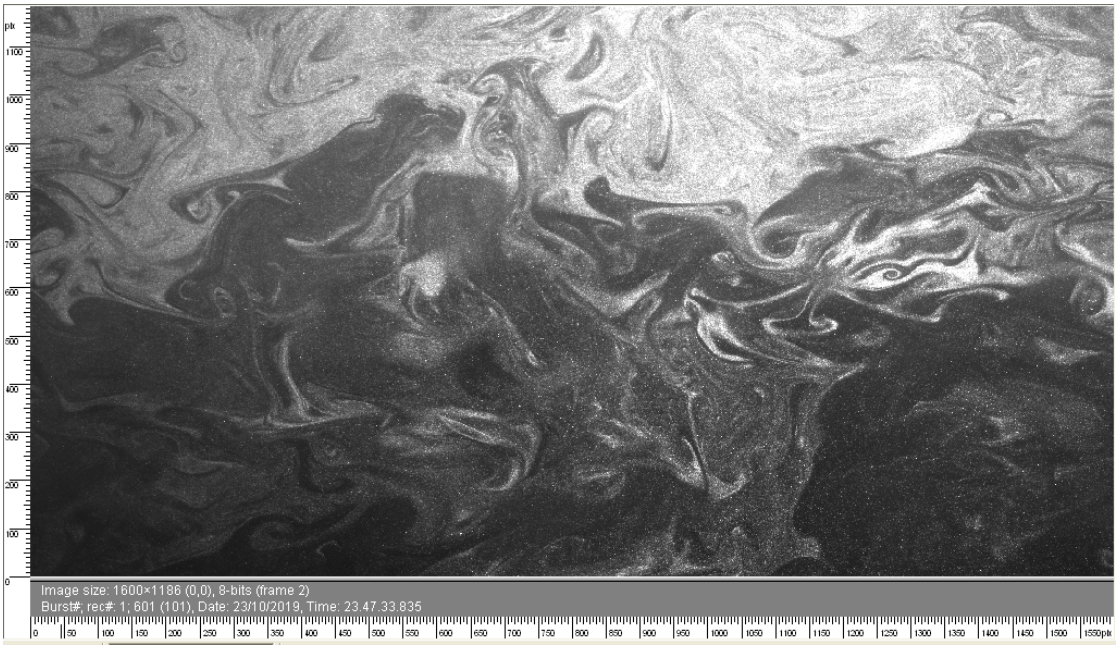

Figure 4.30: Example of a picture watchable in a PIV experiments. In specific, this is obtained during the test conducted with the sample of screen H5220.

Flow-Map software was used to conduct the post-processing of the optical images. Both two cameras usually are used simultaneously in order to obtain a 3D particle image velocimetry; instead, in this case, the experiments were conducted in 2D with both cameras, with particular interest in the out-coming flow, close to the sample, and the flow at the end of the test chamber. After a proper calibration of the system, identifying focus of cameras and the images field of view, the system was used for PIV measurements. In specific, the images were taken with a time pulse step of 400 μs and the smoke time step was managed by the operator. The resulting images will be representative of a velocity vector maps and will be possible to extrapolate instantaneous velocity values from each picture or instead average them in order to obtain an averaged velocity maps, comparable with the CFD results. The fan frequency was set at firstly at 5 and then stabilized at 10 Hz, around a 1 m/s of air velocity. The results obtained from the case of 10 Hz was the ones used for the comparison with CFD model results. Examples of pictures obtainable from

the measurements are showed in figure 4.30. In particular, the results consisted in forty raw velocity vector maps representative of the air flow velocity in a specific moment (forty pictures), which were preliminary analyzed by Flow-Map software applying the moving average filter. After this process, was possible to elaborate the data also through Matlab, with the idea of obtaining averaged velocity values from the instantaneous results coming from the PIV measurements. From each image, was elaborated an average of the phenomenon by calculating the mean values of each profile present in every picture, within every image obtained in the test. This results should be comparable with the CFD results, considering them a average values of the flow.

4.2.3 Research outcomes

Experimental results

Referring to the measurements in wind tunnel to determine the screens characteristics, the data pressure collected were related to the air velocity in order to obtain a relation, which describes the behavior of the screens. Was expected to find relations that would have this form (Eq. (4.15)):

$$\Delta P = au^2 + bu, \tag{4.15}$$

considering the equation would intercept the origin of axes. By fitting data, should be possible to obtain similar equations and to evaluate from them the permeability and the inertial coefficient, characteristics of each screen. The results of the data fitting are showed in figure 4.31. The regression process showed values of coefficient of determination, R^2, close to 1, which means that these new relations explain and predict well future outcomes. Moreover, the correlation of pressure and air velocity of these samples shows that they have a different effect on the air flow, mainly attributable to the differences on the texture. The curves of screens H4215 and H5220 have a similar trend and consequently they have comparable coefficients of the equations. It is recognizable in each curve when there is only the contribution of Darcy's term (linear part) and when starts also the contribution of Forchheimer's term (parabolic profile). Equating the expression in (eq.(4.15))and the Forchheimer equation (eq. (4.10)), was possible to determine the permeability, K, and the inertial factor, Y, for each screen type. In particular, the permeability ant the Forchheimer coefficient were computed thanks to the expressions:

$$K = \frac{\Delta x \mu}{b} \tag{4.16}$$

$$Y = \frac{a\sqrt{K}}{\Delta x \times \rho}, \tag{4.17}$$

where ρ is 1.225 (kg/m^3), μ is 1,81 $\times$ 10^{-5} (Pa s) and Δx is the thickness of samples, which was measured by a mechanical feeler. The results of the data elaborations and calculations were summarized in table 4.6.

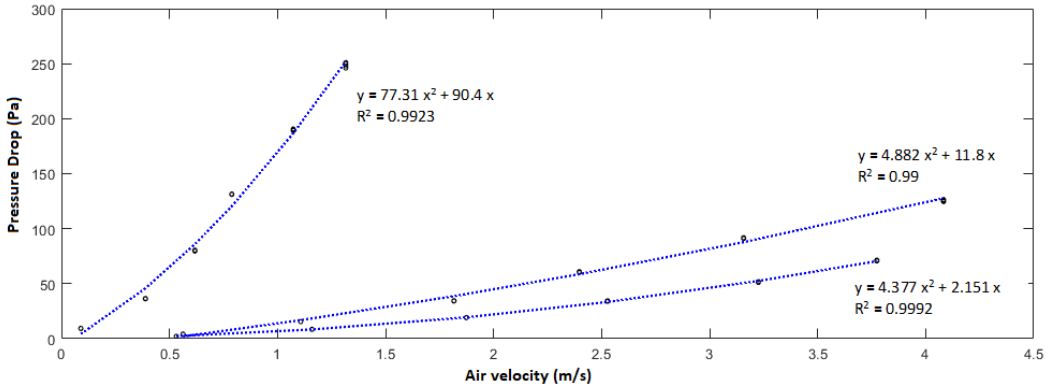

Figure 4.31: Characteristic curve of screens: from left to right H3647, H5220 and H4215, with their relative precision.

Table 4.6: Data obtained from the elaborations of data collected in experiments and parameters calculated.

	a	b	Δx	Y	K
H4215	4.377	2.151	0.00032m	0.5794	2.6627 $\times$ 10^{-9}
H5220	4.882	11.8	0.00032m	0.2759	4,9085 $\times$ 10^{-10}
H3647	77.31	90.4	0.00036m	1.4883	7.2080 $\times$ 10^{-11}

These results outline the fact that the **permeability (K)** values differ from each other by an order of magnitude. Despite the permeability tends to decrease from sample to sample, the **inertial coefficient (Y)** does not increase according to the same trend.

In parallel, was conducted the Matlab image processing, which leads to a definition of a value of porosity for the samples. For each screens, three different images were taken and was calculated a porosity value by an average of the results obtained from them, as presented in table 4.7.

Table 4.7: Results of image analysis of screen samples, with each single value obtained and the average of them.

	1	2	3	average
H4215	0.2133	0.2076	0.20	0.2070
H5220	0.1727	0.1635	0.1639	0.1667
H3647	0.0338	0.0294	0.0273	0.0302

It is possible to observe that the porosity has the same trend of the permeability, as outlined for the data in table 4.6. This fact confirms that the permeability is strictly linked and dependent on porosity. However, as anticipated in section 4.2.2, the result related to H3647 was not considered totally reliable, considering the resulting the images from manipulation so different from those obtained from the scanner, in figure 4.25. In spite of this fact, the result obtained can be considered representative of the situation and can remark the significant difference of H3647 from the other screens. Starting from the porosity evaluation of a screen, the relations present in literature, such as (4.12), (4.13) and (4.14), could be applied to derive the permeability values and inertial factors. In fact, has been decide to calculate them based on the estimated porosity and, afterwards, to compare them to the one experimentally obtained (see tables 4.8 and 4.9). Tables 4.8 and 4.9 reported the results obtained by literature expressions using porosity, available in tables 4.7, and compare them to the experimental results in the last column of the tables.

Table 4.8: Values of permeability based on literature equations and comparison with experimental value.

	K_1	K_2	K_3	K_{exp}
H4215	2.768×10^{-10}	1.300×10^{-10}	1.017×10^{-9}	2.663×10^{-9}
H5220	1.957×10^{-10}	7.782×10^{-11}	4.922×10^{-10}	4.909×10^{-10}
H3647	1.272×10^{-11}	1.448×10^{-13}	1.601×10^{-12}	7.208×10^{-11}

Considering reliable from images manipulation only the porosity of H4215 and H5220, it is clear that the equations 4.14 gives results comparable to the experimental data. It gives more precise values for the permeability than for the inertial factor.

Table 4.9: Values of inertial coefficients based on literature equations and comparison with experimental value.

	Y_1	Y_2	Y_3	Y_{exp}
H4215	1.232	0.353	0.203	0.579
H5220	1.953	0.453	0.355	0.276
H3647	74.3	3.291	29.74	1.488

CFD model and PIV results

The model consisted in a scaled representation of the wind tunnel, with the H5220 screen placed in the center of the test chamber. The preliminary simulations were conducted with two different air velocities, measured in the experimental phase corresponding to 5 and 10 Hz of fan frequency. From the simulation results, were compared the values of pressure drop (ΔP) calculated based on two sections, before and after the screens, with the measured data. The data, chosen for the simulations, were averaged values of the static pressure data, of the plane placed on the position of the experimental measurements.

Table 4.10: Values of pressure drops measured and simulated, caused by the presence of the screens.

	5 Hz	10 Hz
Measurements	4.13	15.48
CFD	12.70	40.63

The comparison between these data shows a large difference between the measured data and simulations results results which are around 3 times bigger. Has been hypothesized that this situation could be caused by a possible overestimation of the magnitude velocity due to the accuracy of the instrument used and the relative small number of measuring points. Moreover, was not possible to collect pressure drops data directly inside the wind tunnel due to the nature of the instrument and the probable perturbations caused by its application. For these considerations, based also on the results obtained from the PIV for velocity magnitude, was progressively reduced the air velocity in inlet. Firstly, was decided to reduce only the case related to 5 Hz of fan frequency from 0.56 to 0.45 m/s, but still the pressure drop was too high compared to the ones measured. Considering the fact that the majority of the data collected were related to 10 Hz of fan frequency, the

sharpening of the simulation was conducted based on them. In fact, taking in account PIV results, was possible to better evaluate the air velocity to apply as boundary condition. As first step, was decided to consider only 20 images and, from these, calculate an averaged value of air velocity. In particular, were selected seven profiles, averaged on the twenty results, and then calculated an averaged speed rating. In fact, as explained previously, each image taken from this technique is exportable as a matrix of velocity values and positions (in pixels or mm), which in this case are matrix 49 × 36, where the columns are the number of air velocity profile obtainable from each image. In figure 4.32 has been presented the seven velocity profiles relative to different positions of the image section.

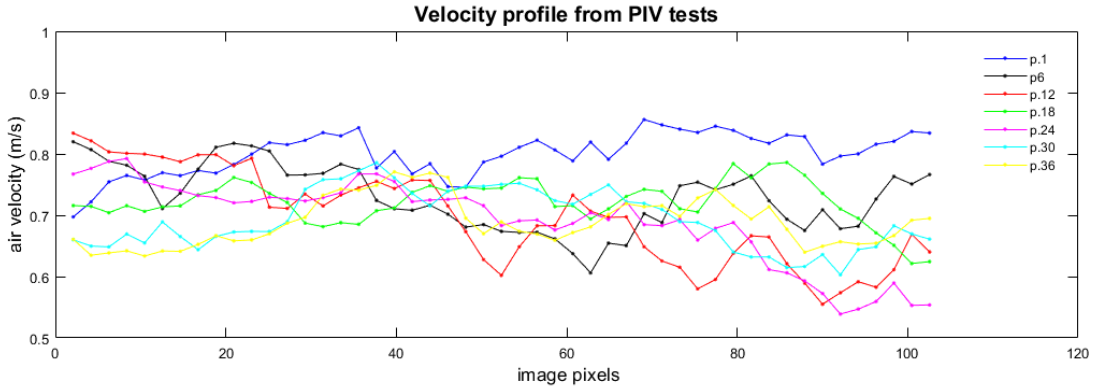

Figure 4.32: Seven air velocity profile obtained by the average of twenty images form PIV. In the legend are reported the positions in the picture where the profiles have been taken.

It is notable a drop of velocity magnitude which goes from a maximum of 0.9 m/s to a minimum of around 0.55 m/s. Form a mediation of the air velocity data, the value obtained was 0.71 m/s, which is practically 30 % less than the measured value, using the pitot tube. Considering this, were conduct new simulations with 0.7 m/s as inlet velocity and with 0.39 m/s, which is the air velocity, recorded by the pitot tube at 5 Hz of fan frequency, lowered by a 30 %.

As done before, from the simulations were collected the static pressure data on the planes at measurement positions and was calculated the value of the pressure drop through the screen. In these cases the value obtained, showed in table 4.11, were closer than before but still too high compared to the pressure data, measured in wind tunnel tests. For this reason, was decided to further reduce the air speed to an initial velocity of 0.65 (m/s) and 0.34 (m/s) respectively. The value of 0.65 m/s velocity magnitude was confirmed by a wider analysis of the PIV measurements, taking in account a bigger number of images and also to limit the interest on velocity profiles to the ones not affected by the screen. Practically, the velocity

Table 4.11: Values of pressure drops measured and simulated, caused by the presence of the screens. In this case, the simulations have been conducted with inlet velocity reduced of a 30 % compared to the previous ones.

	5 Hz	10 Hz
Measurements	4.13	15.48
CFD	6.12	19.9

profiles of 40 images were taken in consideration and the averaged profile was calculated for the velocity profiles. However, considering the fact that the profiles close to the sample could be significantly affected by the reduction of the air passage section and consequently could have an increase of speed magnitude, was chosen to exclude the first six profiles, equal to a distance of 1.6 cm from the screen.

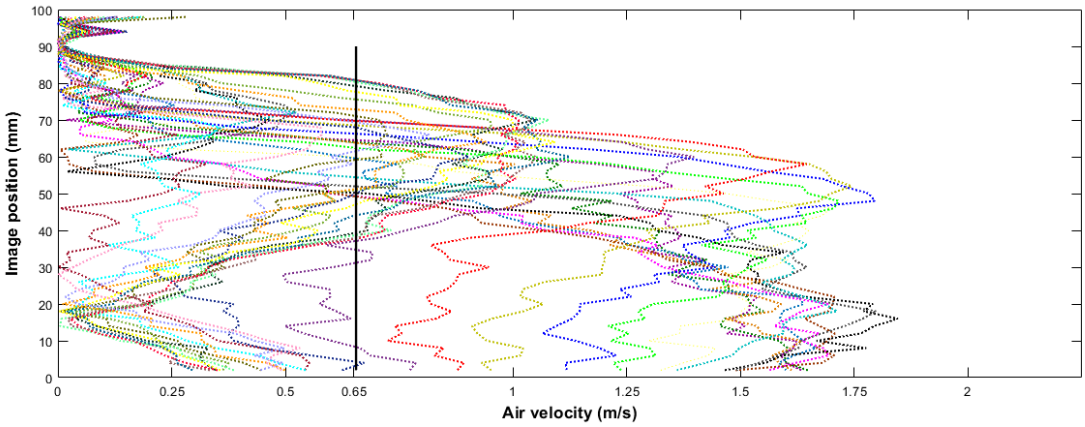

Figure 4.33: The dashed lines are the selected profiles for the calculation and the black straight line is the air velocity value got from the average of all the showed profiles.

This choice was made also due to the fact that the velocity magnitude should correspond to a value, comparable to a value applied as boundary condition and, for that, not affected by the turbulence given by the passage between the meshes of the sample. In figure 4.33 are reported the velocity profiles considered in the calculation and the averaged value, obtained from the calculation process. The calculated averaged value was 0.6552, which differ from the simulated value of a 0.8 %. Following the same steps done until that moment for evaluating the CFD results, the comparison between the static pressures in the two cases (0.65 m/s and 0.34 m/s as initial velocity) and the measured data underlined the achieving of

very similar values. In fact, the simulated static pressures were 4.5 Pa, for 0.34 m/s initial velocity, and 15.4 Pa, with 0.65 m/s as initial velocity. The relative errors were equal to the 8.3 % and to the 0.55 % respectively. In this way, it had been possible to improve the model that now should matched with the data obtained from PIV and this should allow to conduct a comparison between the actual air flow patterns (PIV) and the ones obtained in the simulations(CFD), in order to understand if the phenomenon could be considered properly developed by the CFD model.

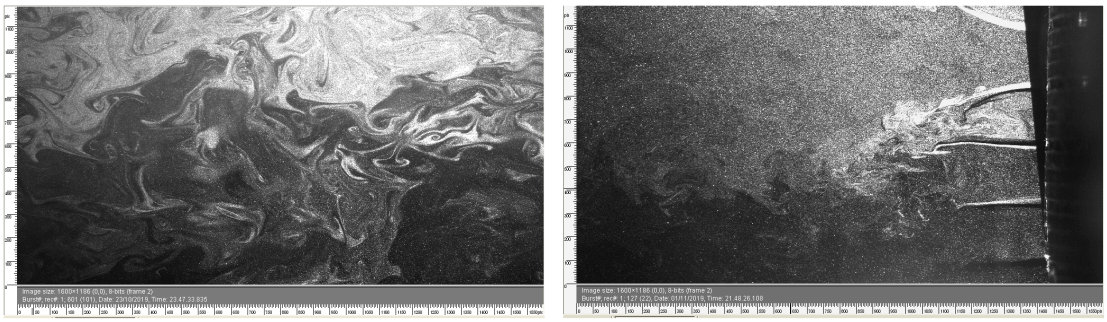

Figure 4.34: The two images were taken during the PIV measurements. The image at the left is representative of the section further from the screen, instead the right one is representative of the section close to it.

In fact, the Particle Image Velocimetry, a explained in section 4.2.1, is able to catch the velocity field of a gas flow in a specific moment. Practically, the system took images with an interval of 400 μs which could be representative of the air flow patterns and velocity. During the tests, were considered two areas: one was immediately downstream of the screen and the other one was the furthest section, where the flow should be less affected by the perturbation given by the screen presence. In figure 4.34 are presented two images taken from PIV so as to understand which kind of output is obtained from these measurements. Already form this images, it can be observed how the flow dynamic is totally different in the two sections. However, the outputs obtained from the PIV technique were actually raw velocity vector maps. Thanks to FlowMap software, it is possible to filter the solution through several mathematical possibilities. In this case, it was applied a moving average filter. This validation method is a continuity type method where vector values are assessed in the context of the neighboring vectors. To clarify this explanation, in figure 4.35 has been shown the previous images in fig. 4.34, the respective raw vector maps and the results of the moving average method.

In the last row of the figure 4.35 are located the moving average method results and several vectors are colored in green because they are the ones modified by this method. The first image allows to understand better the air flow pattern close

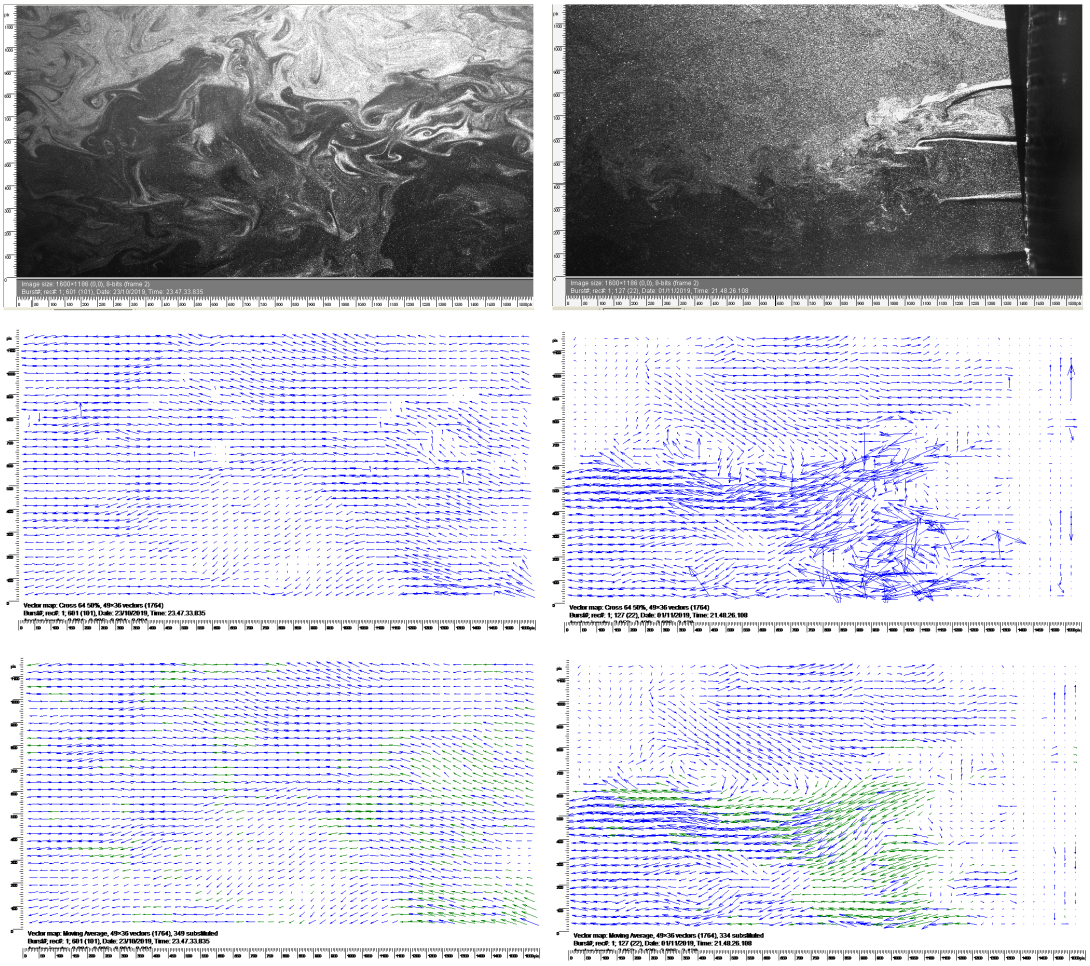

Figure 4.35: Taking into account the images presented in fig. 4.34, below them are presented the raw maps and the maps resulting from the moving average method. In order to underline the differences, the changed obtained on the raw maps are reported in green.

to the screen, thanks to the overlapping of the vector map to it. The first image shows a more chaotic flow, with few vortexes present in the map. On the contrary, in the second image, it is interesting to see how actually are not present significant vortexes in the section far from the screen.

The vector map of this section shows a more organized and regular behavior of velocity field. The further step was to compare the results obtained through the PIV tests and the CFD model, in order to understand if it can be representative of the fludo-dynamic, characterizing this situation. To do a better comparison, a portion of the section, where it is located the air flow through two strips with

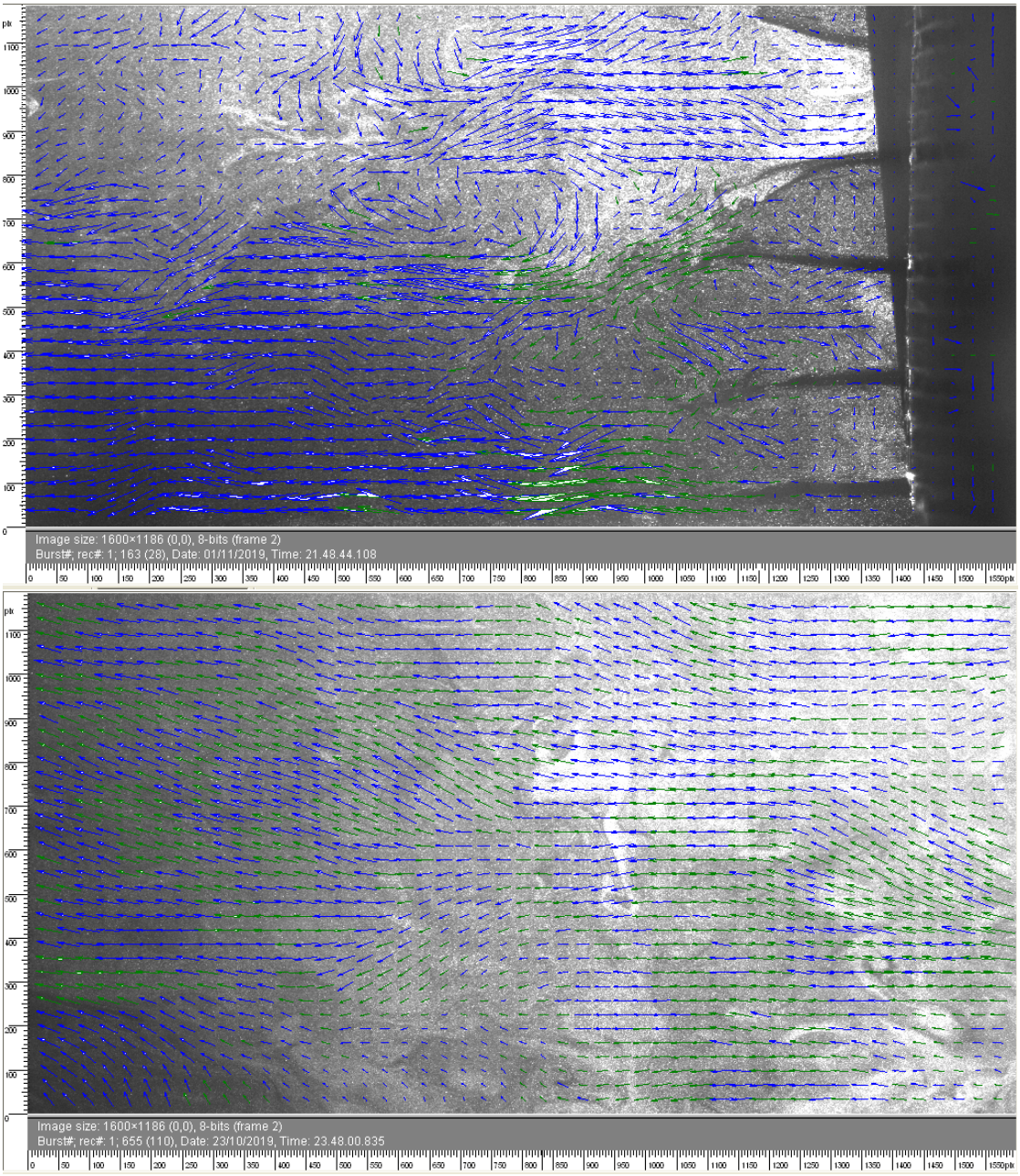

Figure 4.36: Overlap of the images cached from the cameras during the test and the related vector maps, with applied the moving averaged method.

thread, was separated and the differences between the simulated case and PIV outcome were evaluate. The vector map obtained from the middle section of the CFD model is presented in fig. 4.37, related to the maps of the PIV result. In both

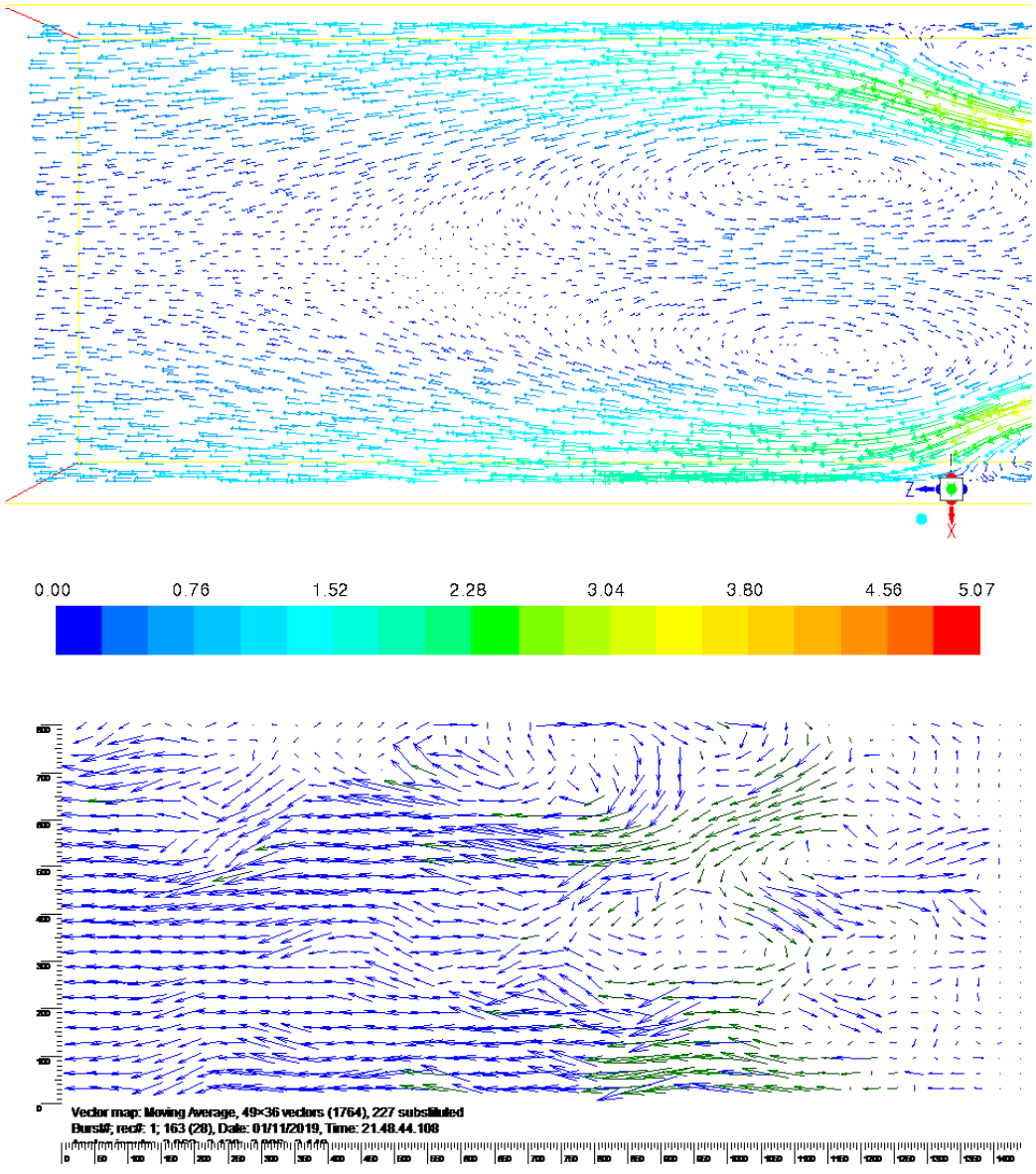

Figure 4.37: In the upper part a vector map, obtained from the simulation with initial air velocity of 0.6 m/s, is reported with below the vector map resulting from PIV measurement.

images two jet flows are identifiable at the level of the strips with only thread and a recirculation area between them. It is also clear that moving far from the screen

the air flow starts being more regular, as saw also in figure 4.36. The simulated case replicates the fluid dynamic of the real case in adhering way, even though a preliminary speed assessment work had been necessary. This aspect of different initial speed could be due to a deterioration of the fan applied in the tests, or to the way and the instrument used for the collection of data. In fact, could be preferable to apply an anemometer for the air velocity measurements instead of a pitot tube, which is more imprecise. However, this would be possible only by a variation of the test chamber, being able to insert the instrument in such a way as to be able to seal the chamber and not to disturb the measurements. This modification of the measurements methodology would imply the purchase of an insert-able anemometer in the test chamber or in the enlargement of the last one. Despite these considerations, the CFD results showed a significant consistency and accuracy with the achievements obtained by the PIV. Due to these, the CFD model could be considered validated and consequently a reliable methodology for the definition of screens characteristics or, at least, to investigate the fluidynamic of the air passage through a porous surface.

4.2.4 Considerations

Shading screens can be placed internally and externally in a greenhouse and they can significantly affect the air flow patterns inside the structure. Nevertheless, in literature the studies are mainly focused in type of screens with a regular texture, which is not the case of the new type of shading screens available on the market. For these screens, any methodology is available for their practical characterization, which can be important considering then the complex texture. Starting from these considerations, an experimental approach and a computational approach have been tested and evaluated.
In particular, several type of shading screens have been analyzed and experimentally characterized by wind tunnel tests, air velocity and pressure drop measurements. These procedure allowed to define the specific behavior of each screen and then to investigate their effect inside the greenhouse (section 4.3). However, the experimental may can not be applicable in all situation and maybe can not be available the instruments and the technologies to conduct these tests.
Then, the CFD approach could be an efficient approach in this case. In fact, can be performed a 3D model of a real test experiment, and, by the validation of this model, afterwards can be obtained the same type of relations, given by the experimental procedure. It has been demonstrated that the CFD application allow to describe the phenomenon in a comparable way to the experimental situation, described by the PIV. Thanks to the observation of the phenomenon by the PIV, it has been calibrated and refined the CFD model, which can be positively considered

a methodology, applicable for the determination of the parameters, linked to the air flow through a screen. This characterization process is necessary for analyzing and evaluating the real effect of screens, with different characteristics, on the internal fluid-dynamic of a greenhouse.

4.3 Optimization of shading screen type in greenhouse case

According to the knowledge acquired and the improvements that had been done on the shading screens characterization methodology, it was considered the evaluation of the effects of screens H4215, H5220 and H3647 on the greenhouse ventilation. In fact, the previous cases can lead to an evaluation on how the ventilation could be affected by the presence of different shading screens but also on how the choice of one respect to another could determine a better internal ventilation. Considering this, to be able to conduct this comparative study, few improvements on the results until that moment obtained had been necessary.

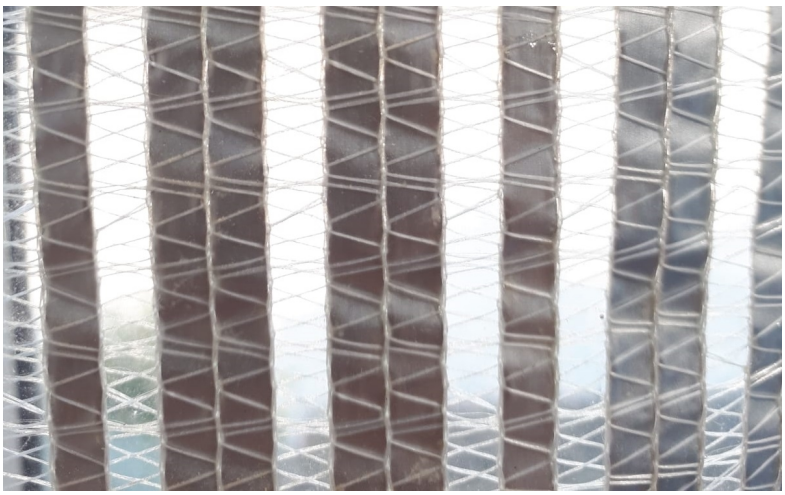

Figure 4.38: Picture of XLS 16 where are recognizable the aluminum and plastic strips.

In fact, thanks to the deepen study of screens characteristics it was possible to reach more accurate results about XLS 16 screen, modifying some preliminary assumptions and consequently avoiding few inaccuracies revealed. First of all, it was clear that the contribution of the inertial coefficient could be better estimate thanks to the fact that, considering the texture of XLS 16 composed by 2 aluminum, 1 plastic, 1 aluminum, 1 plastic strips (visible in figure 4.38) alternately, it can be considered more similar to H3647, based a qualitative point of view. For this reason, can be derived the porosity value and the Forchheimer coefficient from the permeability coefficient, obtained from the data previously collected. In fact, the data measured for the XLS 16 were characteristic of the linear part of the Darcy-Forchheimer's law and for this reason could be considered reliable the value of K computed equal to 5.72×10^{-11}. Since for these kind of screens has been

outlined that equation 4.14 can be applied with low error margin, it is possible to calculate the porosity of XLS 16.

$$\alpha = \left(K\ 2 \times 10^{-7}\right)^{\left(\frac{1}{3.3531}\right)} = 0.13266 \tag{4.18}$$

On the contrary, starting from the porosity, the inertial coefficient could be better evaluate thanks again to equation 4.14 and the resulting value computed is reported in 4.19.

$$Y = 0.342 \times 10^{-2}\alpha^{-2.5917} = 0.6422. \tag{4.19}$$

Considering all three screens, it is possible to compare and evaluate the different effects on greenhouse ventilation. The simulations were conducted in the same way as done in section 4.1.2. Nevertheless, had been necessary to conduct again the mesh convergence study because newly made by ICEM CFD.

4.3.1 Modeling and simulation

Other modifications had been considered since the first model validation, not only an improvement about the permeability and inertial coefficient definitions of the screen XLS 16 but also about the formulation of the wind profile, the dissipation rate and the kinetic energy. In fact, was decided to express these parameters not depending from the boundary layer, (δ), but depending on the friction velocity, u_*, which is equivalent to the air velocity measured in a specific point. In specific, despite the equations 4.1, 4.2 and 4.3, these profiles were modified based on **?**, in a form which is more frequently applied in studies in the agricultural sector. The wind velocity profile equation is

$$U = \frac{u_*}{K}\log\left(\frac{z + z_0}{z_0}\right), \tag{4.20}$$

where u_* is the friction velocity measured in a defined height and K is (0.40) is the von Karman's constant. In particular, the friction velocity definition is based on measurements on field and can be calculated as

$$u_* = \frac{Ku_h}{\log\left(\frac{h+z_0}{z_0}\right)}, \tag{4.21}$$

where h is the measuring height point. In this case, the friction velocity had been measured around 9 meters of distance from the structure at an height of 3 m, with an hot-wire anemometer. The velocity magnitude has been recorded each second for 2 minutes. The resulting value is the averaged magnitude, equal to 1.67 m/s. Regarding the wind, it was blowing with a S-E direction for all the

data collection, monitored thanks to the meteorological station integrated to the greenhouse structure. Consequently, also the dissipation rate and the kinetic energy were expressed depending on the friction velocity:

$$k = \frac{u_*^2}{\sqrt{C_\mu}}, \tag{4.22}$$

and

$$\epsilon = \frac{u_*^3}{K(z + z_0)}, \tag{4.23}$$

These equations had been written in a user defined function (UDF) and compiled as boundary conditions for the new simulations. The process of meshing and grid analysis was conducted again because was necessary to performed new grids using ICEM cfd. For this reason, six new grids were prepared and simulations were conducted with equations 4.20, 4.22 and 4.23 as boundary conditions. In analogy of what had been done in the previous studies, were calculated $\|L\|_\infty$ and $\|L\|_2$ norms, with similar results. For this reason has been reported the $\|L\|_\infty$ results in figure 4.39.

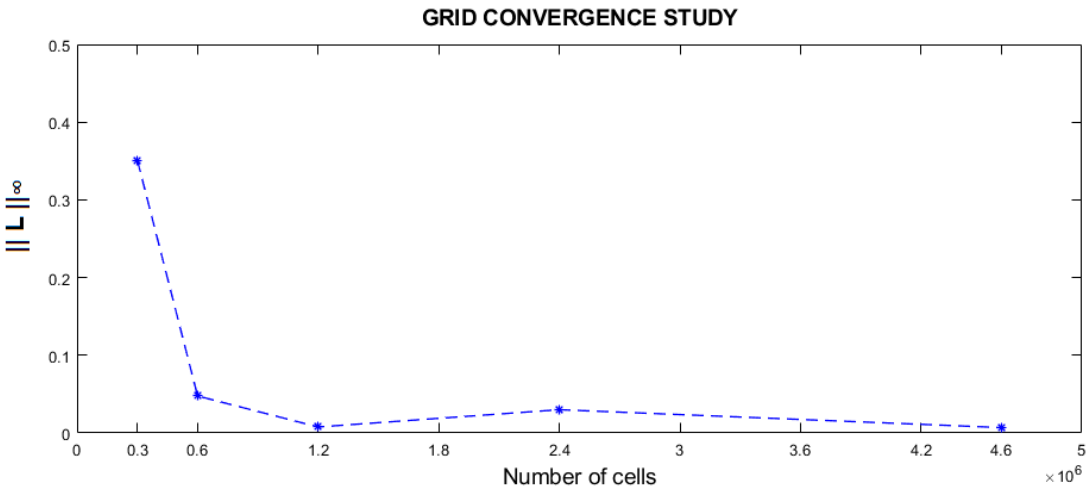

Figure 4.39: $\|L\|_\infty$ calculated based on twelve velocity profiles, located on the central section of the domain.

The mesh of 4.6e+06 was chosen for the other simulations.

4.3.2 New Validation

The model was validated in the study presented in section 4.1 with an a reliability of errors under the 30 %, but with one error close to that percentage and another one even over, on a total number of five data used for the comparison. However, as outlined in the previous sections of this chapter, several changes and enhancements had been done in the modeling and in the simulation conditions. Considering these, it was supposed necessary to validate again the model against the already collected data, comparing the results with what was previously obtained. In figure 4.40 the averaged velocity values are compared to the simulation results, showed as vertical air velocity profiles. Each measured data is represented with the range of error, equal to the deviation standard based on the average of air velocity.

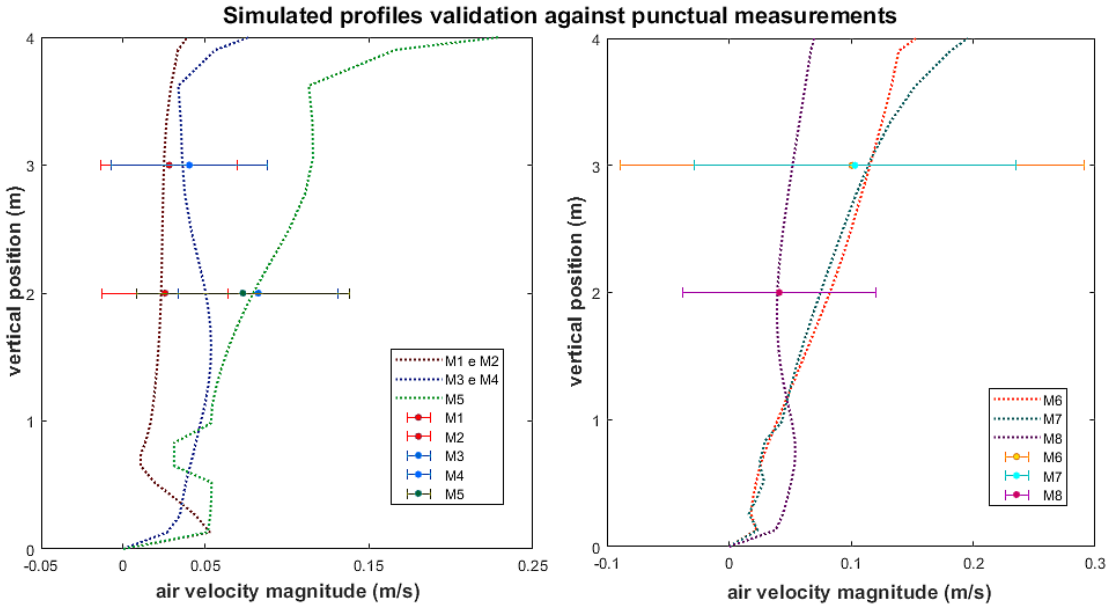

Figure 4.40: The first plot (left one) shows the comparison of three simulated profiles and the relative data collected in positions, belonging at that profile. The second plot (right one) presents other three profiles and the relative three measurements.

Quantitatively the relative errors between measured values and punctual simulated values were calculated for all the validation points, reported in table 4.12 and in table 4.13. The first table concerns the five measurements already taken into account in tab. 4.3. In fact, are compared the relative error obtained in the previous validation process and the new ones. Two points (M1 and M5) shows comparable errors and other two (M2 and M4) presents even a lower value. However, a point (M3) presents an highest errors (56 %) but it was characterized by a quite high percentage also in the previous validation (26 %). However, the problematic points

are M3 and M4 in both cases, probably because they are the ones located in the back of the greenhouse, close to the screen and the internal wall (as visible in fig. 4.10).

Table 4.12: Comparison between measurements and simulations

Measurements	Error %	Error first validation %
M1	11.2	10
M2	9.3	22.5
M3	56	26
M4	24.4	35
M5	8.7	2.8

Moreover, this time, other three measured velocity data, in different positions showed in figure 4.41, were compared to the simulation results by the percentage of relative error, as shown in table 4.13. These errors are limited under under the 15 % in all the cases.

Table 4.13: Comparison between measurements and simulations

Measurements	Simulated velocity (m/s)	Measured velocity (m/s)	Error %
M6	0.12	0.10	14.5
M7	0.11	0.10	10
M8	0.04	0.041	3.8

It is evident, from the results in tables 4.12 and 4.13, that the relative errors calculated for the new simulations results are all under the 15%, exactly half value of what was obtained in section 4.1, except for M3, which has proved anyway problematic in both cases. Another improvement over the initial validation is the number of the assessable points for the validation. In fact, in this validation process the comparison on seven points was acceptable, unlike that on five points conducted in the previous case. Then, a significant improvement in the case modeling is evident; the new simulation set up leads to globally better validation results, thanks to the changes made for the boundary conditions, the wind velocity profile and the XLS 16 characterization.

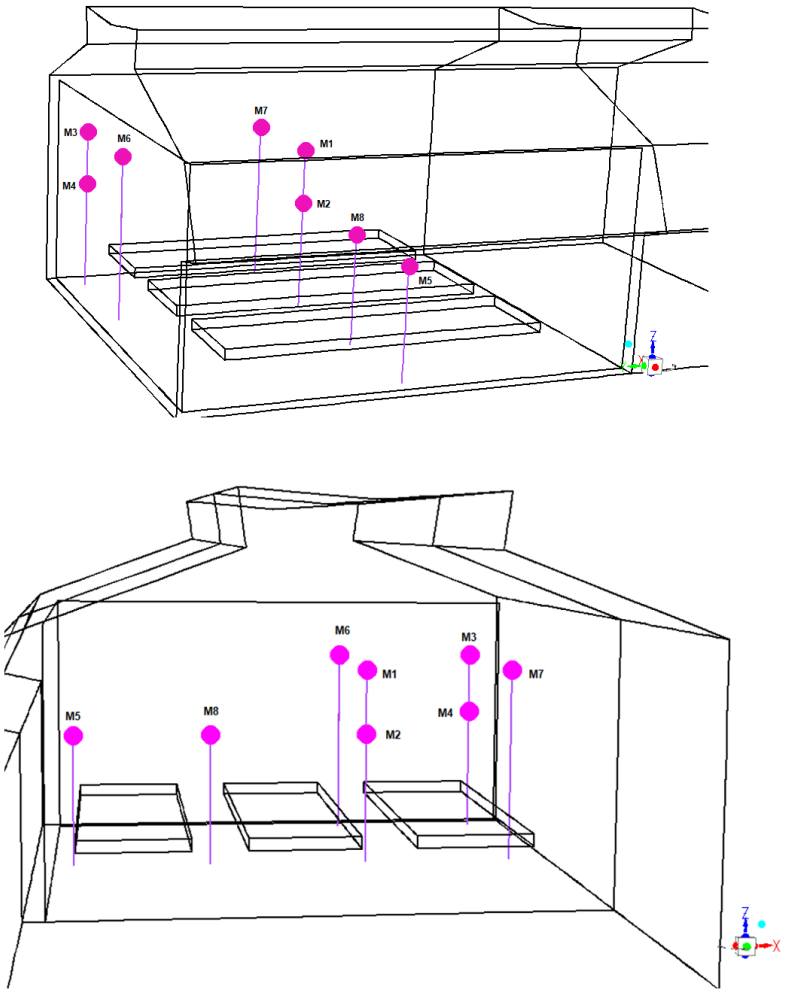

Figure 4.41: In the figure are reported all the collection data positions inside the greenhouse span, in two different point of view.

4.3.3 Outcomes of the case with XLS 16

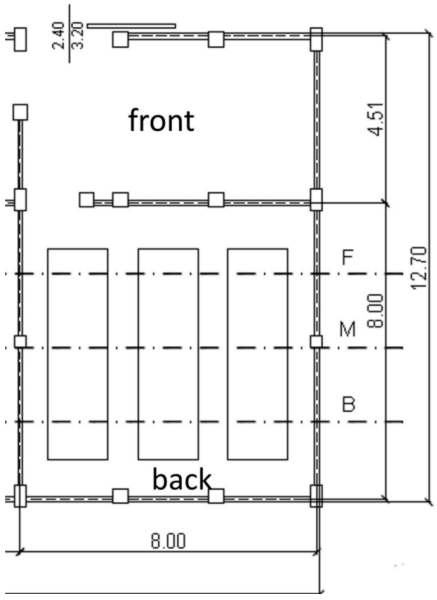

Figure 4.42: Sketch of the greenhouse with the representation of the sections of interest.

The different definitions of wind profile and turbulence parameters made it necessary to again compare the internal fluid dynamics that characterize the greenhouse in the absence or presence of the xls 16 screens. In any case, significant differences are expected between the two cases, as shown in section 4.1, but with possible changes in the air patterns. With the same approach as used before, the contour maps of three different planes were compared, as shown in figure 4.43, in analogy to what was done in fig. 4.18.

The layout of the plans has been reported for a better understanding of the subsequent analysis of the results. The air flow patterns of the case without screens (left column in fig. 4.43) presented a central vortex that affects the whole section. On the contrary, the case with XLS 16 screens, placed inside the structure, (right column in fig. 4.43) shows a central area of the section characterized by really low or zero velocity magnitude. In particular, the benches seem to be immersed in an air stagnation zone.

Qualitatively, the fluid dynamics of the two cases is clearly different. However, the zone of interest was the area around the benches, where the air velocity should be around 0.5 - 0.6 m/s (under 1 m/s) for the optimal growth of the crops. Considering three different distances from the benches (10 cm, 20 cm and 50 cm), chosen thinking about the ornamental plants usually placed here, the air velocity

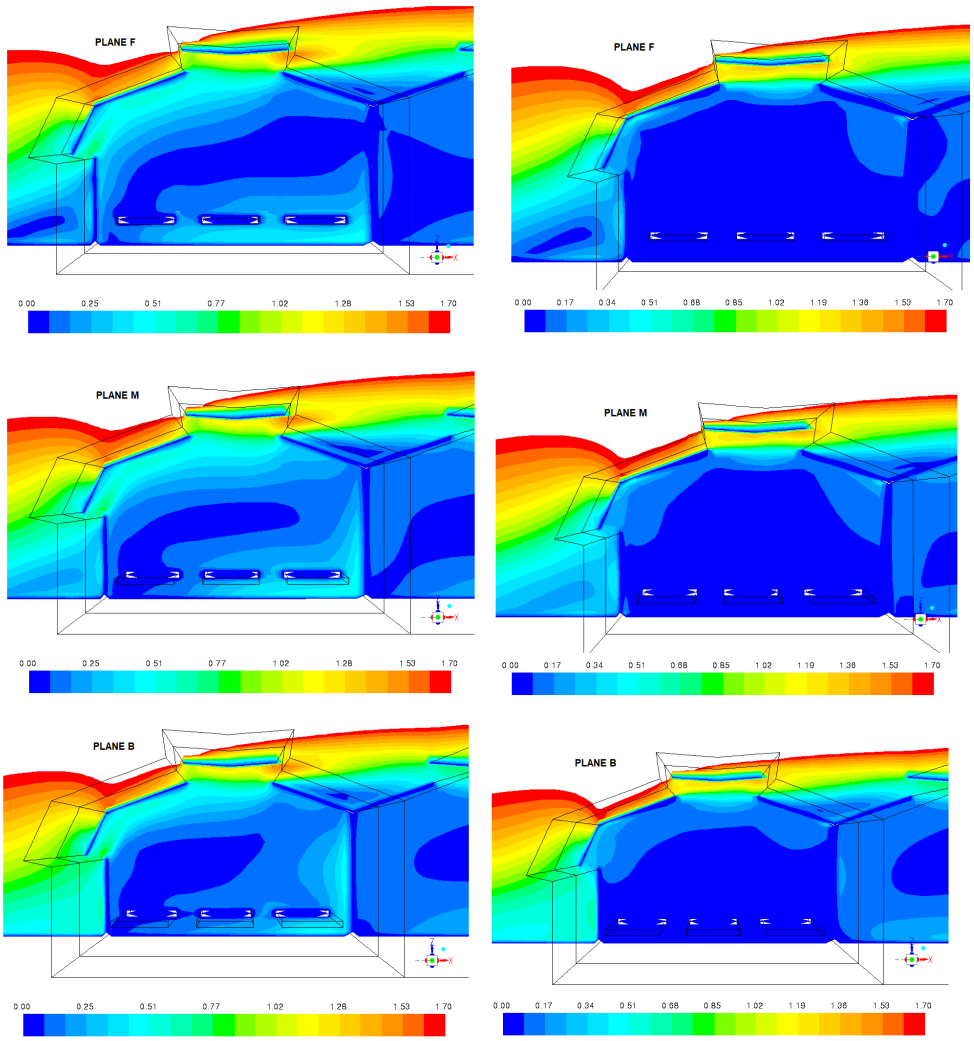

Figure 4.43: Velocity magnitude, without screens (left column) and with screens (right column) on the planes F, M and B.

profiles at these heights were compared, in figure 4.44. The configuration without screens presents a similar trend of air velocity to the case with screens, at 10 cm from the benches. However, clearly the different air velocity magnitude stands out, considering that the velocity with XLS 16 placed is really close to zero. The trends are similar in all three planes for both cases. In particular, it is visible a progressive increase in air speed from the outer wall of the greenhouse to the internal one. This confirms what has been seen in figure 4.43, i.e the presence of a vortex in the middle of the sections of the greenhouse without screens. In fact, this

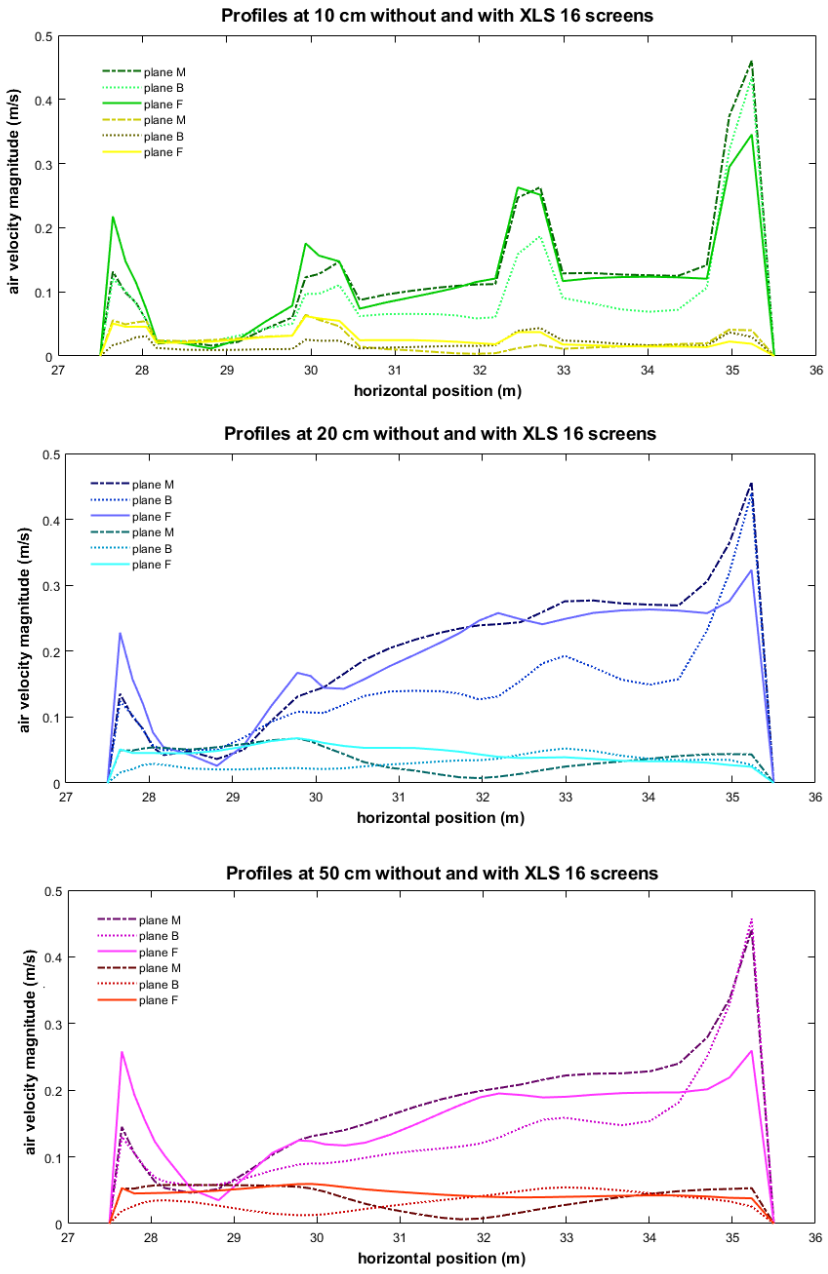

Figure 4.44: Three plots where are compared the air velocity profiles, from the simulation section M B and F, at a peculiar height from the benches. In particular, in the plots: dark green, dark blue and purple profiles refer to the case without screens; light blue, red and yellow profiles refer to the case with XLS 16.

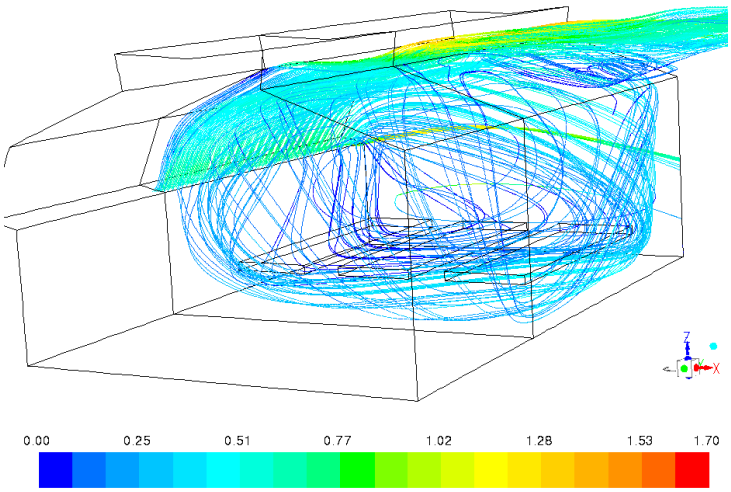

Figure 4.45: Pathlines of the air flow incoming from the lateral window, inside the cultivation ambient.

vortex interests all the cultivation area of the greenhouse as appreciable from the figure 4.45. Moreover, the velocity profiles at 20 cm and 50 cm have the same trend with reference to the respective configurations. Once again, the velocity profiles of the greenhouse without screens, also at these heights, show the presence of the vortex which affects the whole section. Instead, in these cases, the air velocity in presence of XLS 16 screens is practically constant along the greenhouse sections, always with a magnitude of 0.05 m/s or lower, confirming what was visible in the contour maps (fig. 4.43). Considering only the case without screens, it is evident from the totality of the profiles that the bench near the window is in the most disadvantageous position, in terms of optimal ventilation conditions. In fact, at any height, the air velocity magnitude never exceeds the 0.3 m/s, reaching negative picks of 0.05 m/s. This condition should be avoided for the well growth of crops.

4.3.4 Different screens effects

It is clear the presence of the screens can considerably change the distribution and the magnitude inside the structure. For this reason, the choice of the type of screen could make the difference in internal fluid dynamics.

Therefore, the screens, studied in section 4.2 that, which have different characteristics in relation to the air passage, with the same effect on solar radiation, were simulated inside the greenhouse and compared with the outcomes of the case with XLS 16 screens. The simulation set up was analogous to the one applied for the XLS 16 simulation. Also the same approach of analyses of the results has been

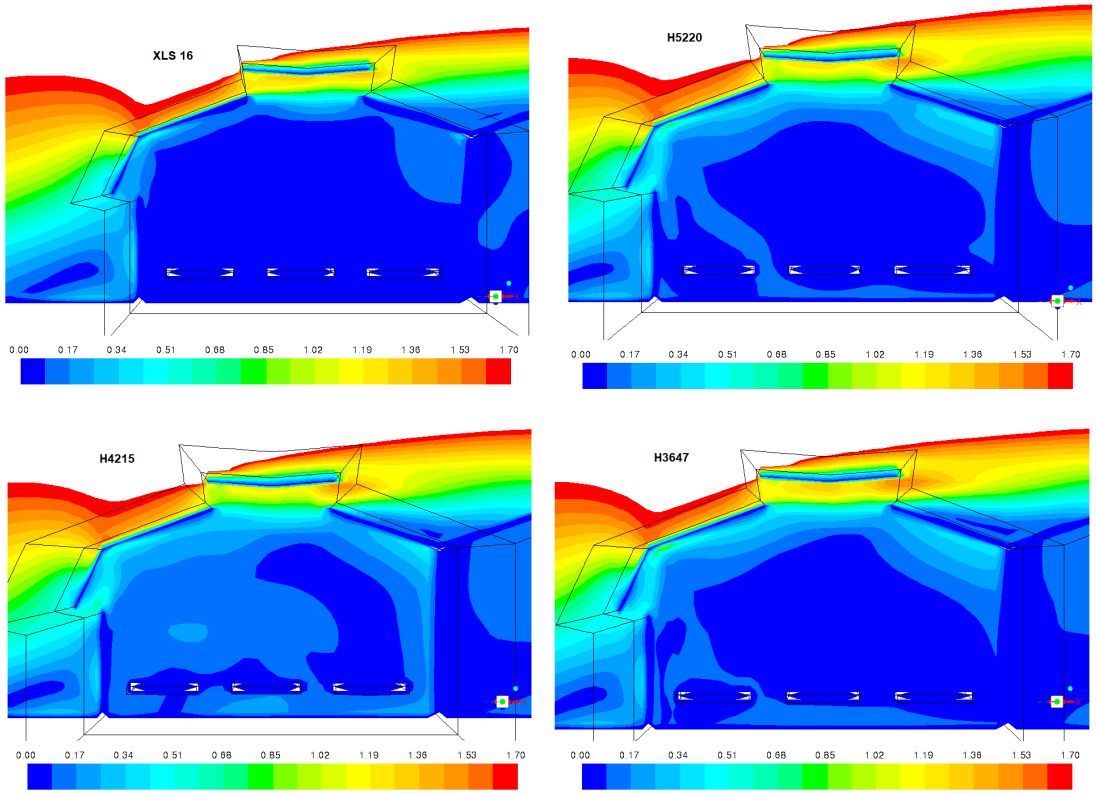

Figure 4.46: Contour maps of the four cases of the section placed in the front of the greenhouse.

followed. The contour maps of the three different planes (front, medium and back) were compared to observe the air flow inside the structure with the four screens type (XLS 16, H5220, H4215 and H3647).

Starting from the front section, the case with XLS 16 has been already analyzed and present really low velocity magnitude in the cultivation area. In figure 4.46, the configuration with H4215 screens shows the highest velocities inside the structure. Moreover, it is present small vortex in the higher part of the section, around 2.5 - 3 m and a low velocity area around the bench, close to the internal wall.

However, around the benches, the air velocity magnitude is around 0.1 - 0.2 m/s. On the contrary, the cases with H5220 and H3647 show a wider area at low speed magnitude in the cultivation are. Furthermore, the maps of these two cases are significantly similar, a condition that will be confirmed in the other sections. Figures 4.47 and 4.48 showed contour maps close to the result, showed in fig. 4.46. In the configuration with H4215, the low velocity area is bigger than the one in the front section. Moreover, the similarity between case with H5220 and H3647 are

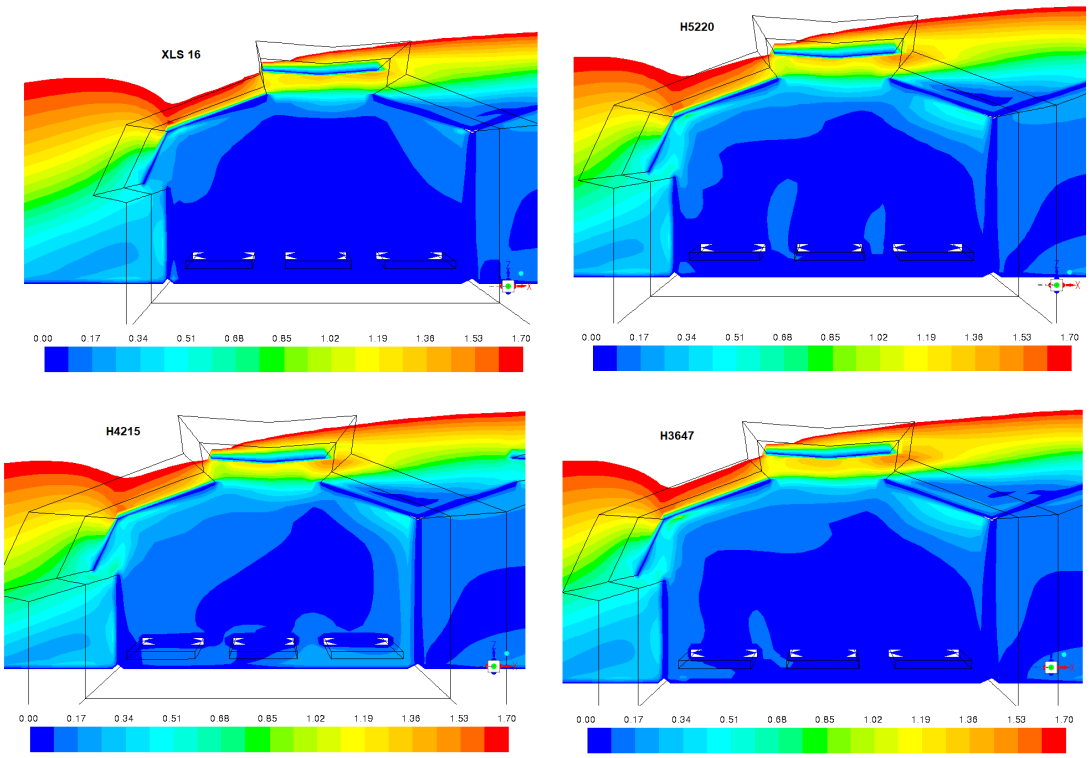

Figure 4.47: Contour maps of the four cases of the section placed in the middle of the greenhouse.

confirmed in the middle section. They show a the highest velocity magnitude in the areas up to the horizontal screen and close to the lateral screen. In fact, the penetration of the air flow incoming from the vents is really limited in small areas close to the screens.

In order to observe better the air flow dynamic inside the structure, the vector maps are presented only for the middle sections. The vortex in the upper part of the section is clearly visible in the case H4215. Moreover, it is visible an air circulation around the benches and also the velocity close to the internal wall change direction. This could mean the presence of an air flow swirl that involves the cultivation area. In the configurations with H5220 and H3647 screens, three vortexes are present around the benches, but with really low air velocity.

However, the areas of interest are around the benches, where the optimal conditions for the growth of the plants are looked for. For this reason, are compared the air velocity profiles at the same heights as done in previous section. The figure 4.50 show the greater magnitude velocity for the H4215 and a similarity of profiles through the sections for all screens. The analogy of the air velocity trends of H5220

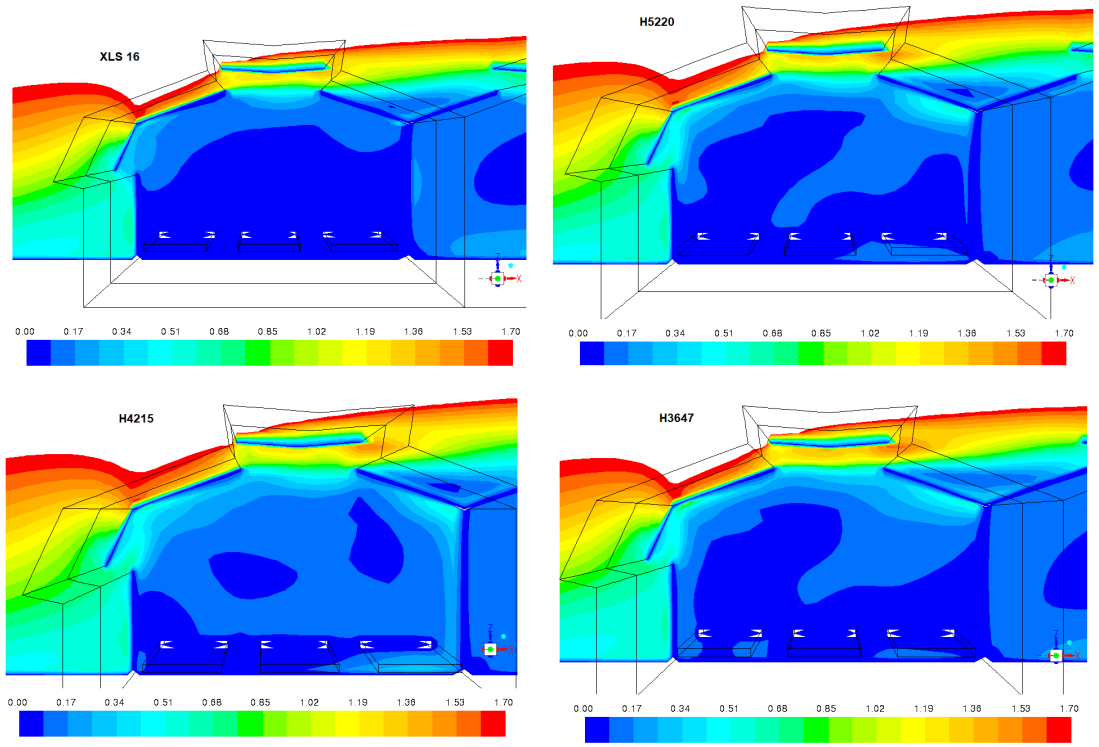

Figure 4.48: Contour maps of the four cases of the section placed in the back of the greenhouse.

and H3647 is confirmed, so much to coincide in some areas.

The air velocity presents in any case an increase close to the right lateral limits of the section, already noticed in the contour maps, even exceeding 0.2 m/s in the middle and back sections. In the front section, the screens H4215 shows a significantly linear trend, except for a decrease of the air velocity close to the left lateral limit of the section. In this position, the grater air magnitude refers instead to the H5220 case. In the cases at 20 cm of height, the profiles doesn't show any peculiar difference compared to the results at 50 cm of height.

On the contrary, in figure 4.52 it is important to notice that the screens H4215 doesn't show significant and important improvements, only the increasing velocity close to the internal wall. In fact, the trends are similar in all section for any cases. They present velocity magnitude picks between the benches. A peculiar thing visible in these sections is the fact that the configuration with screen H5220 present greater velocity than the H4215 case, not only in the back but also in the central section.

In order to quantify and analyze the variations of the air velocity magnitude

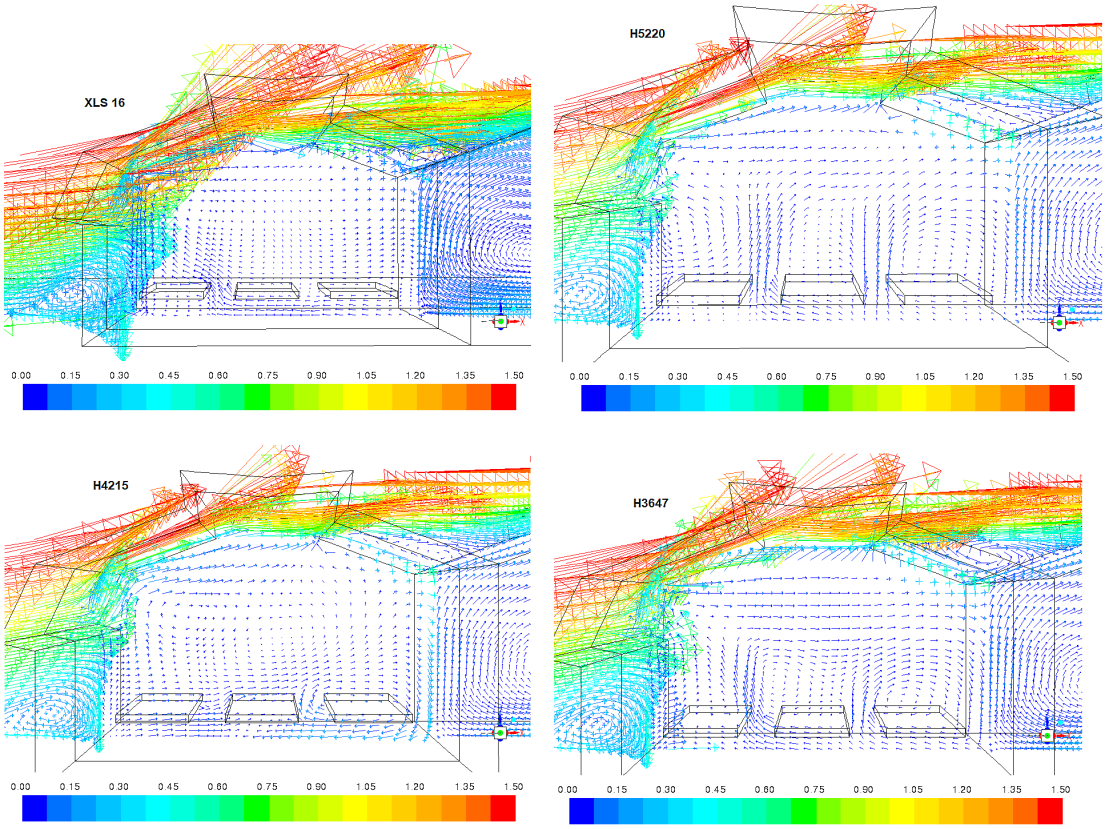

Figure 4.49: Vectors map of the four cases of the section placed in the middle of the greenhouse.

between the cases, the average air velocity at each height, regarding a specific greenhouse section, has computed and compared for all simulated case. In table 4.14 the averaged air velocity, collected in the back plane of the greenhouse, are reported and the percentage of air velocity reduction due to the presence of the screens is calculated. The reduction was computed based on the average velocity of a profile belonging to a specific distance from the benches and the same profile of the case without screens.

The data shows an almost invariant reduction between profiles at 10 cm and 20 cm from the benches. The percentage reductions related to the profiles at 50 cm from the benches present are decreased compared to the results related to the other two planes. The reduction related to the case with H5220 presents percentage going from a maximum of 64.4 % to a minimum 53.5 %, similar to the values characterizing the case with H3647. In fact, this case shows a limited range of variation, going from a maximum reduction of 62.6 % to a minimum value of 55.9

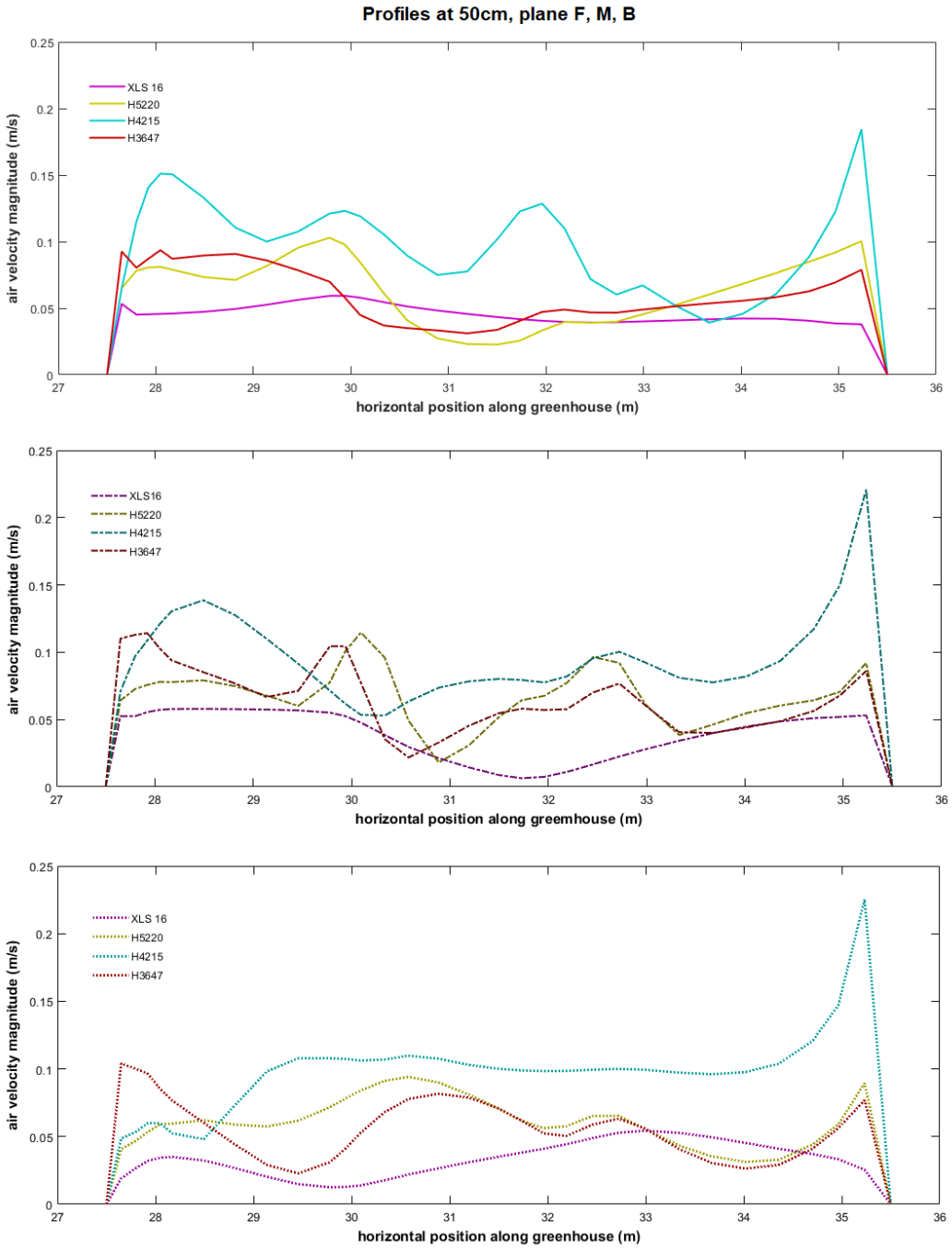

Figure 4.50: Air velocity profiles, related to back, front and middle sections, regarding the area at 50 cm from the benches of the four screen types simulated.

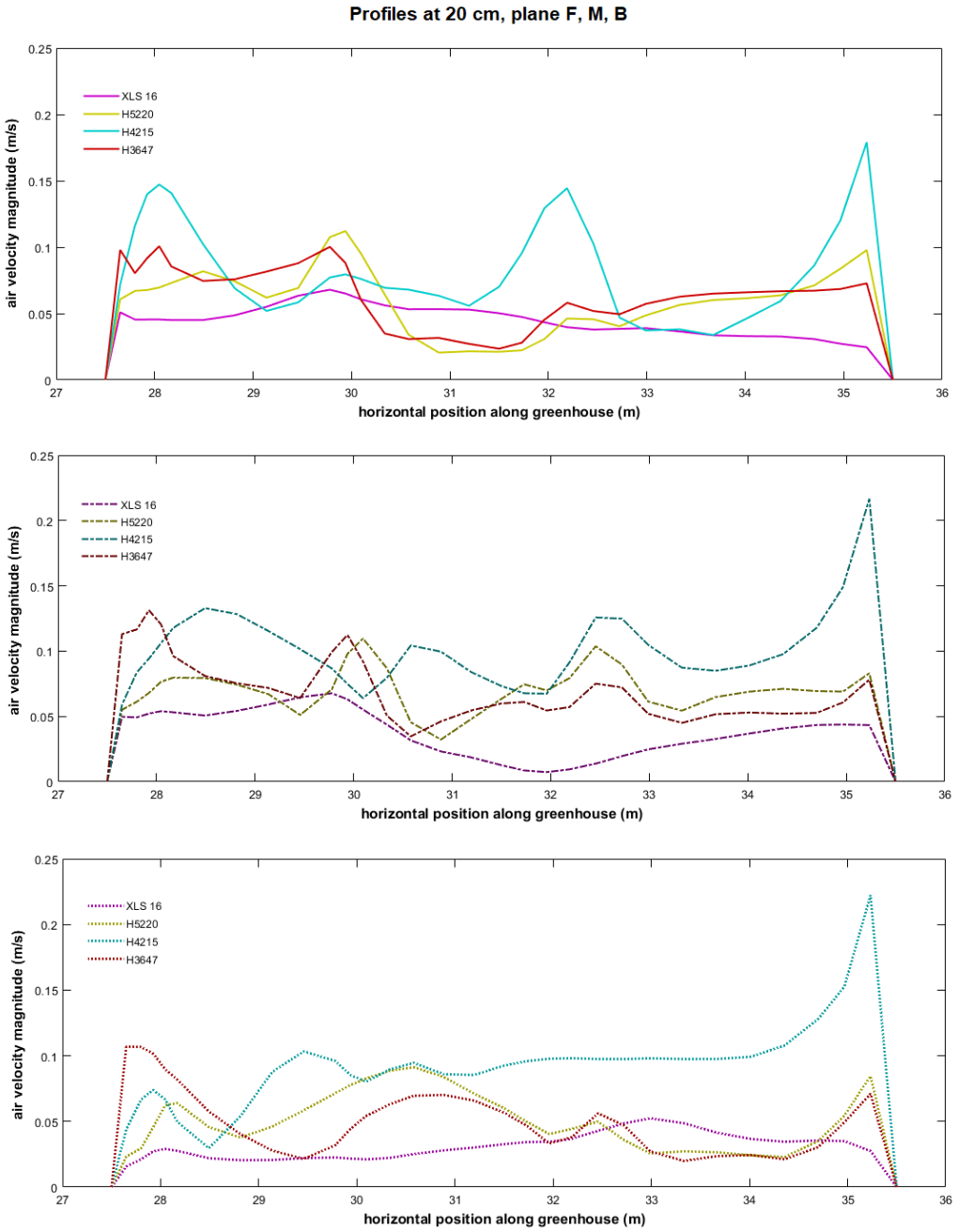

Figure 4.51: Air velocity profiles, related to back, front and middle sections, regarding the area at 20 cm from the benches of the four screen types simulated.

%. However, the most limited reduction is the one of the simulated case with H4215 screen type and the worst results are those of XLS 16 case.

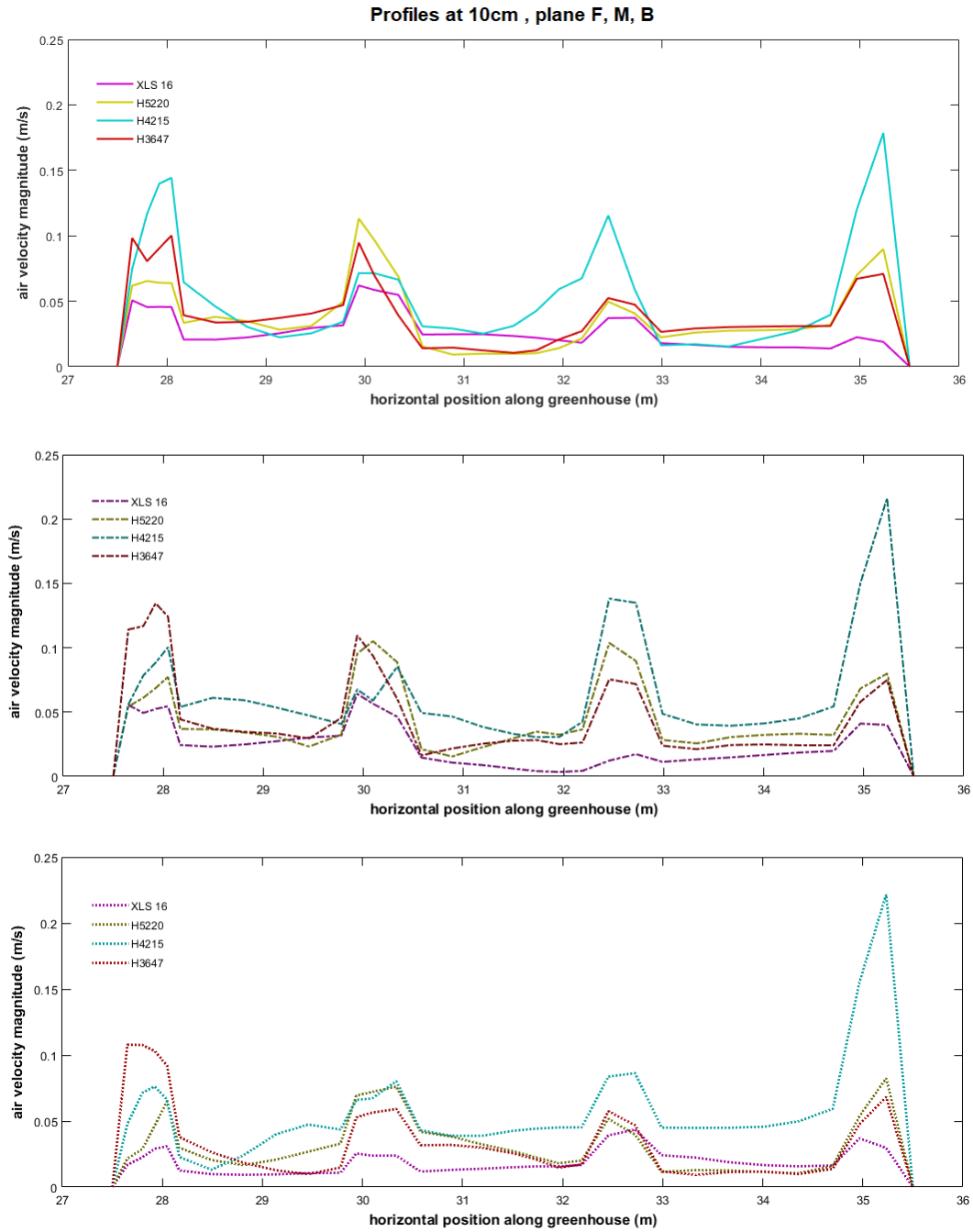

Figure 4.52: Air velocity profiles, related to back, front and middle sections, regarding the area at 10 cm from the benches of the four screen types simulated.

Table 4.14: The average speeds were calculated for all the profiles related to the greenhouse back section and the variation compared to the results of the case without screens was quantified.

	10 (cm)	Reduction (%)	20 (cm)	Reduction (%)	50 (cm)	Reduction (%)
XLS 16	0.019	79.2	0.029	78.2	0.031	75.6
H5220	0.032	64.4	0.049	63	0.058	53.5
H4215	0.056	37.8	0.087	34.2	0.092	26.7
H3647	0.036	60	0.049	62.6	0.055	55.9

Table 4.15: The average speeds were calculated for all the profiles related to the greenhouse central section and the variation compared to the results of the case without screens was quantified.

	10 (cm)	Reduction (%)	20 (cm)	Reduction (%)	50 (cm)	Reduction (%)
XLS 16	0.025	79	0.036	80	0.037	77
H5220	0.046	61.5	0.066	63.2	0.065	59.7
H4215	0.063	49.5	0.095	47.5	0.09	44.1
H3647	0.049	58.6	0.068	62.1	0.065	59.7

In table 4.15, the results shown refer to the central plan of the greenhouse. They are similar to the ones presented in tab 4.14, if not for a visible increase in the percentage reduction in the case with the screen H4215. In fact, in this section the percentages passed from a range between 26.7 % and 37.8 % to values close to 45 % or more. In addiction, it is visible that the percentages of all cases vary within a narrower range than in the results of the previous section. This is due to more homogeneous speed values between the various distances considered above the benches.

Instead, in table 4.16 are reported the results related to the front section of the greenhouse. In this section, similar results are obtained to those obtained for the back section (tab. 4.14, where a significant decrease in the percentage reduction of speeds is visible at 50 cm from the benches, mainly for the case with H4215 screen type. Nevertheless, the reduction percentages of air velocity, at 10 cm and 20 cm in the front section, are the highest ones for the case with H4215, compared to all

Table 4.16: The average speeds were calculated for all the profiles related to the greenhouse frontal section and the variation compared to the results of the case without screens was quantified.

	10 (cm)	Reduction (%)	20 (cm)	Reduction (%)	50 (cm)	Reduction (%)
XLS 16	0.028	76.9	0.043	75.6	0.043	70.8
H5220	0.039	67.2	0.057	67.4	0.06	59.5
H4215	0.056	52.7	0.081	54.1	0.095	36
H3647	0.042	65.1	0.06	65.6	0.057	61.3

those presented before. In this section, this would be the positions characterized by the worst conditions for plants cultivation. On the contrary, the H5220, H3647 and XLS 16 cases showed values not very different between the various sections and between the various positions, showing also that the worst results are obtained with the presence of XLS 16 screens, confirming what has been seen so far.

4.3.5 Observations

From these results, it is possible to understand that the placements of the H4215 screen could give better air velocity conditions in the cultivation area. Moreover, the simulation with XLS 16 present the worst condition possible between the different configuration. Another unexpected outcome is the similarity between the air flow inside the structure in H5220 and H3647 cases. In fact, in the section 4.2, from the experimental characterization of the screens, the H5220 gave results closer to the H4215 case than H3647. For this, it was expected to have more similarities between H4215 and H5220 than H3647. Nevertheless, the configurations show too low air velocity magnitude for the optimal growing conditions of the plants.
However, could be interesting, for further studies, to evaluate if the effect of the different screens could give different and more significant results with the increasing of the wind velocity or even the wind direction. Another aspect could be study different dispositions for these type of screens, starting with the present condition which demonstrated to be critical.

4.4 Wine cellar case study

The process of preparation of wine consists in several steps, which one of the most important is the wine-aging. In this step, temperature and humidity play a fundamental role, since they can strongly affect the quality of the final products, which improves in constant and suitable environmental conditions (Boulton et al., 1999), as already anticipated in section 2.4. Regarding this, the improvement of internal ventilation can have a significant role in achieving the best conditions. In this chapter, a CFD study for the design of a ventilation system, which is created as a support of natural ventilation for a wine cellar, is presented. The basic idea is to obtain a mechanical ventilation system able to modify the air flow patterns and in this way to reduce, if not eliminate, the areas of air stagnation.

4.4.1 Wine cellar description

The natural ventilation in a cellar is usually made by a window and several outlets to the outside. Considering this, a ventilation system has been designed in order to be placed in a wine cellar, as addiction to the existing ventilation. The users of this system should be small or medium wine producers. In specific, a wine-aging room of an Italian wine-growing and producing farm, which already had been collaborating with the research group on other aspects of the wine-making process, was chosen as case study (farm winery located in the Emilia-Romagna region, Italy, with average production of 1500 hl/year and worldwide export). The farm is located in the eastern part of the Emilia Romagna Region, where viticulture and fruit farming are widespread and consolidated activities (Barbaresi et al., 2015). Figure 4.53 shows two pictures of this wine cellar.

Figure 4.53: Pictures of the wine cellar.

The room (see figure 4.53)is a north-east oriented parallelepiped, 9.80 m long, 5.20 m wide and 2.60 m high and it has a window located on the north-east wall,

a door on the north- west wall. It can contain up to 45 french barrels, called barriques, 89 cm long, diameter 59-71 cm each. The barrells are placed close to the walls and few of them also in the middle of the room. The four walls and the floor are in contact with the ground, the ceiling with a conditioned room. The cellar is naturally ventilated.

However, the only natural ventilation had showed several inconveniences for the wine conservation. In fact, the air velocity could be too low around the barriques, raising in this way the possibilities of mold formation, or even stagnation areas not reached by natural ventilation. About this, it was validated the 3D model of the cellar and was investigated the air flow distribution inside in a condition of natural ventilation. Moreover, considering the critical aspect of this ventilation system, has been considered to adapt and apply a well consolidated ventilation technique in residential buildings, such as perforated tubes, also in agricultural field.

4.4.2 Cellar ventilation

The airflow patterns within wine cellars has been investigated by CFD simulations validated against experimental trails. In specific, the built environment of the farm includes a two - story building with an underground cellar for wine aging. The cellar is naturally ventilated through the access door and a single window, as illustrated in fig. 4.54. Inside plan dimensions of the cellar are 4.70 m 9.80 m; the internal height is 2.50 m, with floor plan located 2.90 m below the ground.

Figure 4.54: Picture of the farm building with the indication of the underground wine cellar location.

The numerical model of the cellar, including the wooden barrels inside was developed in Fluent environment based on the 3D digital model represented in

figure 4.55, which includes the door and window openings and three holes placed in the South-Western wall and ceiling, which should contribute to air exchange with the outdoor. For the CFD model was created an unstructured mesh with 4 $\times 10^6$ cells, carried out with robust octree method. The mesh was refined in several areas: holes, fan, door, window and big barrels. Convergence criteria adopted for simulations is 10^{-5} for all parameters and 10^{-3} for continuity.

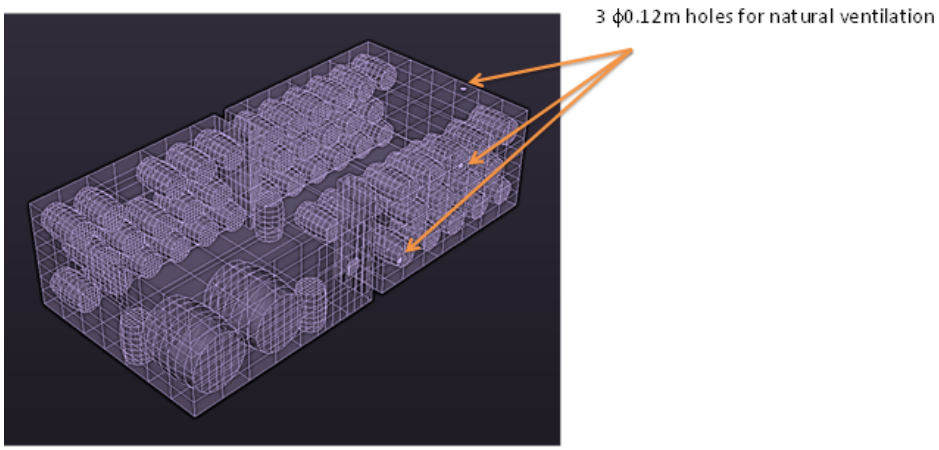

Figure 4.55: Geometrical 3D model of the wine cellar.

An experimental trial in controlled conditions of ventilation was set to validate the CFD model.

Validation measurements

The validation data were collected in controlled conditions inside the structure. Specifically, the window and the ventilation holes were left open, while the door was closed with cardboard, except for a circular hole with diameter of 0.4 m and center on the vertical axis of symmetry of the door, at 1.20 m height. This hole was fully covered by a circular fan with the same size of the hole and known mechanical features, so that a controlled forced ventilation inlet condition was created.

Measurements of inlet air velocity were carried out by means of vane probe anemometer Delta Ohm AP472 S1 with the following features: 100 mm diameter, velocity range of 0.4 m/s - 30 m/s, resolution of 0.01 m/s, accuracy corresponding to $\pm$ (0.1 m/s + 1.5% full scale). The inlet air velocity was characterized by measuring air speed at a distance of 5 cm from the fan surface, in nine points equally spaced with distance of 1/3 radius, distributed along the vertical and horizontal diameters of the fan. Air velocity was measured in each point for 60s with 1s sampling interval, and the average value of these measures excluding the outliers was considered as air the velocity in each point. Then a three-dimensional

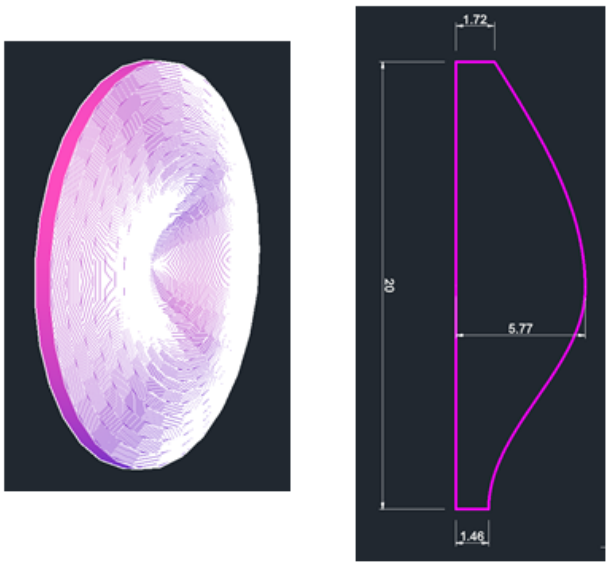

Figure 4.56: 3D velocity profile (on the left) on a vertical plan at distance of 5cm form the inlet fan and radial section of the profile (on the right). Velocity in m/s, distance in cm.

profile of air velocity was created (Fig. 4.56) and an equivalent uniform profile was assessed, resulting in a circular inlet with constant magnitude of 3.55 m/s, which was adopted as boundary condition.

Under these controlled conditions, the experimental measurements of air speed were carried out by means of hot wire probe anemometer Delta Ohm model AP471 S4 S1 with the following features: velocity range of 0.1 m/s - 5 m/s, resolution of 0.01 m/s, accuracy corresponding to $\pm$ 0.05 m/s (from 0 to 0.99 m/s) and $\pm$ 0.15 m/s (from 1.00 m/s to 5.00 m/s). Air velocity magnitude was measured in a in a grid of 70 measurement points, illustrated in figure 4.57.

Air velocity was measured in each point for 60s with 1s sampling interval. Then the CFD model of the cellar representing the same inlet and outlet conditions adopted for the experiment was set up and steady state simulations were run. Results in term of air speed magnitude on a plan at 1.20 height over the floor is illustrated in figure 4.58.

Simulated velocity magnitudes were computed in the 70 measurement points to validate the model. Overall RMSE was equal to 0.291 m/s. In particular, the fit of simulations to experimental values along the horizontal axis of the inlet fan is represented in figure 4.59, while the fit along the central longitudinal axis of the cellar at the same height is represented in figure 4.60 and figure 4.61.

CFD simulations proved thus to represent suitable tools to study airflow pattern

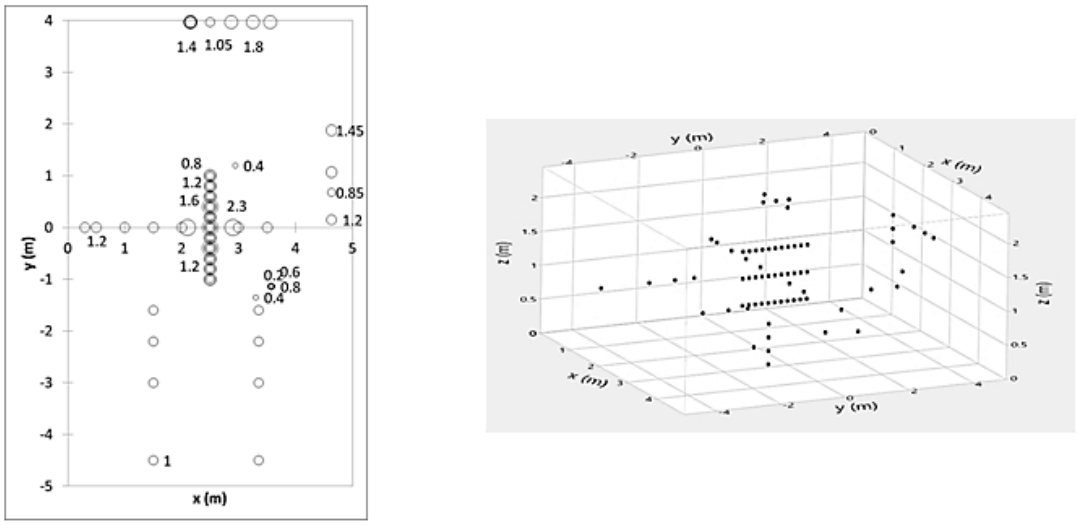

Figure 4.57: Grid of air velocity measurement points inside the cellar. On the left: Plain layout with indication of points heights (proportional to circle diameters). On the right: axonometric view. The origin of the Cartesian System corresponds to the projection of the door axis of symmetry on the floor.

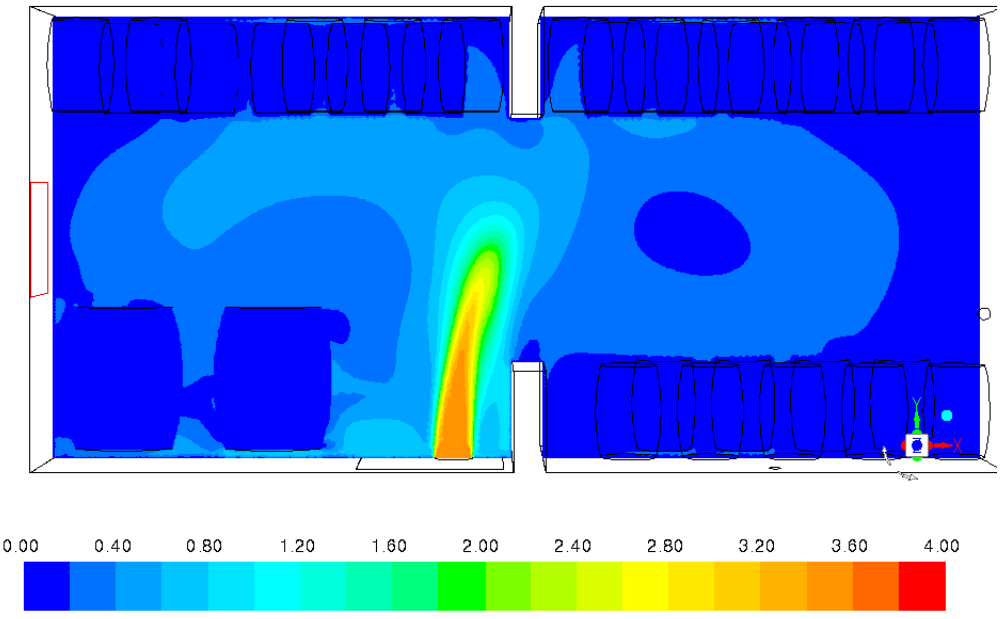

Figure 4.58: Simulated velocity magnitude on a plan at 1.20 height over the floor under validation conditions.

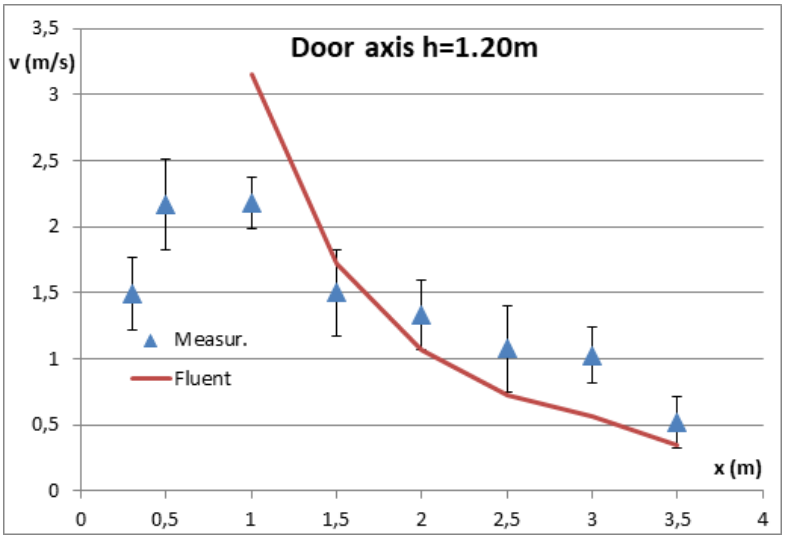

Figure 4.59: Simulated and measured air velocities along the horizontal axis of the inlet fan.

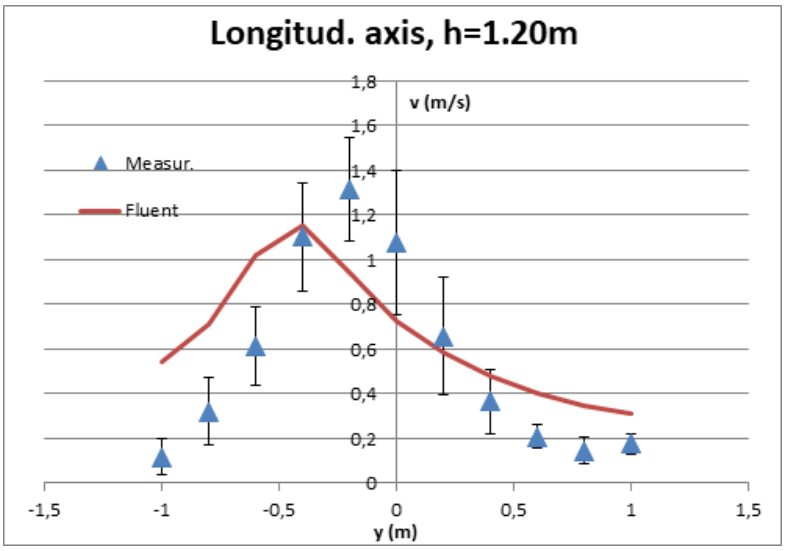

Figure 4.60: Simulated and measured air velocities along the central longitudinal axis of the cellar at 1.20 m height.

inside the cellar. As a first outcome, the validation model allowed to underline that the space between the barrels and the walls behind was affected by negligible air velocity magnitude, even under conditions of forced ventilation from the door and the open window, as it is clearly shown in figure 4.58.

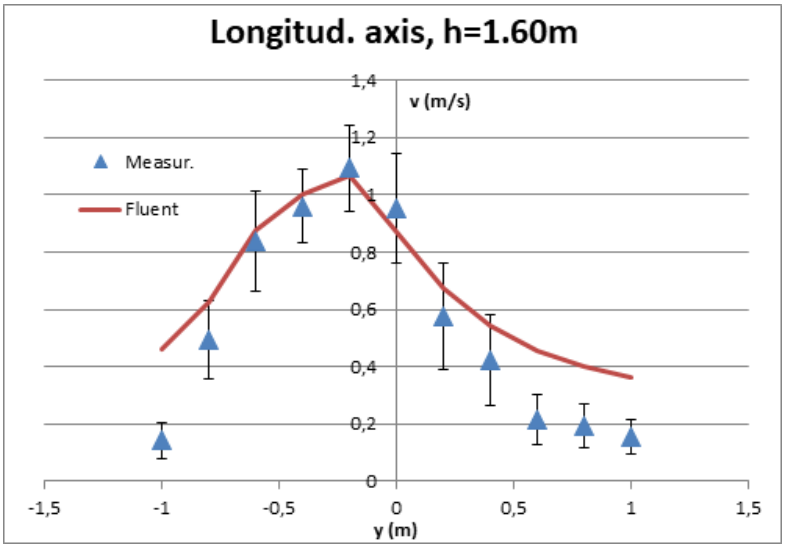

Figure 4.61: Simulated and measured air velocities along the central longitudinal axis of the cellar at 1.60 m height.

CFD results

The validated model was then used to simulate a different condition of ventilation, based on the available inlet openings. In particular, a condition with 1 m/s uniform air speed entering from the window and the door closed has been considered, in order to verify if the increase of air speed entering from the window could be an effective strategy to achieve distributed ventilation throughout the cellar. The results are shown in figure 4.62 in terms of velocity magnitudes at different heights. The results clearly highlight that a great drop in air velocity occurs passing from the central zone of the cellar to the area between barrels and the walls behind, independently from the height above the floor. The only exception is represented by very small areas around the holes in the Sout-Western wall, where velocity peaks can be noted, but they cannot contribute to ventilation behind the barrels, as they represent only local phenomena causing great heterogeneity of ventilation rate.

Therefore, in the North-Eastern wall the zones behind the barrels are characterized by very small velocity magnitude, as reported in tables 4.17 and 4.18. These values are calculated as average velocity values of profiles behind the barriques.

The area between barrels and South-Eastern wall, northern part, is characterized by extremely variables velocity values at height of 0.5 m and 2 m, due to the presence of holes, as noticed above. At 1.25 m, 0.10 m from the wall, the average velocity over the cells is 0.31 m/s, with standard deviation of 0.1 m/s, which means that it is about 50 % of the velocity in central zone of the cellar. Therefore the simulations clearly showed that the ventilation entering either from the door or the window

Table 4.17: Air velocity behind barrels on NE wall, southern part (statistic over the cells at 0.10 m from the walls).

Height (m)	Average velocity (m/s)	Standard deviation (m/s)
0.50	0.10	0.05
1.25	0.11	0.06
2	0.11	0.06

Table 4.18: Air velocity behind barrels on NE wall, northern part (statistic over the cells at 0.1 m from the walls).

Height (m)	Average velocity (m/s)	Standard deviation (m/s)
0.50	0.18	0.05
1.25	0.11	0.06
2	0.15	0.05

does not represent an effective strategy to achieve uniform air exchange inside the cellar, independently from the inlet velocity. In particular, the zones behind the barrels located near the walls are affected with poor or negligible ventilation, with the consequent issues of mold formation, humidity concentrations and temperature inhomogeneities. This part of the study underlined that the improvement of the air velocity distributions is an important opportunity in wine cellar to optimize micro-climatic conditions by achieving high uniformity of air speed and humidity. Moreover, the combination of on-site measurement and CFD simulation represent a fundamental tool for the identification and characterization of airflow patterns in wine cellars. Finally, the results clearly indicate the opportunity to develop proper specific systems, such as micro-ventilation, to increase uniformity of air velocity in wine aging cellars.

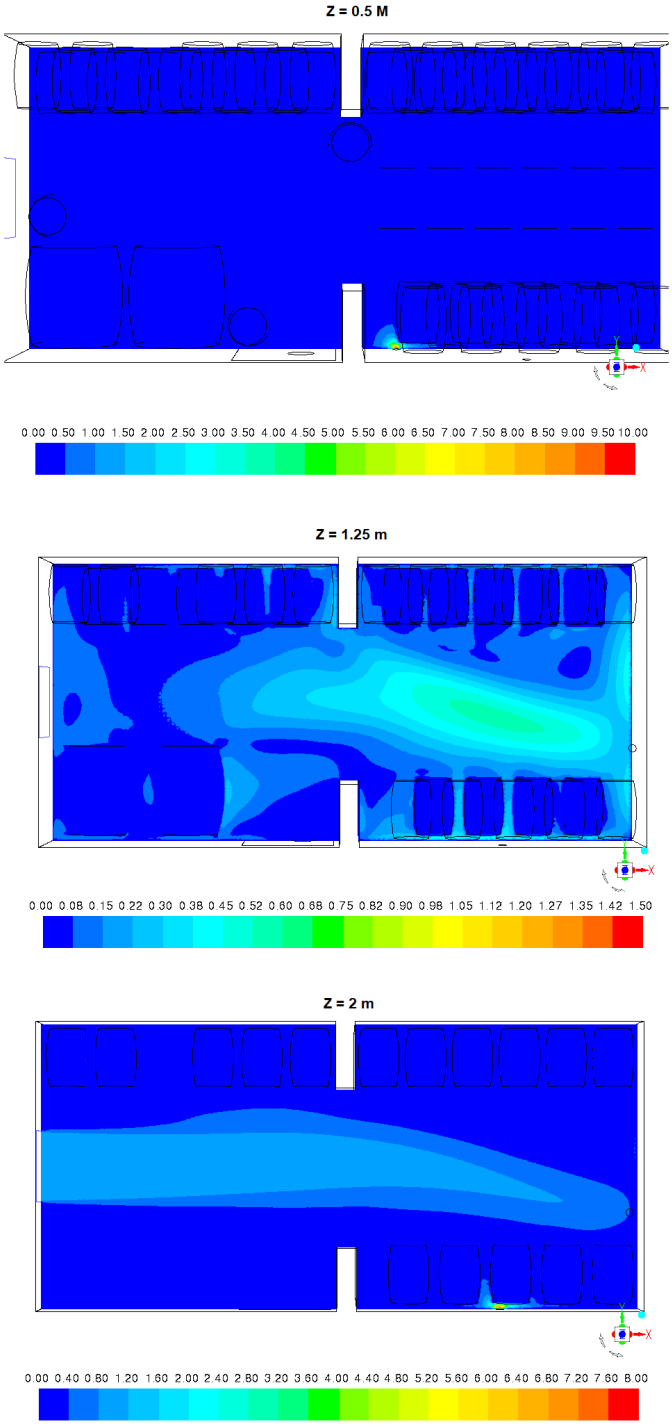

Figure 4.62: Contours of air velocity magnitude at three different horizontal section under condition of 1 m/s airflow inlet from the window and door closed.

4.4.3 Ventilation system

Tube ventilation is a unique method that gently introduces fresh air into enclosed environments without introducing damaging cold drafts. This system creates environments that are infused with fresh air. For this reason, it could be ideal for any kind of buildings, such as calf barns and other animal rearing facilities, including poultry and swine as well as greenhouses, commercial buildings, industrial settings. Despite this, in literature are only few the studies on this type of system in agricultural field (Mondaca and Choi, 2017; **?**; Wells and Amos, 1994). There are several studies focused on modeling the tube system such as (El Moueddeb et al., 1997, 1998; Brundrett, 1990; Wells and Amos, 1994). For example, El Moueddeb et al. (1997) validate a simplified one-dimensional model, based on the fundamental equations of thermodynamics and fluid mechanics for an incompressible and inviscid fluid. The model is based on eq. 4.24 and 4.25:

$$P_2 = \rho[V_1((\frac{1}{2})(V_1 + V_2 - V_0 cos(\alpha)) + \frac{(V_0^2 - V_2^2)}{2}] \tag{4.24}$$

$$C_r = K_{e1} - [(\frac{2}{((V_1 + V_2)V_1)}][(\frac{(V_0^2 - K_{e2}V_2^2)}{2}) - \frac{P_2}{\rho}], \tag{4.25}$$

where P_2 is the downstream pressure expected from a single or a pair of outlets to the duct average air velocity (V) and to the outlet air jet exchange angle (α) and velocity (V_0). Moreover, C_r is the regain coefficient and K_e are energy correction coefficients. Furthermore, El Moueddeb et al. (1998) developed a new design model for perforated ventilation ducts based on the previous one. It compares also the actual airflow distribution pattern of the three perforated ducts to those predicted from the model. Finally was tested the hypothesis that the effective delivery area of the fan is equal to the effective outlet area of the duct. Wells and Amos (1994) presented the possible steps for designing an air distribution system for a greenhouse. In fact, it was identified a design procedure for a perforated polyethylene tube:

1. Calculate the total air circulation rate;
2. Determine the number of ducts, position and length;
3. Determine the number of rows of holes;
4. Determine discharge jet throw distance;
5. Select static pressure fro the duct;
6. Calculate hole size;

7. Calculate number of holes;
8. Calculate duct diameter;
9. Check aperture ratio and inlet pressure (back to point 7 if necessary);
10. Check jet throw and hole size (back to point 6 if necessary);
11. Draw system curve, including losses in supply ducts, elbows and takeoffs. Select inflation fan (back to point 5 if necessary);

In this procedure is assumed that all holes will have the same size and spacing, with the idea of obtaining a duct which should be easy to be manufactured.
The application of CFD approach is not frequent in literature study of this type. For example, Mondaca and Choi (2017) creates and validates a computational fluid dynamics (CFD) model capable of replicating the flow distribution created by a positive-pressure polyethylene tube ventilation system. In addition, Mondaca and Choi (2017) has been tried to determine the feasibility of adding jet deflectors to aim the jets at specific targets without affecting the entire performance of the system. Taking into account the problems given by a not optimal natural ventilation and knowing which are the usual air velocity magnitude characteristic of a natural ventilated cellar, this work aims to define a low cost system for the mechanical ventilation in addiction to the natural ventilation. In specific, the system consists in a polyethylene perforated duct. It was validated the model of the preliminary configuration of the system and then were investigated different set up solutions in order to identify which should be the best configuration possible between the several hypotheses.

System description and construction

The duct ventilation system has been taken in account as technological solution to improve the climatic condition inside the wine cellar, in specific around the wine barrels. For this reason, there are geometrical limitations for the system that must be respect. In fact, to be placed behind the barriques, between them and the wall, the tube can not have a diameter greater than 20 cm. Moreover it can not be longer than 4.80 m, which is the length of the wall, as visible in figure 4.63. The system was performed using materials that are easy to find and not expensive. Was considered the use of a PVC tube of 0.12 m and 0.08 m of diameter and a pc fan of 80 and 220 V, with the proper dimensions to be connected to the tube (both long 2 m). Both kind of tubes were perforated with a drill of 0.005 m and were tested several combinations of tubes and fans, in specific:

- Tube of ϕ=0.125 m and fan 220 V;

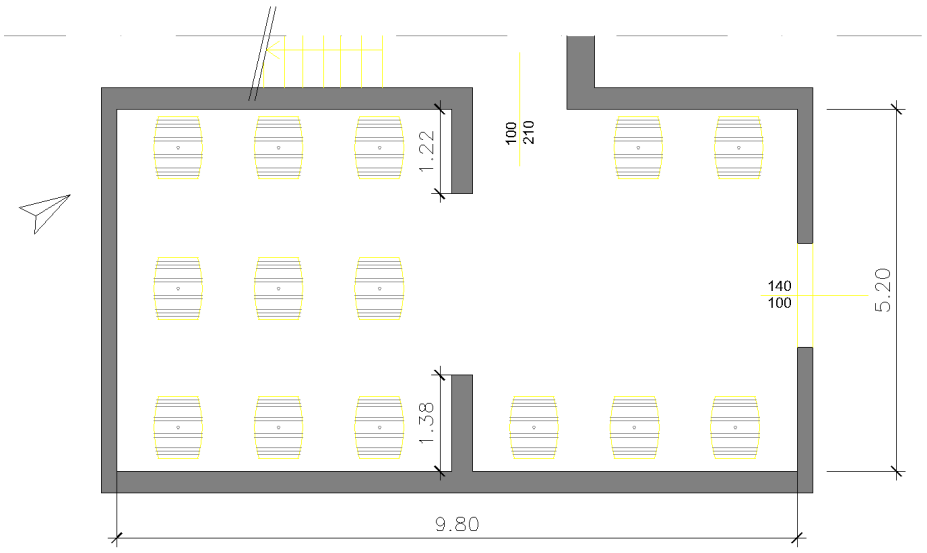

Figure 4.63: 2D representation of the room, with a simplified disposition of the barrels on one row.

- Tube of ϕ=0.08 m and fan 220 V;

The two components, in every solution, were connected through a frame of polystyrene and insulating tape. The ratio between holes distance and diameter, $\frac{d}{\phi}$, has been defined equal to 12. Few preliminary air measurements has been performed with an hot wire anemometer,(Delta Ohm with an uncertainty of 0.01 m/s), at 0.40 m from tubes. The optimal range of velocity wanted, based on Geyrhofer et al. (2011) was up to 0.40 m/s, which is a normal value obtainable by NV, and 1 m/s, which can cause too significant wine losses. Between the first two configuration, this range of velocity was respected only by the configuration **of ϕ = 0.125 m tube and fan 220 V**. Starting from this first system, firstly the case was modeled and validated and consequently were studied different configuration to improved and define a better set up.

System modeling

As defined in the previous paragraph, the configuration modeled in CFD was a tube 2 m long, of 0.125 m of diameter. The fan was a pc fan of 220 V. The geometrical model was carried out by Autodesk Inventor. The global dimensions of the domain were 3 m of width, 4.025 m long and 1.2 m height (see fig. 4.64)

In particular, had been necessary to model the fan as surface inserted inside a solid body. In particular, had been design as an internal surface of a small cylinder,

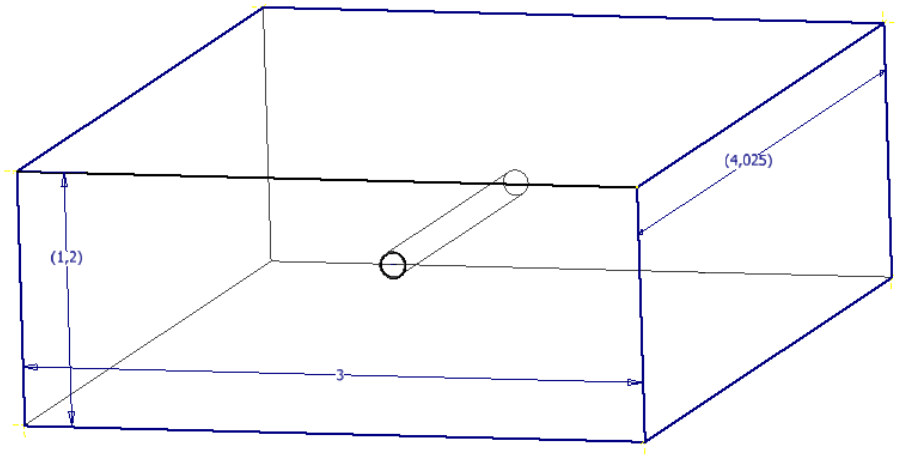

Figure 4.64: 3D model of the validation case, with dimensions reported in (m).

of which the closing surfaces were defined as interiors. The cylinder was created with an height of 2.5 cm and the fan surface was cutting the cylinder exactly in the middle. This had been done in order to be able to model that surface as a fan in Ansys-Fluent, avoiding the complete 3D design of the fan structure. Globally boundary conditions of these cases had been defined as visible in figure 4.65

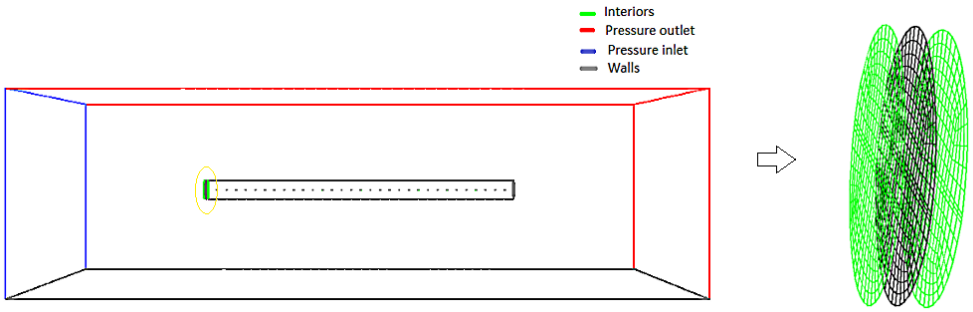

Figure 4.65: 3D model of the case, with outlined boundary surfaces specification. It has been highlighted with a yellow ring the part concerning the fan and has been done an enlargement of it, at the right. The three surfaces visible are the two interior surfaces, in green, and the fan surface in black.

On this model, were performed four different grids with cells number from 8×10^{05} to the finest one of 6.4×10^{06}. In the same way as performed for the other models, has been performed a convergence study as presented in figure 4.66

The resulting mesh, chosen for the simulations, was the one of 3.2×10^{06}. In this preliminary step of the study, the fan has bee already defined with the real

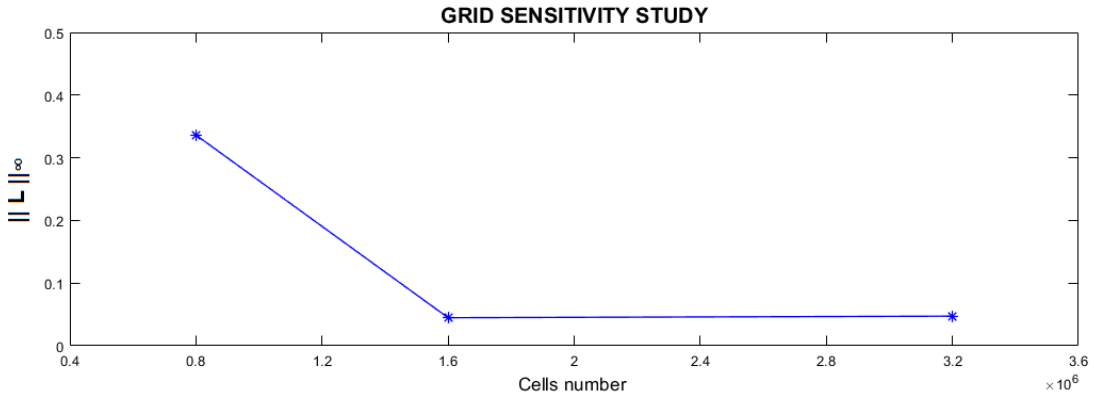

Figure 4.66: Grid convergence study for the four different meshes, by the calculation of $\|L\|_\infty$.

characteristics, for the validation process. In fact, it was configured with a static pressure of 45 Pa, the center of rotation exactly at the center of the surface with a diameter of the internal body equal to half of the fan diameter (0.06 m, see fig. 4.67). Moreover, it has been imposed a tangential velocity of 15.4 m/s derived from

Figure 4.67: Image of the pc fan, form the data sheet, with specified dimensions.

the data sheet. The simulations were conducted with a standard k-ϵ model, which will maintained for the future simulations.

Model validation

In order to be able to validate the model presented, the system has been subject to measurements of air velocity. In particular, data were collected at two different distances from the tube. The measurements has been done using an hot-wire anemometer (Delta Ohm with an uncertainty of 0.01 m/s), provided with a metal cover for the wire protection. This cover is a spherical grid of around 6 cm of

diameter. A series of measures had been taken at 40 cm from the system, in four different positions along the tube, as presented in figure 4.68.

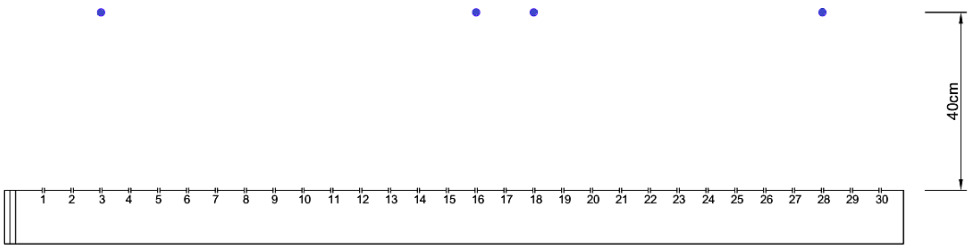

Figure 4.68: This is a simplified scheme of the measurements positions (blue points) with respect to the tube.

This distance should be the representative distance of the barrels from the tube, once placed in the wine cellar. The time of measurements was of 2 minutes of recording with a time step of 2 s of sampling.

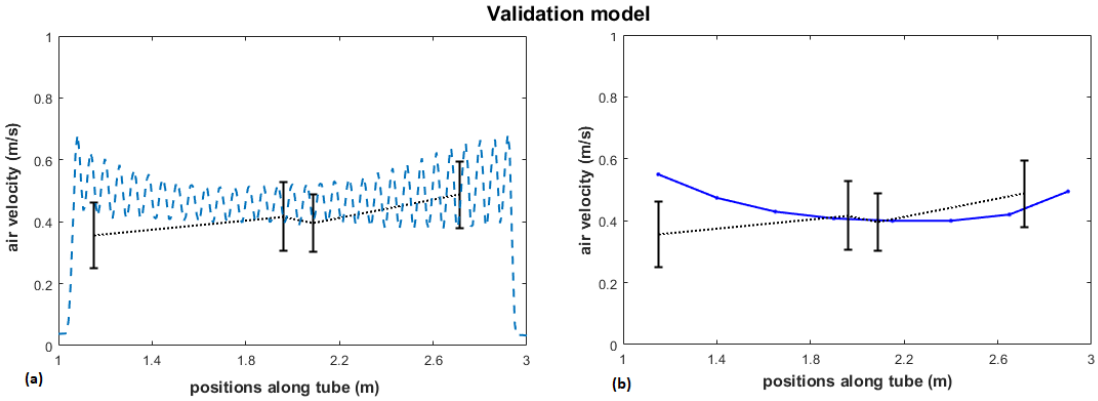

Figure 4.69: In the figure the comparison between measured and simulated velocity magnitudes is showed, collected at 40 cm from the tube. In **(a)**, the profile velocity from the model compared to the profile of collected data (dashed profile) is shown . In **(b)**, instead the measurements profile compared to the linearized profile of simulated results are shown.

In figure 4.69, the graph at left shows the profile of air velocity at 40 cm from the tube extrapolated from the simulation compared to the measured data. It is already visible that the numerical solution is really close to the real data. In order to better observe the two trends compared, the result of simulation has been linearized as visible in the graph at the right. Calculating the relative error between the data measured in the points and the simulation results in the same positions,

three on four error are less than 10 %, precisely are 5, 2 and 1 %. Only respect the first position, the error is higher, around 27 %, however is still lower than the 30 %, the upper limit established to consider validated a model. This could be due to the swirl of the fan, which determine in the reality a more unstable air velocity at the first section of the tube, as explained in (Brundrett, 1990). Considering the variation on the measured data expressed by the standard deviation, it is possible to consider the differences between real and simulated data not significant and for this the model is validated.

4.4.4 Best system design

The first design considered for the system was the one already considered in the validation procedure. Starting from this, were considered other possible solutions, with the aim of find the best configuration to obtain the most homogeneous air velocity profile, with a magnitude settled in a range between 0.3 m/s and 1 m/s, at 40 cm from the tube. Firstly, was decided to increase the diameter and consequently, maintaining the length of the tube and the $\frac{d}{\phi}$ ratio, to thin out the number of holes. It was fixed a new diameter of holes equal to 8 mm, instead of 5 mm, at a distance of 9.6 cm. The simulation was conducted at the same conditions presented in section 4.4.3. As first step, has been compared the air velocity profiles of the two configurations at 40 cm (figure 4.70)

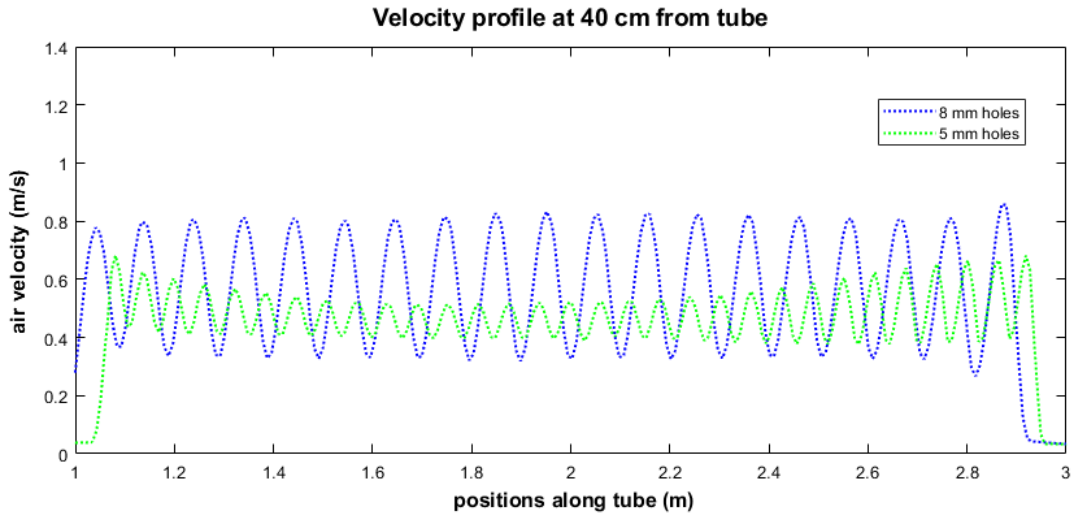

Figure 4.70: Comparison between the solutions with 5 mm and 8 mm holes. These are the two profile at 40 cm from the tube and represents the velocity magnitude starting from the end of the pipe to the fan.

The configuration with 8 mm holes presents a wider variation than the other set up. In fact, the velocity in this case swings between 0.8 and 0.2 m/s, with greater picks in correspondence of holes. Then, on average the air magnitude is higher than the configuration 1 but it is still contained in the evaluated range. However, the solution with 8 mm holes presents a more homogeneous magnitude. On the contrary, the 5 mm holes solution shows an increasing air velocity in the first and last few holes. This fact has been linked to the turbulent nature of the flow and the dependence on the swirl of the fan. Starting from this preliminary results and considerations, were developed and evaluated other system configurations.
First, two solutions were provided with the same number and diameter of holes of the first models, with the addiction of 20 cm of tube at the beginning. In this way, it was supposed to reduce the effect of the fan rotation (Brundrett, 1990) and the high turbulence of the flow around the inlet. In another two configurations, starting from the solution with 8 mm holes, was maintained the holes diameter but was reduce the $\frac{d}{\phi}$ ratio of one third or halved, decreasing in this way the distance between holes and increasing their number. The idea was to obtain a reduction of the range of variation of the velocity magnitude, compared to the starting configuration. As done for the case with 8 mm holes, other two solutions consisted in the model with 5 mm, in which the holes were refined with a distance of 4 cm in one configuration, with $\frac{d}{\phi}$ ratio reduced of one third, and in the another one with a distance of 3 cm, with the $\frac{d}{\phi}$ halved. The same supposition of reducing the variation range of velocity, obtaining in this way a more linear profile, led to these configurations. Totally were provided and analyzed eight different system set ups summarized in table 4.19.

The evaluated configurations should improve the results obtained from the starting configurations. Keeping configurations 1 and 2 as reference base, the velocity profiles of the other cases were compared and analyzed. The figure 4.71 shows in fact, the comparison between the basic configurations, configurations 3 and 4 and, in figure 4.73, between basic configurations, configurations 5 and 6.

An unexpected result characterize the configuration 3, where the air magnitude significantly decrease at the level of half tube, reaching values really low, around 0.2 m/s. Moreover, the trend of the speed doesn't change that means the addiction of twenty centimeter of tube close to the fan doesn't affect the resulting velocity at 40 cm of distance from the tube. Referring to configuration 4, the increase of centimeter to the tube doesn't modify the trend of air velocity, except for the pick at fan level, which was not present before. The variation of air velocity is totally similar to the starting configuration. In fact, air jets penetration distances were comparable in configuration 2 and 4, as visible in figure 4.72. On the contrary, the air jets penetration distances of configuration 3 are significantly reduced compared

Table 4.19: Configurations of the tube analyzed in this study: n is the number of holes, L is the length of tube and ϕ is the diameter of holes.

Configurations	n	ϕ (mm)	$\frac{d}{\phi}$	L (m)
1	30	5	12	2
2	19	8	12	2
3	30	5	12	2.2
4	19	8	12	2.2
5	44	5	8	2
6	27	8	8	2
7	58	5	6	2
8	35	8	6	2

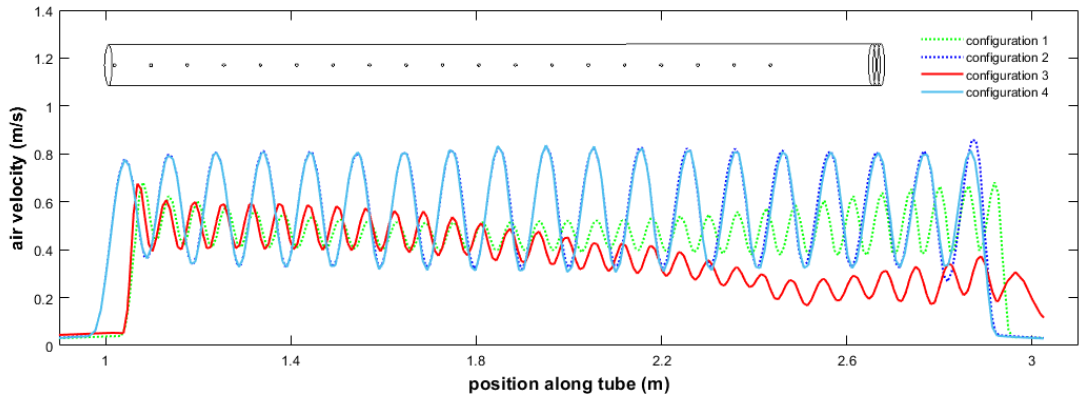

Figure 4.71: The dashed lines are the basic configurations and the whole lines are the configurations with 20 cm in addiction of tube.

to the starting configuration 1 (fig. 4.72).

In fact, the positions of the profiles (black line in figure 4.72) concerns a zone where every air jet is still quite defined. Instead, at a short distance, an area with a more homogeneous air velocity can be observed, where there is no longer the separation of the single jets.

On the contrary, the air jets of configuration 1 and 3 are characterized by a more restricted penetration distances. In particular, configuration 3 presents an area where the contour profiles are not presents, where the air velocity is under the lower limit defined (0.05 m/s). This configuration definitely has a very limited

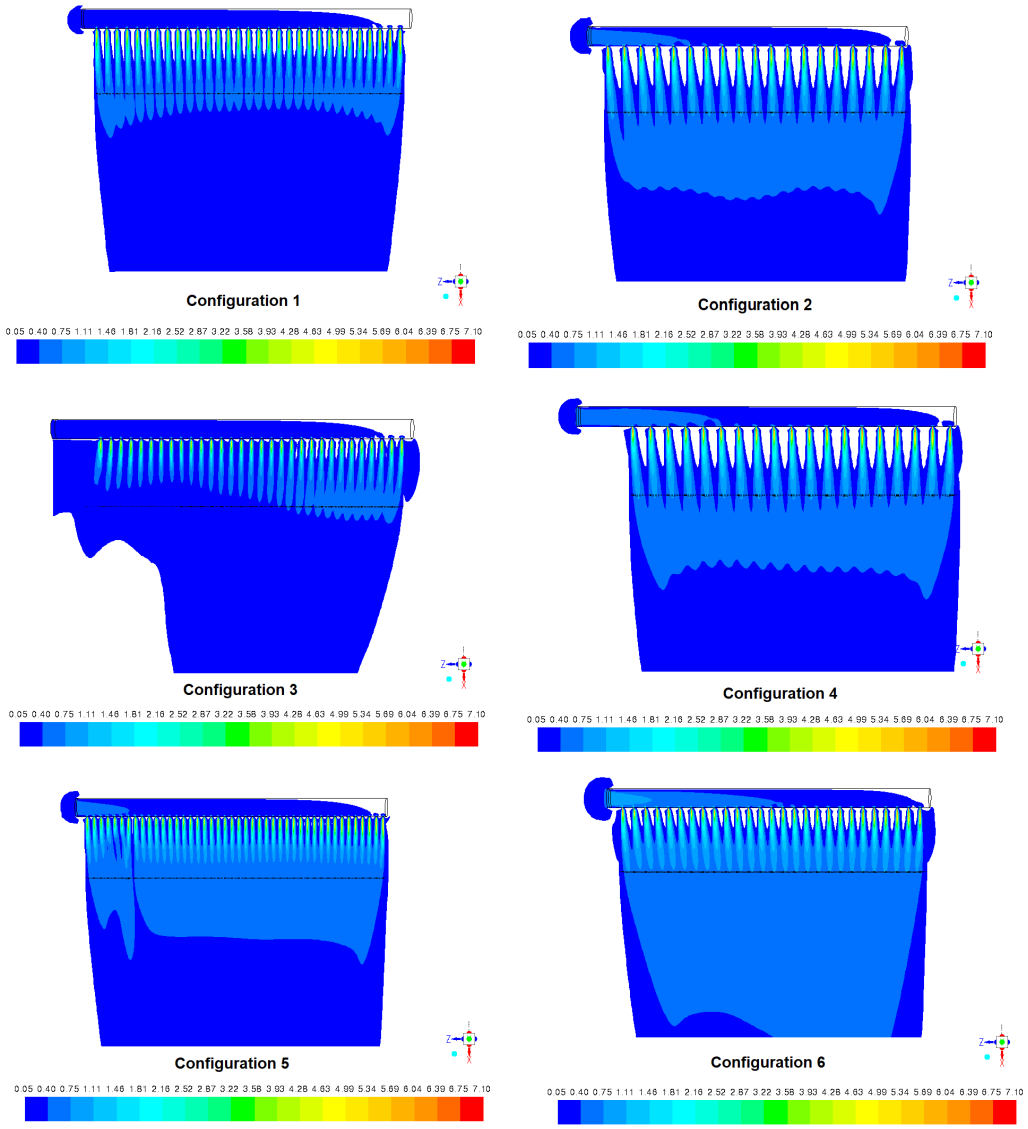

Figure 4.72: Contour maps of the configurations from the first one to the sixth one. The air velocity profiles, at 40 cm of distance from the pipe, are showed in black.

area of action. However, considering the application of the system and the desired air velocity, the new configurations (3 and 4) allow to obtain results far from what is looked for. The same comparison was performed between configurations 1,2 and 5,6, as presented in figure 4.73. The configurations 5 and 6 show an air velocity variation really limited, around 0.6 m/s for the fifth configuration and between 0.8

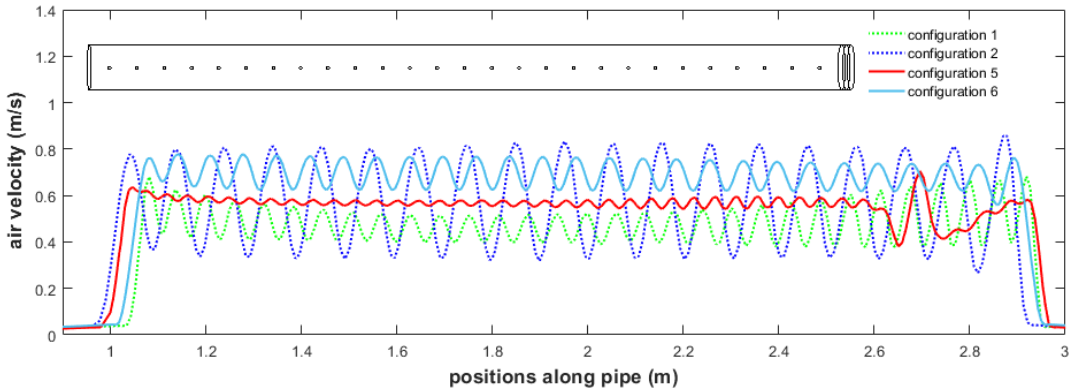

Figure 4.73: The dashed lines are the basic configurations and the whole lines are the configurations with refined holes. The pipe is the configuration 6, for understanding that the profiles are from the end to the top of the tube.

and 0.6 m/s for the sixth configuration. Configuration five presents also an initial wider variation of air speed, at the level of the first five holes, but still limited between 0.6 and 0.4 m/s.

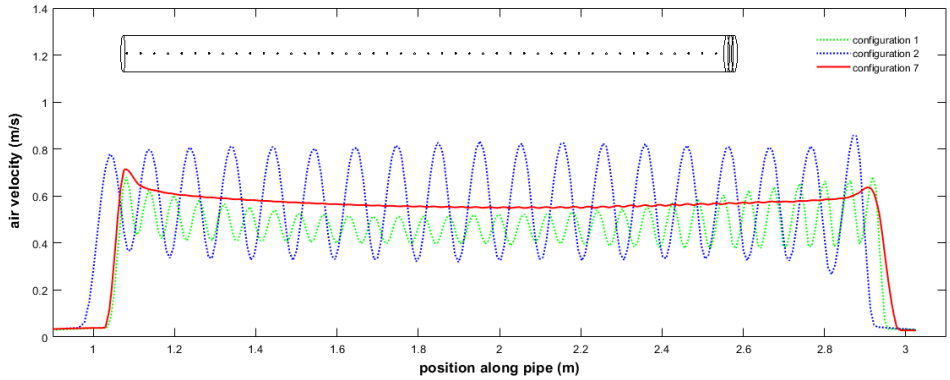

Figure 4.74: The dashed lines are the basic configurations and the whole line is the configuration with refined holes. The pipe showed to understand that the profiles are from the end to the top of the tube.

However, it remains an isolated episode in the profile. In addiction, for the purposes of the system it would not affect its functionality and it is still in the range of the desired velocity magnitude. Moreover, based on figure 4.72, in configuration 5 the profile is located in the area where any single jet is no longer identifiable but where there is a more constant and homogeneous air velocity. A similar result characterize configuration 6, with the only difference that the velocity magnitude

is larger than configuration 5. However, these configurations significantly improve the results obtained with the initial configurations, 1 and 2. Nevertheless, these results can be considered less satisfactory than those concerning configurations 7 and 8, as shown in in fig. 4.74 and in fig. 4.75. In fact, in configuration 7, the profile demonstrates to be more homogeneous and stable at 0.6 m/s, compared to the previous cases. In the profile, the velocity undergoes a small increase at the beginning and end areas of the pipe. However, these variations are very limited, just around 0.7 m/s. For these reasons, this configuration can be definitely considered similar to the sought results.

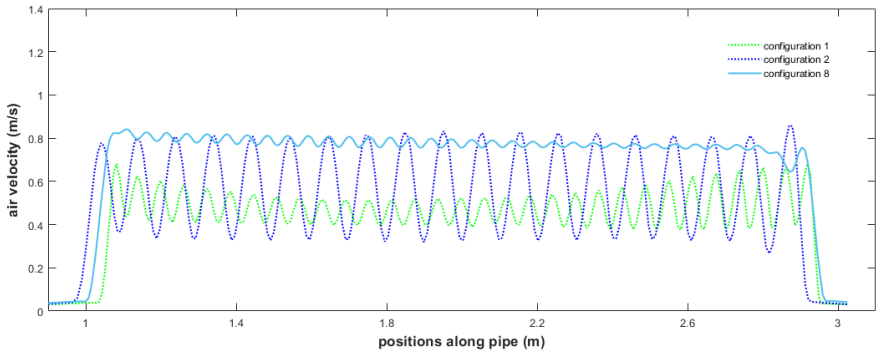

Figure 4.75: The dashed lines are the basic configurations and the whole line is the configuration with refined holes. The profiles as done before are from the end to the beginning of the tube.

In analogy to this configuration, the outcome profile of configuration 8 is presented in figure 4.75. As visible, the result is similar to the one obtained for configuration 7 (fig. 4.74 because the profile presents reduced oscillations, and so a more homogeneous trend, with a velocity magnitude settled around 0.8 m/s. In this case, there is a slight decrease in the magnitude in the initial part of the profile, but that does not result in a significant variation in the trend.

Considering all the configurations and the relative results and based on the defined limits of air velocity, configurations 7 and 8 were chosen to be the best system designs for the future application of the pipe. They have already shown differences that would be interesting to investigate further the air flows, resulting from the two configurations. In fact, taking into account that the system is planned to be placed inside a wine cellar, could be useful to understand how far from the tube could be appreciable the air jet effects. In figure 4.76 the contour map of configurations 7 and 8 are reported, showing the air velocity magnitude of the area around the system. It is clear that the air jets, coming from the system, have a wide area of action in both cases. In fact, downstream of the pipe stagnation areas (air velocity equal to 0 m/s) are not detected, however areas at rally low velocity

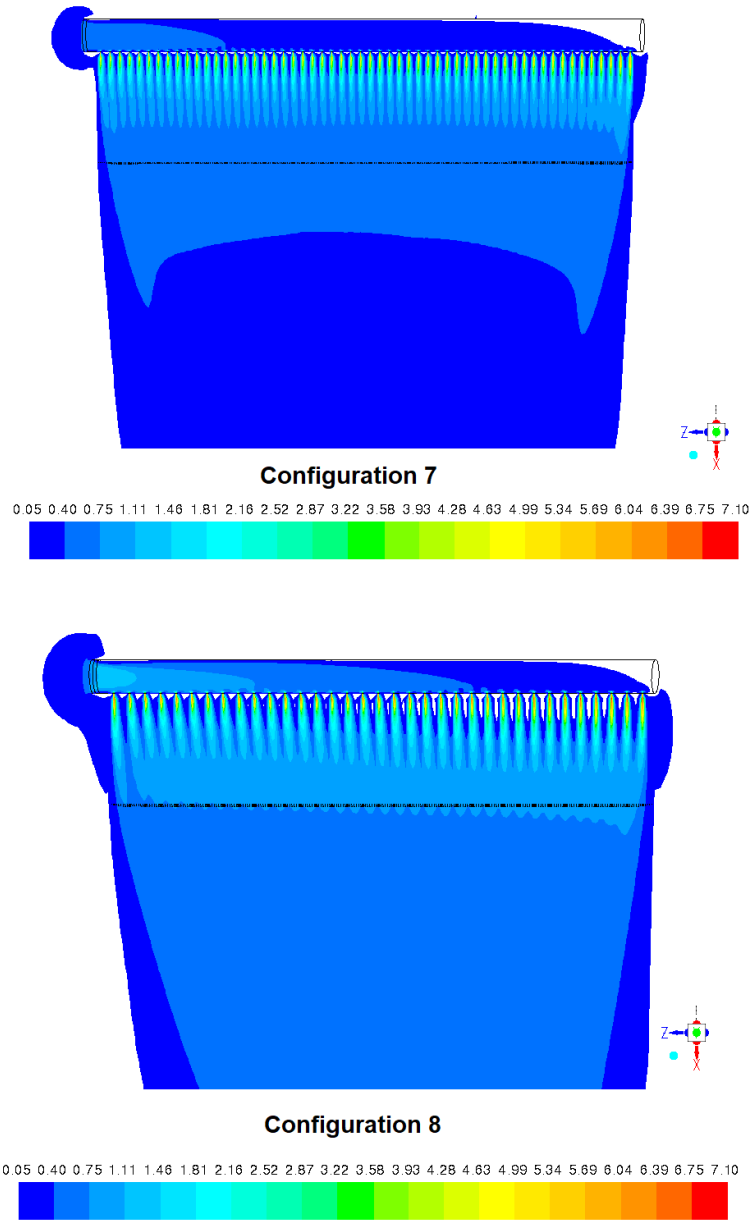

Figure 4.76: The contour map of the air velocity, due to the air jets of the pipe, for configuration 7 and 8. The magnitude lower limit was settled at 0.05 m/s, in both cases.

(0.05 m/s) are present in the case of configuration 7. On the contrary, configuration 8 shows wider effects, presenting an area at air velocity higher than 0.4 m/s from

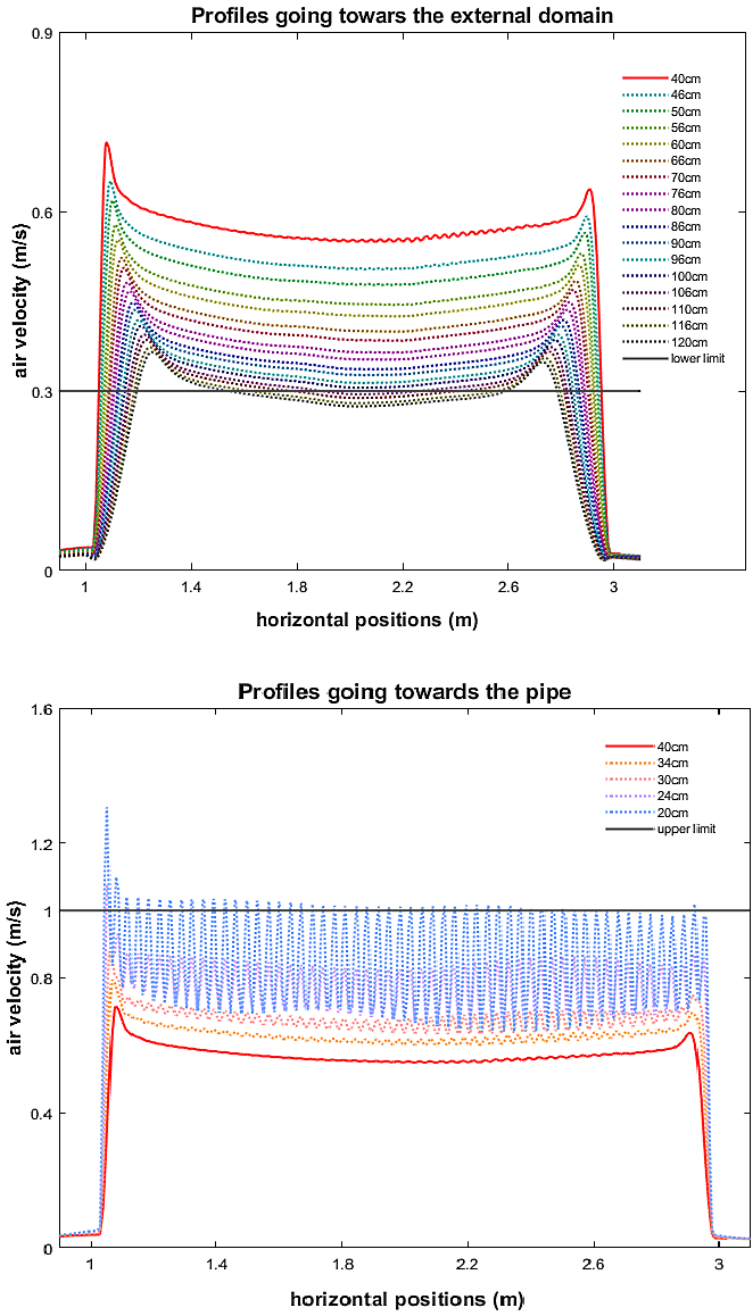

Figure 4.77: The first plot (up) presents the trend of the velocity profiles, increasing the distance from the pipe. The second plot (down) shows the same situation but about the profiles with a decreasing distance from the tube.

40 cm up to the limit of the domain, which means over 1.45 m far from the pipe. Recalling the purpose of the system, the velocity values of greatest interest are those that are maintained in the range of 0.3 m/s - 1 m/s. In order to identify at which distance these limits were exceeded, the velocity profiles were extrapolated to every 2 cm of distance, proceeding towards the pipe and the external domain, starting from the initial profile at 40 cm from the tube, for configuration 7. In order to show the results in the clearest way possible, in figure 4.77 are presented the profiles every 10 cm and an intermediate profile at 6 cm, between these. Moreover,the profiles that are placed towards the domain are represented separately from those ones that are placed towards the system.

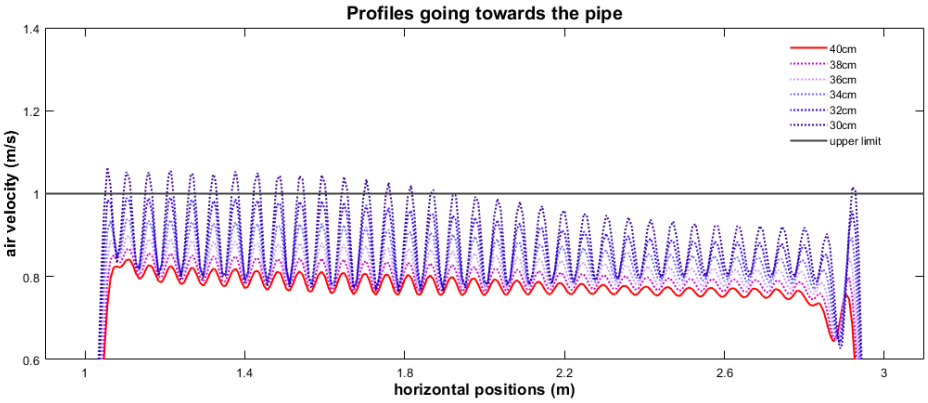

Figure 4.78: The plot presents the trend of the velocity profiles, decreasing the distance from the pipe, in order to identify when the limit of 1 m/s is passed.

As visible in fig. 4.77, the lower limit is exceeded at a distance of 1.06 m from the tube. This distance was confirmed also taking into account the profiles every 2 cm, between 1 m and 1.06 m. About the upper limit, it is exceeded at a distance of 20 cm, since the profile relative to this distance has variations ranging from 1 m / s to 0.7 m/s. Then, the action area of the system is enclosed between 20 cm to 1 m of distance from the system.
On the contrary, can not be identified the distance from the tube where the lower limit could be exceeded, for the configuration 8, but instead the exceeding of the upper limit can be investigated, as done in figure 4.78. The limit of 1 m/s is exceeded at a distance of 30 cm from the system, where the air velocity profile shows several picks, located from the half of the pipe to the end of it, overcomes the defined limit. Then it has been possible to restrict the area of action of this configuration between 30 cm and 1.45 m from the tube.
These informations are essential to evaluate the positions inside the room, where the system should be arranged. Moreover, it can be an useful information to better reflect on other aspects regarding possible layouts, such as the optimal number of

pipes to be placed in the cellar.

4.4.5 Discussion

The wine cellars are rooms for the aging of the wine and, for this process, it is very important to have the climate conditions. Usually the ventilation system of this ambient is natural and control temperature and humidity, presenting several issues, as already widely explained previously. In this study, a CFD model of the cellar has been validated and applied for the study of cellar ventilation. The natural ventilation of the room presented wide stagnation areas at several heights in the domain. In particular, the area behind the barriques at the North-Est wall was characterized by low or zero air velocity. This situation could cause problems in the wine aging process.
According to these results, the design and test process of a smart mechanical ventilation system, which would act as a support for natural ventilation, for small or medium wine farms, has been conducted. In particular, was created a first set up of the system and was created a model of it, which was validated against experimental data. Then, several configurations were analyzed and compared, defining the best ones between these, based on the system purpose. The final configurations that presented the optimal results had these sets up:

- holes of 0.5 mm of diameter, spaced 3 cm from each other;
- holes of 0.8 mm of diameter, spaced 4.8 cm from each other.

The CFD approach gave the chance to observe the behavior of each system hypothesized, going to identify the negative aspects in relation to the desired results. Finally, it was possible to optimize the system, without having to build any new system, saving time and materials. Moreover, this approach allowed also the investigation of other useful aspects for the further system implementation, such as the zones of air velocity, within the defined magnitude range. All these can be considered essential for a proper placement of the system inside the room. Starting from these results, it would be interesting to investigate how the implementation of the system could affect the global air flow distribution inside the wine cellar. In addiction, it could be a step further in the research the comparison of different system positions within the environment as well as a combined action of several tubes, always having as ultimate goal the optimal conditions for the aging of wine.

Chapter 5

Conclusions

The advantages for the agricultural and agro-industrial sector linked to the improvement of ventilation and therefore of climatic conditions in buildings and structure for vegetable and animal production is well known, according to different points of view. In fact, the ventilation can play a key role in the variability of the environmental parameters in agricultural buildings. In particular, air velocity can significantly affect the growth of crops in greenhouses, as well as product, aging and conservation in a wine cellar. However, ventilation itself is affected by several factors, such as wind velocity and direction, solar radiation or presence of insect or shading screens. About wine cellars, ventilation allows to reduce the formation of molds around the barriques, during the aging phase, but, due to the fact that is usually archived through a natural ventilation system, it is subject to various critical issues.

This thesis has addressed these issues with the aim of identifying several possible solutions improving the environmental conditions of these two types of agricultural buildings. First of all, the results obtained in this study have highlighted that any choice can have positive or negative consequences on ventilation rate and air flow distribution inside an agricultural buildings. In fact, the study has allowed to estimate and observe the ventilation in a case-study greenhouse under several wind velocity profiles. In addition, the results have shown that the presence of internal shading screens can considerably modify the air flow patterns and reduce the air velocity magnitude all around the cultivation areas. These new outcomes led to conduct a more in-depth research on the specific characterization of a set of new types of shading screens.

In fact, the outcomes of this study have clearly shown that growers should pay careful attention to the choice of the most suitable shading screen. Considering the great amount of types of shading screen on the market, the choice should not be made only based on its effect on solar radiation. In fact, different screens can have a totally different behavior respect to the air flow passing through them, for a

given effect on solar light. In particular, these new products are characterized by a plastic texture with a complex mesh. For these reasons, it was expected to notice differences between them, and consequently also differences on the fluid-dynamic inside the buildings where they can be placed. It has been necessary to find out a methodology to collect the data for the characterization of screens. Based on wind tunnel tests and velocity and pressure drop measurements, the characteristic curve and the parameters characterizing the screens behavior have been defined. In alternative to an experimental approach, a CFD scaled model has also been validated, applicable for the determination of the screens properties, when any experimental apparatus is available.
The tested screens showed significantly different properties that can also influence ventilation in a structure, such as a greenhouse. About this, the CFD approach has been applied to observe and evaluate the different effects of these screens on the internal fluid dynamic of a greenhouse, compared to the situation observed in absence of any screen. Their effect on ventilation is significant and visible, since they can considerably reduce air speed in the cultivation area and modify the air flow patterns. However, the choice of most suitable type of screen can lead to better conditions in the cultivation area, even when further improvements are still possible. This result suggests that, besides choosing the most suitable type of screen, the most efficient ways of arranging the screens inside the structure should also be carefully evaluated, based on the fluid dynamic properties.
About natural ventilation, it has been modeled and validated a case-study of a wine cellar, in controlled conditions. In this way, the CFD model allowed to detect the critical aspects, such as stagnation or low velocity areas, of the natural ventilation. In particular, low air velocities have been observed on the North-Est side of the room, behind the barriques. Then, it has been considered to design a mechanical ventilation system to be added to the natural ventilation system of the cellar, in order to improve these critical issues of insufficient air velocity and stagnation areas.
A 3D CFD model of this system has been validated. Then several configurations of the system have been simulated, analyzed and compared. Two system configurations proved to be able to provide the defined ventilation conditions, based on the literature references available. These configurations have similar results but with some differences that affect their applicability in a closed environment, such as a cellar. In fact, the results have shown that both systems can be used but it is necessary to evaluate their optimal positioning inside the room and the number applicable, always considering the aim of creating a more homogeneous ventilation condition. In fact, it should be considered its effect on the indoor air flow patterns, highlighting the improvements in the area around the barriques. However, this process has allowed to optimize the design of the system without

conducting any type of experimentation, thus reducing the working time but also the use of materials.
From a global point of view, the CFD approach has allowed to identify the critical issues of the ventilation conditions of agricultural buildings but also to study several possible improvements. This approach proved to be an useful and fast tool to study and evaluate a multiplicity of scenarios, providing useful evaluation tools also for producers and growers. In fact, it can be applied not only as a tool for the design of new buildings but also as a tool for the improvement of existing buildings or their management by the producers/growers themselves. Finally, it has also proved to be an excellent decision-making tool on products on the market.

Bibliography

Alabi, O.O.. Validity of Darcy's Law in Laminar Regime. Electronic Journal of Geotechnical Engineering 2011;16:27–40.

Almuhanna, E. A., . Ventilation in Agricultural Buildings: Characteristics and Measurements Methods (Review). International Journal of Agriculture Innovations and Research 2016;4(5):872–882.

Amstrong, H.. Shut down the roof and save energy:. Fruit & veg tech 2003;3(5):6–9.

Annese, V., De Venuto, D.. On-line shelf-life prediction in perishable goods chain through the integration of wsn technology with a 1st order kinetic model. 2015. p. 605–610. Cited By 7.

ANSYS, I.. ANSYS Fluent Theory Guide, 2013. `arXiv:ArXiv ID`.

Avramidis, S., Siau, J.F.. An investigation of the external and internal resistance to moisture diffusion in wood. Wood Science and Technology 1987;21(3):249–256.

Baeza E. J., P.P.J.J.L.J.C., Montero, J.I.. Simulation of natural ventilation of parral greenhouse with a baffle device below the greenhouse vents. Acta Horticulturae 2008;801:885–892.

Bakker J. C., A.S.B.T., Montero, J.I.. Innovative technologies for an efficient use of energy. Acta Horticulturae 2008;801:49–62.

Barbaresi, A.. Modellazione edilizia e simulazione energetica per le analisi delle prestazioni e la progettazione integrata delle cantine aziendali. Ph.D. thesis; Alma Mater Studiorum, Univeristy of Bologna; 2014.

Barbaresi, A., Torreggiani, D., Benni, S., Tassinari, P.. Underground cellar thermal simulation: Definition of a method for modelling performance assessment based on experimental calibration. Energy and Buildings 2014;76:363–372.

Barbaresi, A., Torreggiani, D., Benni, S., Tassinari, P.. Indoor air temperature monitoring: A method lending support tomanagement and design tested on a wine-aging room. Building and Environment 2015;86:203–210.

Bartzanas, T., Boulard, T., Kittas, C.. Effect of vent arrangement on windward ventilation of a tunnel greenhouse. Biosystems Engineering 2004;88:479 – 490.

Baxevanou, C., Fidaros, D., Bartzanas, T., Kittas, C.. Numerical simulation of solar radiation, air flow and temperature distribution in a naturally ventilated tunnel greenhouse. Agricultural Engineering International: CIGR Journal 2010;12:4867.

Benni, S., Santolini, E., Barbaresi, A., Torreggiani, D., Tassinari, P.. Calibration and comparison of different CFD approaches for airflow analysis in a glass greenhouse. Journal of Agricultural Engineering 2017;48. doi:10.4081/jae.2017.568.

Benni, S., Tassinari, P., Bonora, F., Barbaresi A. .and Torreggiani, D.. Efficacy of greenhouse natural ventilation: Environmental monitoring and CFD simulations of a study case. Energy and Buildings 2016;125:276–286.

Benni, S., Torreggiani, D., Barbaresi, A., P., T.. Thermal Performance Assessment for Energy-Efficient Design of Farm Wineries. Transactions of the ASABE 2013;56:1483–1491.

Berckmans,D. and Vranken, E. and Geers, R. and Goedseels, V. journal = Farm Building Progress, p...t..E.v...y... ;.

Blanco, M., Ramos, F., Van Doorslaer, B., Martínez, P., Fumagalli, D., Ceglar, A., Fernández, F.J.. Climate change impacts on EU agriculture: A regionalized perspective taking into account market-driven adjustments. Agricultural Systems 2017;156:52–66.

Boulard, T., Kittas, C., Roy, J.C., Wang, S.. Convective and ventilation transfers in greenhouses, part 2: Determination of the distributed greenhouse climate. Biosystems Engineering 2002;83:129–147.

Boulton, R.B., Singleton, V.L., Bisson, L.F., Kunkee, R.E.. Principles and Practices of Winemaking. Springer US, 1999. doi:10.1007/978-1-4757-6255-6.

Bournet, P.E., Boulard, T.. Effect of ventilator configuration on the distributed climate of greenhouses: A review of experimental and cfd studies. Computers and Electronics in Agricultur 2010;74(2):195 – 217.

Bournet, P.E., Ould Khaoua, S.A., Boulard, T.. Numerical prediction of the effect of vent arrangements on the ventilation and energy transfer in a multi-span glasshouse using a bi-band radiation model. Biosystems Engineering 2007;98(2):224–234.

Brundrett, E.. Prediction of Airflow With Swirl in Perforated Polyethylene Tubes. Journal of Fluids Engineering 1990;112:447.

Campen, J.B.. Greenhouse design applying CFD for Indonesian conditions. Acta Horticulturae 2005;691:605–614.

Campen, J.B., Bot, G.P.A.. Determination of greenhouse-specific aspects of ventilation using three-dimensional computational fluid dynamics. Biosystems Engineering 2003;84:69–77.

Campiotti, C., Bibbiani, C., Campiotti, A., Schettini, E., Viola, C., Vox, G.. Innovative sustainable strategies in agro-food systems and in buildings for energy efficienc. RIVISTA DI STUDI SULLA SOSTENIBILITA' 2016;:79–96.

Campiotti, C.A., Bibbiani, C., Scoccianti, M., Viola, C.. Energy efficiency in agro-food industry 2013;14(S3):42–49. Cited By 2.

Canakci, M., Topakci, M., Akinci, I., Ozmerzi, A.. Energy use pattern of some field crops and vegetable production: Case study for antalya region, turkey. Energy Conversion and Managemen 2005;46(4):655 – 666.

Cañas, I., Mazarrón, F.R.. The effect of traditional wind vents called zarceras on the hygrothermal behaviour of underground wine cellars in Spain. Building and Environment 2009;44:1818–1826.

Castellano, S., Mugnozza Scarascia, G., Russo, G., Briassoulis, D., Mistriotis, A., Hemming, S., Waaijenberg, D.. Design and Use Criteria of Netting Systems for Agricultural Production in Italy. Journal of Agricultural Engineering 2009;(518):31–42.

Ceglie, F.G., Amodio, M.L., de Chiara, M.L.V., Madzaric, S., Mimiola, G., Testani, E., Tittarelli, F., Colelli, G.. Effect of organic agronomic techniques and packaging on the quality of lamb's lettuce. Journal of the Science of Food and Agriculture 2018;98:4606–4615.

Davidson, P.. Turbulence An Introduction for Engineers and Scientists. OUP Oxford, 2004.

De Rosis, A., , A., Torreggiani, D., Benni, S., Tassinari, P.. Numerical simulations of the airflows in a wine-aging room: A lattice Boltzmann-Immersed Boundary study. Computers and Electronics in Agriculture 2014;109(1):261–270.

Di Sabatino, S., Buccolieri, R., Pulvirenti, B., Britter, R.. Simulations of pollutant dispersion within idealised urban-type geometries with CFD and integral models. Atmospheric Environment 2007;41(37):8316–8329.

Djevic, M., Dimitrijevic, A.. Energy consumption for different greenhouse constructions. Energy 2009;34(9):1325–1331.

El Moueddeb, K., Barrington, S., Barthakur, N.. Perforated ventilation ducts: Part 1, a model for air flow distribution 1997;68:21–27.

El Moueddeb, K., Barrington, S., Barthakur, N.. Modeling fan and perforated ventilation ducts for airflow balance point. Transactions of the American Society of Agricultural Engineers 1998;41(4):1131–1137.

Etheridge D., . NATURAL VENTILATION OF BUILDINGS THEORY, MEASUREMENT AND DESIGN. John Wiley & Sons, 2012.

Fabrizio, E.. Energy reduction measures in agricultural greenhouses heating: Envelope, systems and solar energy collection. Energy and Buildings 2012;53:57–63.

Fabrizio, E., Ghiggini, A., Bariani, M.. Energy Performance and Indoor Environmental Control of Animal Houses: A Modelling Tool. Energy Procedia 2015;82:439–444. doi:10.1016/j.egypro.2015.11.833.

Fatnassi, H., Boulard, T., Bouirden, L.. Simulation of climatic conditions in full-scale greenhouse fitted with insect-proof screens. Agricultural and Forest Meteorology 2003;118:97–111.

Fidaros, D.K., Baxevanou, C.A., Bartzanas, T., Kittas, C.. Numerical simulation of thermal behavior of a ventilated arc greenhouse during a solar day. Renewable Energy 2010;35:1380 – 1386.

Flores-Velazquez, J., Montero, J.I.. Computational Screenhouses Fluid Dynamics (CFD) Study of Large Scale. Acta Horticulturae 2008;797:117–122.

Fluent Inc, . FLUENT 6.3 User's Guide, 2006.

Fuchs, M., Dayan, E., Presnov, E.. Evaporative cooling of a ventilated greenhouse rose crop. Agricultural and Forest Meteorology 2006;138(1):203 – 215.

Geyrhofer, A., Weingartmann, H., Mandl, K., Schattauer, D.. Measurements of air flow in the wine cellar. Mitteilungen Klosterneuburg 2011;61:76–81.

Gromke, C., Buccolieri, R., Di Sabatino, S., Ruck, B.. Dispersion study in a street canyon with tree planting by means of wind tunnel and numerical investigations - Evaluation of CFD data with experimental data. Atmospheric Environment 2008;.

He, K., Chen, D., Sun, L., Huang, Z., Liu, Z.. Analysis of the Climate inside Multi-span Plastic Greenhouses under Different Shade Strategies and Wind Regimes. Kor J Hort Sci Technol 2014;32:473–483.

Hemraj, , Sukesha, . Power estimation and automation of green house using wireless sensor network. In: 2014 5th International Conference - Confluence The Next Generation Information Technology Summit (Confluence). IEEE; 2014. p. 436–441.

Hirsch, C.. Numerical Computation of Internal and External Flows. Butterworth-Heinemann; second edi ed.; 2007. p. 680.

Impron, I., Hemming, S., Bot, G.P.A.. Simple greenhouse climate model as a design tool for greenhouses in tropical lowland. Biosystems Engineering 2007;98:79–89.

ISO9053:1991, . Acoustics - Materials for Acoustical Applications - Determination of Airflow Resistance. Technical Report; International Organization for Standardization; Geneva, Switzerland.; 1991.

Jung, S.Y., Govindarajan, B., Baeder, J.. A Hamiltonian-Strand Approach for Aerodynamic Flows Using Overset and Hybrid Meshes. AHS International 72nd Annual Forum 2016;(May).

Katsoulas, N., Bartzanas, T., Boulard, T., Mermier, M., Kittas, C.. Effect of Vent Openings and Insect Screens on Greenhouse Ventilation. Biosystems Engineering 2006;93:427–436.

Kittas, C., Katsoulas, N., Bartzanas, T., Mermier, M., Boulard, T.. The Impact of Insect Screens and Ventilation Openings on the Greenhouse Microclimate. American Society of Agricultural and Biological Engineers ISSN 2002;51:1–15.

Koplik, J., Banavar, J.R.. Continuum deductions from molecular hydrodynamics. Annual Review of Fluid Mechanics 1995;27(1):257–292.

Linden, P.F.. The fluid Mechanics. Fuild Mechanics 1999;.

Maher, A., Kamel, E., Enrico, F., Atif, l., Abdelkader, M.. An intelligent system for the climate control and energy savings in agricultural greenhouses. Energy Efficiency 2016;9:1241–1255.

Martin, S., Canas, I.. A comparison between underground wine cellars and aboveground storage for the aging of Spanish wines. TRANSACTIONS OF THE ASABE 2006;49:1471–1478.

Mazarrón, F.R., Cañas, I.. Seasonal analysis of the thermal behaviour of traditional underground wine cellars in Spain. Renewable Energy 2009;34(11):2484–2492.

Mazarrón, F.R., López-Ocón, E., Garcimartín, M.A., Cañas, I.. Assessment of basement constructions in the winery industry. Tunnelling and Underground Space Technology 2013;35:200–206.

Miguel, A.F.. Airflow through porous screens: From theory to practical considerations. Energy and Buildings 1998;28:63–69.

Miguel, A.F., Van De Braak, N.J., Bot, G.P.A.. Analysis of the airflow characteristics of greenhouse screening materials. Journal of Agricultural and Engineering Research 1997;67:105–112.

Miguel, A.F., Van De Braak, N.J., Silva, A.M., Bot, G.P.A.. Physical Modelling of Natural Ventilation Through Screens and Windows in Greenhouses. Journal of Agricultural Engineering Research 1998;70:165–176.

Mistriotis, A., Arcidiacono, C., Picuno, P., Bot, G.P.A., Scarascia-Mugnozza, G.. Computational analysis of ventilation in greenhouses at zero- and low-wind-speeds. Agricultural and Forest Meteorology 1997;88:121–135.

Molina-Aiz, F.D., Valera, D.L., Álvarez, A.J.. Measurement and simulation of climate inside Almera-type greenhouses using computational fluid dynamics. Agricultural and Forest Meteorology 2004;125:33–51.

Mondaca, M., Choi, C.Y.. A Computational Fluid Dynamics Model Of A Perforated Polyethylene Tube Ventilation System For Dairy Operations. In: 2017 Spokane, Washington July 16 - July 19, 2017. volume 59; 2017. p. 1585–1594.

Montero, J.I., Muñoz, P., Sánchez-Guerrero, M.C., Medrano, E., Piscia, D., Lorenzo, P.. Shading screens for the improvement of the night-time climate of unheated greenhouses. Spanish Journal of Agricultural Research 2013;.

Negrè, E., Françot, P.. Manuel Pratique De Vinification Et De Conservation Des Vins. Flammarion ed. Les Angles, 1965.

Nelson, P.. Greenhouse Operation and Management. 6th ed. Prentice Hall, 2003.

Norton, T.. CFD in the Agri-Food Industry : A maturing engineering design tool. Computers and Electronics in Agriculture 2013;93:149–150.

Ocon, E., Gutierrez, A.R., Garijo, P., Santamaría, P., Lopez, R., Olarte, C., Sanz, S.. Factors of Influence in the Distribution of Mold in the Air in a Wine Cellar. Journal of Food Science 2011;76:169–174.

Perone, C., Fucci, F., La Fianza, G., Brunetti, L., Giametta, F., Catalano, P., Bianchi, B.. Experimental study of a mechanical ventilation system in a greenhouse. Chemical Engineering Transactions 2017;58:811–816.

Picco, A.M., Rodolfi, M.. Assessments of indoor fungi in selected wineries of Oltrepo Pavese (Northern italy) and Sottoceneri (Switzerland). AMERICAN JOURNAL OF ENOLOGY AND VITICULTURE 204;55:355–362.

Piscia, D., Montero, J.I., Baeza, E., Bailey, B.J.. A CFD greenhouse night-time condensation model. Biosystems Engineering 2012;111:141–154.

Ramírez López, B.C., Guzmán, G., Alhalabi, W., Cruz-Cortés, N., Torres-Ruiz, M., Moreno-Ibarra, M.. On the usage of sorting networks to control greenhouse climatic factors. International Journal of Distributed Sensor Networks 2018;14.

Randall, J. M. and Boon, C. R. journal = CAB International, p...t..V.y... ;.

Rico-Garcia, E., Reyes-Araiza, J.L., Herrera-Ruiz, G.. Simulations of the climate in two different greenhoses. Acta Horticulturae 2006;719:325–332.

Rico-García, E., . Aerodynamic study of greenhouses using computational fluid dynamics. International Journal of the Physical Sciences 2011;6(28).

Robles, C.. Low-Cost Fuzzy Logic Control for Greenhouse Environments with Web Monitoring. Electronics 2017;6(4):71.

Rong, L., Liu, D., Pedersen, E.F., Zhang, G.. The effect of wind speed and direction and surrounding maize on hybrid ventilation in a dairy cow building in Denmark. Energy and Buildings 2015;86:25–34.

Rong, L., Nielsen, P.V., Bjerg, B., Zhang, G.. Summary of best guidelines and validation of CFD modeling in livestock buildings to ensure prediction quality. Computers and Electronics in Agriculture 2016;121:180–190.

Ruiz De Adana, M., López, L.M., Sala, J.M.. A Fickian model for calculating wine losses from oak casks depending on conditions in ageing facilities. Applied Thermal Engineering 2005;25:709–718.

San-Antonio-Gómez, C., Manzano-Agugliaro, F., Rojas-Sola, J.I.. Analysis of design criteria in authored wineries. Scientific Research and Essays 2011;6(19):4097–4103.

Santolini, E., Pulvirenti, B.e., Benni, S., Barbaresi, L., Torreggiani, D., Tassinari, P.. Numerical study of wind-driven natural ventilation in a greenhouse with screens. Computers and Electronics in Agriculture 2018;:41–53.

Sase, S.. Air movement and climate uniformity in ventilated greenhouses. Acta Horticulturae 2006;719:313–323.

Schlichting, H., Gersten, C.. Boundary-Layer Theory. Springer, 2017.

Schmitt, F.G.. About Boussinesqs turbulent viscosity hypothesis : historical remarks and a direct evaluation of its validity 2007;335:617–627.

Shih, T., Liou, W.W., Shabbir, A., Yang, Z., Zhu, J.. A new k- eddy viscosity model for high reynolds number turbulent flows. Computers & Fluids 1995;24:227–238.

Simeray, J., Mandin, D., Mercier, M., Chaumont, J.P.. Survey of viable airborne fungal propagules in French wine cellars. Aerobiologia 2001;17:19–24.

Sobieski, W., Trykozko, A.. Sensitivity Aspects of Forchheimer's Approximation. Transport in Porous Media 2011;89:155–164.

Sobieski, W., Trykozko, A.. Darcy's and Forchheimer's Laws in Practice. Part 1: the Experiment. Technical SciencesSciences 2014a;17(4):321–335.

Sobieski, W., Trykozko, A.. Darcy's and Forchheimer's Laws in Practice. Part 2. the Numerical Model. Technical Sciences 2014b;17:321–335.

Sravani, V., Santhosh, K.V., Bhargava, S., D'Almeida, V.. Design and implementation of a smart controller in agriculture for improved productivity. Istanbul University - Journal of Electrical and Electronics Engineering 2018;18:45–51.

Sukop, M.C., Huang, H., Alvarez, P.F., Variano, E.A., Cunningham, K.J.. Evaluation of permeability and non-Darcy flow in vuggy macroporous limestone aquifer samples with lattice Boltzmann methods. Water Resources Research 2013;49(1):216–230.

Tanny, J.. Microclimate and evapotranspiration of crops covered by agricultural screens: A review. Biosystems Engineering 2013;114:26–43.

Tassinari, P., Galassi, S., Benni, S., Torreggiani, D.. The built environment of farm wineries: An analysis methodology for defining meta-design requirements. Journal of Agricultural Engineering 2011;42(2):25–31.

Tate, J.. Thermal Performance Assessment for Energy-Efficient Design of Farm Wineries. Transactions of the ASABE 2013;56(1965):1483–1491.

Teitel, M.. The effect of insect-proof screens in roof openings on greenhouse microclimate. Agricultural and Forest Meteorology 2001;110:13–25.

Teitel, M.. The effect of screened openings on greenhouse microclimate. Agricultural and Forest Meteorology 2007;143:159–175.

Teitel, M.. Using computational fluid dynamics simulations to determine pressure drops on woven screens. Biosystems Engineering 2010;105:172–179.

Teitel, M., Garcia-Teruel, M., Ibanez, P.F., Tanny, J., Laufer, S., Levi, A., Antler, A.. Airflow characteristics and patterns in screenhouses covered with fine-mesh screens with either roof or roof and side ventilation. Spanish Journal of Agricultural Research 2015;19:441–448.

Teitel, M., Liran, O., Tanny, J., Barak, M.. Wind driven ventilation of a monospan greenhouse with a rose crop and continuous screened side vents and its effect on flow patterns and microclimate. Biosystems Engineering 2008;101:111–122.

Teitel, M., Wenger, E.. Air exchange and ventilation efficiencies of a monospan greenhouse with one inflow and one outflow through longitudinal side openings. Biosystems Engineering 2014;119:98 – 107.

Tinti, F., Barbaresi, A., Benni, S., Torreggiani, D., Bruno, R., Tassinari, P.. Experimental analysis of thermal interaction between wine cellar and underground. Energy & Buildings 2015;104:275–286.

Togores, H.J.. Tratado de enología 2003;.

Troost, G.. Die Technologie des Weines / von Gerhard Troost. Eugen Ulmer Stuttgart, zur Zeit Ludwigsburg, [Germany], 1953.

Vadiee, A., Martin, V.. Energy management in horticultural applications through the closed greenhouse concept , state of the art. Renewable and Sustainable Energy Reviews 2012;16(7):5087–5100.

Valera, D.L., Molina, F.D., Álvarez, A.J., López, J.A., Terrés-Nicoli, J.M., Madueño, A.. Contribution to characterisation of insect-proof screens: Experimental measurements in wind tunnel and CFD simulation. Acta Horticulturae 2005;691:441–448.

Vogt, E.. Fabricacion de vinos (Winemaking). Editorial Acribia, 1971.

Vranken, E., Berckmans, D., Goedseels, V.. Control of mechanical ventilation in modern livesock production. Syllabus Study day University Luik 1991;.

Wells, C., Amos, N.. Design of air distribution systems for closed greenhouses. Acta Horticulture 1994;361:94–104.

Yravedra Soriano, M.J.. ARQUITECTURA Y CULTURA DEL VINO: ANDALUCIA, CATALUÑA, LA RIOJA Y OTRAS REGIONES. MUNILLALERIA, 2003.

von Zabeltitz, C.. Integrated Greenhouse Systems for Mild Climates. Springer Berlin Heidelberg, 2011.

Ziganov, O., . Essential computational fluid dynamics. John Wiley & Sons, 2010.

List of Figures

List of Tables